FAKULTÄT FÜR ELEKTROTECHNIK UND INFORMATIONSTECHNIK, LEHRSTUHL FÜR NANOELEKTRONIK, TECHNISCHE UNIVERSITÄT MÜNCHEN

FUNCTIONALIZATION OF SURFACES FOR SENSORS AND OPTOELECTRONICS

ALINA LYULEEVA

Vollständiger Abdruck der von der Fakultät für Elektrotechnik und Informationstechnik der Technischen Universität München zur Erlangung des akademischen Grades eines

Doktors der Naturwissenschaften (Dr.rer.nat.)

genehmigten Dissertation.

Vorsitzende/r: Prof. Dr. Oliver Hayden

Prüfende/-r der Dissertation:

1. Prof. Dr. Paolo Lugli
2. Prof. Dr. Dr. h. c. Bernhard Rieger
3. Prof. Dr. Marc Tornow

Die Dissertation wurde am 10. Januar 2018 bei der Technischen Universität München eingereicht und durch die Fakultät für Elektrotechnik und Informationstechnik am 5. April 2018 angenommen.

To my family

Посвещается моей семье

Meiner Familie gewidmet

“Life is like mountains:

When it happens that you reach a valley,

Watch out for another peak to conquer!”

Vladimir Yurievich Kusov
(Владимир Юрьевич Кусов)

- Just ignore the trees and the clouds, then you will see the stars -

Acknowledgements

I would like to thank *Prof. Dr. Lugli (University of Bozen-Bolzano, Italy)* for being my Dissertation supervisor and for providing the opportunity to work in his group. Already after two weeks of my scientific work, he allowed me to develop a completely new project in the field of a hitherto unknown material. With his confidence in my independent work, I had the freedom to explore different subjects. I chose two-dimensional materials out of personal interest. However, this subject grew rapidly into my new field of expertise. Additionally, many thanks to the Nano-group and especially the group members *Marco Bobinger, Florin Loghin, Andreas Albrecht, Vijay Bhatt (TUM, Chair of Nanoelectronics, Munich) and Dr. Aniello Falco (University of Bozen-Bolzano, Italy)*. Many thanks to *Katharina Melzer* and *Dr. Frank Deubel*, who have advised me especially in the beginning of my work.

Thanks to the Alberta/Technical University of Munich (UofA/TUM) International Gradate School for Hybrid Functional Materials (ATUMS) for its existence and for the opportunity to be part of its development from the very beginning. Many thanks to *Prof. Dr. Dr. h.c. Bernhard Rieger (TUM, Chair of Macromolecular Chemistry, Munich)* and *Prof. Jonathan Veinot (UofA, Chemistry Department, Edmonton, Canada)*, who are the ATUMS German and Canadian Program Directors, respectively. With their help I was able to engage with my Canada- and Germany-based colleagues and initiate collaborative projects, which led to several joint-, first and also second author publications. With that, also many thanks to the whole ATUMS community. In my opinion, it is a special program which is led by very interesting, creative and simply nice people. Thank you guys for the opportunity to be a part of this!

Huge appreciation to the group of *Prof. Frank Hegmann (UofA, Physics Department, Edmonton, Canada)* and of course to Frank himself, who hosted me during my research stays in Canada. Being my second supervisor, he advised me a lot not only in my scientific work, but also in my future career plans and even sometimes karaoke singing!

Many thanks to *Prof. Dr.-Ing. Markus Becherer (TUM, Chair of Nanoelectronics, Munich)*, who has taken over the supervision during my last year of the PhD. He was a great support in scientific discussions, projects and collaborations management and paper writing. Also *Dr. Almudena Rivadeneyra's (TUM, Chair of Nanoelectronics, Munich)* help is highly appreciated. She not only introduced me into the humidity sensor field, but also helped with advice for my first independent steps in science.

Many thanks to my collaboration partners *Marc Kloberg, Philipp Holzmüller and Mary A. Narreto*. Thank you guys for fruitful discussions and exciting research. It was great fun to work with you and see how ideas become reality.

Dr. Tobias Helbich, I thank you for this pleasure to already here and now write "Dr." in front of your name. It was a great honour and lots of fun to walk through all these 9 years of studies at TUM, side-by-side with you. – "komm zurück… pffff!" Also many thanks to my friends from Munich, Scheeßel and St.Petersburg! Without having you and your support, the whole painting would have lost its colors.

Great appreciation to everyone, who helped me to find all the little and not so little mistakes in my thesis!

Great thanks to *Prof. Martin Stutzmann (TUM, Walter-Schottky Institute, Munich)*, who always offered his support and advice. Being not only a great professor, he also helped a lot with advice, due to his massive knowledge background in two-dimensional systems.

Of course, not to forget: huge thanks and great appreciation to *Prof. Sir Kostya Novoselov (University of Manchester, UK)*. Thank you very much for your honesty, hours of discussion, very helpful consulting, guidance during my PhD and advice for my future career plans!

And last but definitely not least: I want to give heartfelt thanks to my whole family in St.Petersburg, Hamburg-Area and Frankfurt(-Area). Especially my grandparents **Margarita Fyodorovna Kusova** and **Vladimir Yurievich Kusov**, my mother **Irina Vladimirovna Adam** and my sister **Yuliana Maksimovna Lyuleeva** together with my little niece **Lara Schöfer**! I am very lucky to have had your support day and night, either spring, summer, autumn or winter, even if it was just a simple hello on the phone.

Thank you all!

1 CONTENTS

TABLE OF ABBREVIATIONS

0D	zero-dimensional
1D	one-dimensional
2D	two-dimensional
AFM	atomic force microscopy
DFT	density functional theory
EDX	x-ray spectroscopy
EPR	electron paramagnetic resonance
FET	field-effect transistors
FTIR	Fourier transform infrared spectroscopy
hBN	hexagonal boron nitride
LED	light emitting diode
MMA	methacrylic acid
MW	microwave
OSiNS	oxidized silicon nanosheets
PS	polystyrene
PAA	poly(acrylic acid)
PMMA	poly(methacrylic acid)
RH	relative humidity
SEM	scanning tunneling microscopy
SiNS	silicon nanosheets
SiNC	silicon nanocrystals
SiNW	silicon nanowires
^{t}BMA	*tert*-butyl methacrylate
TMDC	transition metal dichalcogenide
XPS	x-ray photoelectron spectroscopy

INTRODUCTION AND OUTLINE

ENGLISH

With the potential to overcome barriers in current silicon-based semiconductor technology, two-dimensional (2D) materials is a rapidly developing field in nano-scale applied sciences. This dissertation provides guidance for the fabrication and application of functionalized 2D silicon nanosheets (SiNSs), which show remarkable (opto)electronic properties. Their incorporation into well-known fabrication techniques leads to highly sensitive solution-gated field-effect transistors, photodetectors and humidity sensors.

Among 2D materials, graphene was the first one to be successfully characterized by Novoselov *et al.* in 2004. Following this, the synthesis and possible application of 2D silicon became a more central concern than has hitherto been the case. Silicon in its 2D configuration is believed to exhibit outstanding (opto)electronic properties. Some few examples are the consistent green photoluminescence, the possibility of band gap opening and its semiconducting behavior. The thickness of the layered material is only a few nanometers, but at the same time lateral sizes can go up to micro dimensions. Both 2D silicon configurations and the development in the field of nanomaterials are presented in the first chapter.

This work presents also guidance for the fabrication of nano-devices based on novel hybrid materials. Starting from the fundamental understanding of the physics of the discovered material, it is also explained how to control its properties for further use. With the SiNSs as an example, precise engineering of the surface with the help of radical hydrosilylation reactions is introduced. This surface modification was carried out to perform covalent functionalization, which enables the protection and stabilization of the sheets against damage from UV light and oxygen exposure. Consequently, this simple step increases the lifetime of the SiNSs and provides a facile integration of the modified material into well-known deposition techniques. This work has been carried out in close collaboration with the groups of the Alberta/Technical University of Munich (UofA/TUM) International Gradate School for Hybrid Functional Materials (ATUMS). Especially the synthesis and the surface modification of the herein used material has been mainly carried out by Dr. Tobias Helbich and his students from the Chemistry Department of the TU Munich.

As a result of this surface modification, an established way towards the fabrication of novel devices could be guaranteed at the chair of Nanoelectronics (TU Munich). These fabrication techniques are presented and explained in more detail in chapter 4. The first application is the fabrication of improved SiNS-substrate/P3HT based solution-gated field-effect transistors. These transistors show increased

sensitivity with higher transconductance and ON/OFF ratios. The second presented application is a prototype of a highly sensitive photonic sensor (chapter 4.2.). SiNS-polystere@polysterene composite has been synthesized and integrated into the device as a light sensitive material for that purpose. Finally, a capacitive humidity sensor is being developed (chapter 4.3.) which shows the first steps towards response to surrounding molecules and conditions such as water at certain temperatures. The broad range of the predicted application areas comprises diverse nanoelectronic devices, sensors and lithium-ion batteries based on monolayer silicon nanomaterials.

GERMAN

Die Suche nach neuen Möglichkeiten aktuelle Grenzen der Si-Halbleitertechnologien zu überwinden, treibt in den nanobasierten angewandten Wissenschaften die Forschung der zweidimensionalen (2D) Materialien voran. Diese Dissertation bietet eine Orientierungshilfe für die Herstellung und Anwendung von funktionalisierten 2D-Silciumnanoschichten (SiNSs), die bemerkenswerte (opto)elektronische Eigenschaften aufweisen. Ihr Einbau in konventionelle Technologien führt zur Herstellung von hochsensitiven Feldeffekt-Transistoren, sowie Licht- und Feuchtigkeitssensoren.

Im Bereich der 2D Materialien war Graphen der Vorreiter, nachdem es von Novoselov *et al.* in 2004 erfolgreich charakterisiert wurde. Daraus resultierend bekam stärker als bisher die Synthese und die mögliche Anwendung von 2D Silicium ein zentrales Anliegen. Es wird erwartet, dass Silicium in seiner 2D Konfiguration außergewöhnliche Eigenschaften aufweist. Einige Beispiele sind die konsistente grüne Photolumineszenz, die Möglichkeit die Bandlücke des Materials zu öffnen und sein Verhalten als Halbleiter. Die Schichtdicke des Materials ist nur einige Nanometer groß, wobei die lateralen Dimensionen bis zu einer Größe von einigen Mikrometern reichen. Beide Formen des 2D Siliciums und die Entwicklung im Bereich der Nanomaterialien sind im ersten Kapitel im Detail beschrieben.

Diese Arbeit bietet ebenso eine Anleitung für die Anfertigung von Nanogeräten, welche auf neuartigen Hybridmaterialien basieren. Angefangen mit dem grundlegenden Verständnis der Physik des entdeckten Materials, wird im Folgenden auch erklärt, wie dessen Eigenschaften für weiterführende Nutzung kontrolliert werden können. Mit den SiNSs als Beispiel wird das präzise Engineering der Oberflächen mit Hilfe von radikalischer Hydrosilylierungsreaktionen vorgestellt. Diese Oberflächenmodifizierung wurde mit Hilfe von kovalenten Funktionalisierungsreaktionen ermöglicht, die den Schutz und die Stabilisierung der Nanoschichten gegen Zerstörung durch UV-Licht und Sauerstoff Exposition bieten. Als Resultat verlängert dieser einfache Schritt die Lebensdauer der SiNSs und bietet eine mühelose Integration des modifizierten Materials in bereits bekannte

Depositionstechniken. Dieser Teil der Arbeit entstand in enger Kollaboration mit den Gruppen des Internationalen Graduiertenkollegs „Alberta/Technical University of Munich Graduate School for Functional Hybrid Materials“ (ATUMS, International Research Training Group, IRTG 2022). Insbesondere die Synthese und die Oberflächenmodifizierung des hierbei eingesetzten Materials wurde durch Dr. Tobias Helbich und seine Studenten an der Fakultät für Chemie der TU München durchgeführt.

Ausgehend von der präzisen Oberflächenmodifizierung wurde eine bewehrte Methode für die Herstellung von neuartigen Geräten am Lehrstuhl für Nanoelektronik (TU München) erarbeitet und vorgestellt. Diese Anwendungsmethoden werden im Kapitel 4 im Detail erläutert. Die erste Anwendung stellt die Herstellung von verbesserten SiNS-Substrat/P3HT basierten Feldeffekttransistoren dar. Sie zeigen angestiegene Sensitivität mit einem höheren Gegenwirkleitwert und AN/AUS Verhältnis. Die zweite hierbei vorgestellte Anwendung (Kapitel 4.2.) ist der Prototyp eines sensitiven photonischen Sensors. Dafür wurde das Verbundmaterial SiNS-Polystyrol/Polystyrol synthetisiert und in das Gerät als lichtsensitives Material integriert. Zu guter Letzt wurde ein kapazitiver Feuchtigkeitssensor entwickelt (Kapitel 4.3.), der die ersten Schritte in Richtung sensorischer Rückmeldung auf umgebende Moleküle und Bedingungen wie Wasser in der Atmosphäre bei verschiedenen Temperaturen zeigt.

Auf Basis von Silicium-Einzelschichten wurde eine große Auswahl an Anwendungsbereichen vorhergesagt, welche unter Anderem diverse nanoelektronische Geräte, Sensoren und Lithium-Ionen-Batterien umfassen.

1. NANOMATERIALS AND THEIR SURFACE ENGINEERING

1.1. CONTROL OF THE PROPERTIES OF NANOMATERIALS *VIA* SURFACE FUNCTIONALIZATION

Functional nanomaterial-based sensors are widely used in medical and industrial applications. New properties can arise with lowering the dimensionality of the material. A few examples include: quantum confinement (Brus 1994; Wilcoxon et al. 1999), band gap opening (Balendhran et al. 2015), conductivity with ideal electronic and transport properties (Oscar D. Restrepo, Krymowski, et al. 2014) and photoluminescence (PL). (Jiang et al. 2015) For successful applications, however, the devices typically require surfaces that are durable, highly sensitive, cheap and biocompatible. Varying morphology (Sukhanova et al. 2011), chemical reactivity (Gatoo et al. 2014), band gap tuning (Brennan, Morishita & Michelle J. S. Spencer 2016) and charge transport (McNeil et al. 2012; Skrypnychuk et al. 2015) on the interface between different materials in a composite can be exploited for new device engineering at the nanoscale. A general overview of low-dimensional materials towards 3D structures is presented in Figure 1.

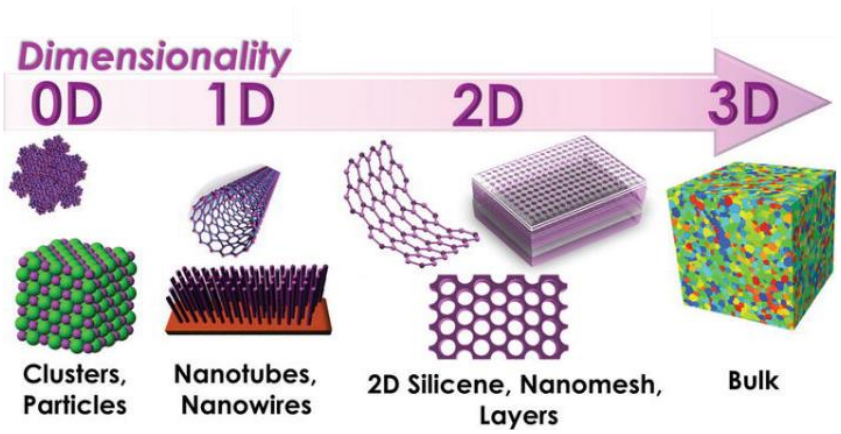

Figure 1: Dimensionality of materials going from left to right: 0D for quantum dots, clusters and nanoparticles, 1D for nanotubes and nanowires, 2D for nanosheets and nanomeshes and 3D for bulk materials such as crystalline silicon. Adapted from Pérez-Taborda et al. (Perez-Taborda et al. 2017) *with permission of The Royal Society of Chemistry, © 2017 Pérez-Taborda JA, Caballero-Calero O, Martín-González M. Published in [New Research on Silicon – Structure, Properties, Technology,] under CC BY 3.0 license. Available from: https://www.intechopen.com/books/new-research-on-silicon-structure-properties-technology/silicon-germanium-sige-nanostructures-for-thermoelectric-devices-recent-advances-and-new-approaches.*

The discovery and investigation of graphene in the beginning of the 21st century laid the foundation for a thus-far unexplored research branch of 2D nanomaterials. (Geim & Novoselov 2007) Based on this work, further 2D materials followed shortly after. Novoselov *et al.* (Novoselov et al. 2004) have practically proven the accessibility of two-dimensionality in graphite. Their discovery and analysis of the zero-overlap semimetal graphene, after the mechanical exfoliation of atomically thin monolayers,

has evoked an explosive amount of work worldwide. Until now, the main purpose was not only finding further analogues of graphene, but also on understanding its fundamental properties to finally pave the way towards applied science. (Arivalagan et al. 2011) This prompted researchers in the fields of materials science, physics and chemistry, which deal with the interface phenomena (for example charge transfer, or molecular interaction), to start searching for new insights in the 2D nanomaterials world. The applied physics and (electro)engineering fields also rapidly discovered potential in the use of these materials for innovative technologies. 2D materials might help overcome the present challenges (*e.g.,* band gap control and ease of manufacturing) and fulfil the desired goals (*e.g.,* reduction of power consumption and semiconductor scaling (Kim et al. 2003; Handy 2014)) in today's applications.

2D materials can be classified into metals (*e.g.,* $NbSe_2$), semiconductors (*e.g.,* silicene and MoS_2) and insulators (*e.g.,* hexagonal boron nitride (hBN)), as presented in Figure 2.

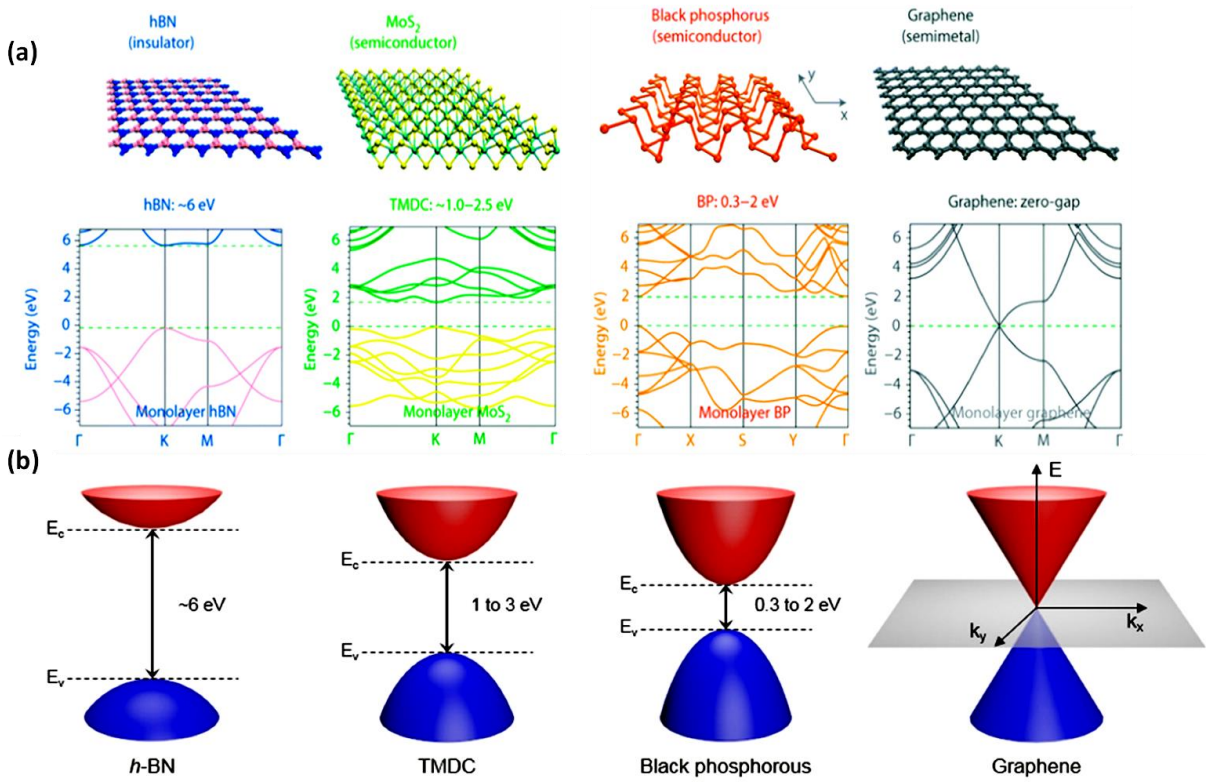

Figure 2: 2D materials with their crystal structure (a) and the corresponding energy diagrams (b). From left to right: hBN as insulator, molybdenum disulphide (MoS_2) and black phosphorus (BP) as semiconductors, graphene as semimetal. Adapted from Rahman *et al.*(Rahman et al. 2016) with permission of The Royal Society of Chemistry (a) and Lee *et al.*(Lee et al. 2016) (CC BY 4.0)

Elemental analogues such as germanene and stanene have already been discovered, studied and successfully presented (Balendhran et al. 2015), as well as heterostructures such as transition metal dichalcogenides (TMDCs) with the formula MX_2 (*e.g.,* WTe_2, MoS_2, $MoSe_2$) (Wilson, J. A.; Yoffe 1969; Velusamy et al. 2015) which have attracted interest due to their outstanding electronic, optical, mechanical and chemical properties. (Wilson, J. A.; Yoffe 1969; Yoffe 1993)

Silicon, as one of the group IV family members, has also 2D representatives: silicene as an analogue to graphene (Vogt et al. 2012; Chiappe et al. 2012; Liu et al. 2013; Xu et al. 2012; Tao et al. 2015; Aufray et al. 2010); silicane, which is a hydrogenated silicon monolayer (Hussain et al. 2013) and siloxene with -OH and -H surface termination. (Dahn et al. 1993) Silicene has attracted attention already in 1994 (Takeda & Shiraishi 1994), when it was theoretically explored by Takeda and Shiraishi *et al.* This nearly planar material with a honeycomb lattice configuration shows structural and electronic properties which are comparable to those of graphene. (Zhao et al. 2016) Nevertheless, due to its sp^2-hybridization, it suffers from the same disadvantage as graphene: the difficulty of stable and irreversible functionalization. This modification step would also allow a controlled opening of the band gap without the destruction of material's surface, which would allow the controlled opening of the band gap. Both, covalent (Bekyarova et al. 2009; Elias et al. 2009) and non-covalent (Wang & Hersam 2011; Chen et al. 2007; Wang & Hersam 2009) functionalizations of planar graphene have been investigated in detail for precise shift of its Fermi level (Lomeda et al. 2008) for the desired need in applications.

Silicene is also governed by sp^2-hybridization, which makes the treatment of this nanomaterial difficult. Furthermore, in conflict with the outstanding features of 2D silicon *(vide supra)* and due to its puckered and crinkled structure (Brumfiel 2013; Merali 2013), silicene is rather unstable in ambient conditions and needs to be protected from UV light and oxygen. (G. Liu et al. 2014; Helbich, Lyuleeva, Höhlein, et al. 2016; Helbich, Lyuleeva, Ludwig, et al. 2016) As soon as this material is exposed to air and light, it starts to degrade, forming SiO_x (x = 1,2), which is an insulating material. Nevertheless, despite these difficulties, Akinwande *et al.* succeeded in 2015 in building a silicene based field-effect transistor (FET), which was operating even at room-temperature. (Tao et al. 2015) For the first time, it was experimentally proven that silicene exhibits the predicted ambipolar Dirac charge transport (Scalise et al. 2014; Cahangirov et al. 2009; Liu et al. 2011) and a room-temperature mobility of about 100 $cm^2V^{-1}s^{-1}$ attributed to acoustic phonon-limited transport (X. Li et al. 2013) and grain boundary scattering. However, in general, most of the elemental analogues of graphene, such as germanene (Cahangirov et al. 2009; Liu et al. 2011; Ni et al. 2012), phosphorene (Guo et al. 2016; H. Liu et al. 2014), and silicene need to be encapsulated with additional molecules or materials, which requires an additional fabrication step.

Still, due to the allotropic affinity of 2D silicon (Feng et al. 2012) to bulk silicon and the latter's more facile synthesis, which can be carried out at low temperatures, it promises to be a good alternative to current mainstream semiconductor technology.

1.1.1. Non-covalent Surface Modification

As already mentioned, before all these nanomaterials can be incorporated in various device fabrication steps, it is necessary to gain a basic understanding of the interaction mechanism between surfaces and their surrounding molecules. The physics and chemistry, present during the covalent bond formation and non-covalent interaction steps, provide a variety of different ways for reversible and also irreversible attachment of molecules to the surface of the nanomaterials, which will be presented in the following. Either with the help of often relatively weak non-covalent interactions, such as van der Waals bonds, ionic interactions, or hydrogen bond formations; or covalent bonds, which are desired due to their stability, surfaces can be modified. The latter, covalent attachment, is one of the chemically most stable ways of connection, which is based on strong chemical forces. It will be discussed in the next chapter 1.1.2.

Non-covalent modification of the surface is a very facile method to control the properties of the material. It is mainly based on physical forces, where electrons are not shared between participating atoms. There are four principles of non-covalent forces: ionic, hydrophobic, van der Waals interactions and hydrogen bonds. (Lodish et al. 2000) These bonds alone provide only relatively low binding energies. The interaction energies range from 4 to 21 kJ/mol. Nevertheless, with multiple non-covalent bonds good chemical stability can be achieved, without the need of chemical reactions to occur. In ionic interactions, opposite charges can be formed on the involved atoms (Hünenberger & McCammon 1999), which are based on their differences in electronegativity (EN).

Hydrophobic interactions occur as nonpolar bonds between molecules. (Privalov & Gill 1988) The immiscibility of such a molecule in water leads to confined encapsulation, micelles (Kataoka et al. 2001) and highly ordered structures. The drive to avoid any polarity, like the one present in water (H_2O), leads to the self-organization of such molecules, which can be found in *e.g.,* self-assembled layers.

Van der Waals forces represent a very weak interaction between two atoms (or molecules), which come to close proximity. (Dalgarno & Kingston 1959) They create an unspecific attraction (van der Waals attraction), resulting from random fluctuations in the electrons distribution.

Hydrogen bonds are electromagnetic attractive forces between polar, protic molecules. They are a result of a high EN difference between the hydrogen atom (hydrogen bond donor) and an atom such as oxygen or fluorine (hydrogen bond acceptor) to which it is attached. (Lodish et al. 2000) Such a hydrogen atom within a hydrogen bond can also jump between the molecules, which is for example present in the Grotthuss mechanism and was also described by Walbran *et al.* as proton transport in polarizable water, for example. (Walbran & Kornyshev 2001)

With respect to the structure of many monomers and polymers used in (opto)electronic applications, such as polystyrene and poly(3-hexylthiophene) (P3HT), it is further important to mention π-π-stacking, which is presented in Figure 3. It is based on electrostatic interactions of π-electron orbitals with other π-systems, anions, metals or simply other molecules. (Anslyn & Dougherty 2005) It plays an important role in organic thin films, which photovoltaics, or FETs' fabrication is based on. They influence not only the stacking structure and thus molecule order and crystallinity of the material, but also the charge transfer between two different materials, involved in the present composite or blend.

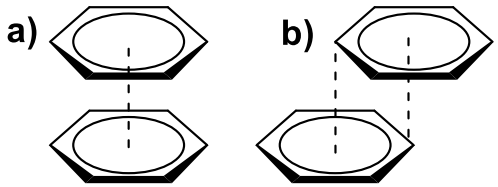

Figure 3: π-π interaction between two systems with delocalized π-electrons. a) Rather unstable sandwich conformation, (maximized overlapping of the π-systems). b) Parallel-displaced conformation, which can be found in e.g., graphite structure.

Physisorption also plays a significant role as a possible surface modification technique. It is based merely on the character of the molecules and the corresponding electron orbitals. (Baum & Brittain 2002; Edmondson et al. 2004) Physisorption can be a very facile method for surface coating and sometimes an important step for subsequent chemical reactions.

In short, the main characteristics of non-covalent modification techniques are their reversibility and the possibility of surface functionalization without its degradation, or introduction of additional defects. Both characteristics are certainly a big advantage for the long-term use of the treated material. Nevertheless, it makes these techniques less reliable, since devices based on these non-covalent modification processes do not possess enough stability to hold against harsh external influences. Thus, further techniques and chemical reactions need to be introduced, which allow stable modification and synthesis of multifunctional hybrid materials *via* covalent bond formation.

1.1.2. Covalent Surface Modification

The bond dissociation energy (BDE) between two carbon atoms is about 347 kJ/mol, which is only surpassed by C-H (410 kJ/mol) and C-F bonds (490 kJ/mol). (Smith & March 2006) Therefore, any molecular structure based on C-C bonds provides a suitable template for stable composites. (Blanksby & Ellison 2003) Because of this, the functionalization of for example *via* chemical vapor deposition (CVD) grown graphene as 2D carbon monolayer (Whitener 2014), or freestanding graphene nanosheets (RamanathanT. et al. 2008), graphene nanotubes (R. Wang et al. 2010), carbon nanotubes (CNTs) (Yan et al. 2007) and also aerographite (Mecklenburg et al. 2012) has been intensively studied during the last decades. However, with the rise of further novel nanomaterials, additional bond formations and synthesis techniques of various hybrid systems have emerged becoming more significant. (Chandiramouli & Nagarajan 2016; Dasog et al. 2013)

The BDE of Si-Si bond is 222 kJ/mol (King 2006), which is lower than C-C bonds. The energy for Si-H bonds (318 kJ/mol) (King 2006), is smaller than C-H bonds, promising an easier cleavage of the bond and subsequent modification of the Si based material surface. This allows less harsh reaction conditions at for example lower temperatures, which is desirable for industrial use. This enables silicon, one of the most prominent elements in industry, to be successfully modified. (Walsh et al. 2005)

Bulk silicon has been modified over decades by several research groups. (Lu et al. 2009; Hu et al. 2001; Islam et al. 2016) The main goal was the functionalization of the silicon surface for interface processes and surface engineering. Buriak *et al.* have shown that Si(100) and Si(111) surfaces are important for various electronic applications. (Buriak 2002) Additionally, both faces possess stability during operation at atmospheric pressures and at high vacuum, while being exposed to different solvents. At the same time, they have the already mentioned high reactivity at the surface, which is desirable for the ease of chemical reactions. This makes them suitable for modification and functionalization reactions with low energy requirements. (Buriak 2002)

Silicon nanocrystals (SiNCs) surfaces are also highly reactive. Thus, going back to the nano-dimensions, but keeping the silicon as our main element, SiNCs have been successfully functionalized with various molecules and their properties controlled. Dasog *et al.* demonstrated a wide range of modification methods for the nanocrystals' surface (Dasog et al. 2016), which allow a precise engineering of their luminescent properties (Figure 4).

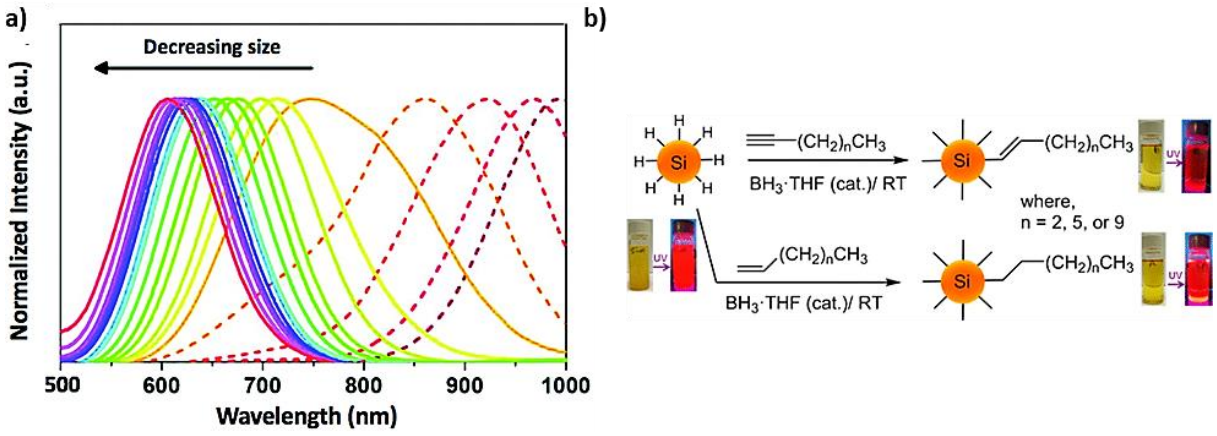

Figure 4: a) PL of SiNCs depending on different sizes of the material. Adapted from Mazarro et al.(Mazzaro et al. 2017) *b) Borane-catalyzed functionalization of SiNCs with alkene and alkenylene molecules. Adapted with permission from Purkait et al.*(Purkait et al. 2014) *Copyright © (2017) American Chemical Society.*

The size of the crystals together with their surface chemistry can influence the stability, solubility and mechanical along with the (opto)electronic properties of the nanomaterial. Not only the well-known radical hydrosilylation reaction can be used for the covalent surface modification, but also *e.g.,* borane-, platinum-catalysed, or even surface self-initiated hydrosilylation reactions were investigated in more detail and proven to be accessible by Veinot *et al.* (Dasog et al. 2016) This modification feature addresses primarily the (opto)electronic industry in connection with the Si-based application as quantum dots. Aside from the (opto)electronic properties, the nanocrystals offer lower toxicity, biocompatibility and possibly simplified incorporation into the existing semiconductor industry infrastructure. (Svrcek et al. 2016; Liu et al. 2009) With the ability to control the wavelength of the emitted light from excited SiNCs, light emitting diodes (LEDs) (Qian et al. 2011; Kong et al. 2014) and solar cells (Chuang et al. 2014; Kramer et al. 2015) can be fabricated. These materials can also be used for bio-imaging (Li & Zhu 2013; Kairdolf et al. 2013), lasing (Ledentsov 2011; Huffaker et al. 1998) and sensing purposes.(Yue et al. 2013; McCulloch et al. 2006)

Additionally, silicon nanowires (SiNWs) can be covalently functionalized, as shown in Figure 5. Galvanostatic electrochemical polymerization with thiophene, or pyrrole can be carried out, as Belhousse *et al.* have demonstrated. Furthermore, Liu *et al.* have shown that SiNWs can be also modified with –COOH groups and then even further decorated with porous crystalline materials, such as metal organic frameworks (MOFs) *via* a simple step-by-step growth method at room temperature. (Liu et al. 2012) Also, organic surface modification *via silanization* (de Smet et al. 2011) can be carried out, providing linker groups for further molecule attachment. An example would be the binding of biomolecules, which has been demonstrated by Aswal *et al.* in 2005. (Aswal et al. 2006)

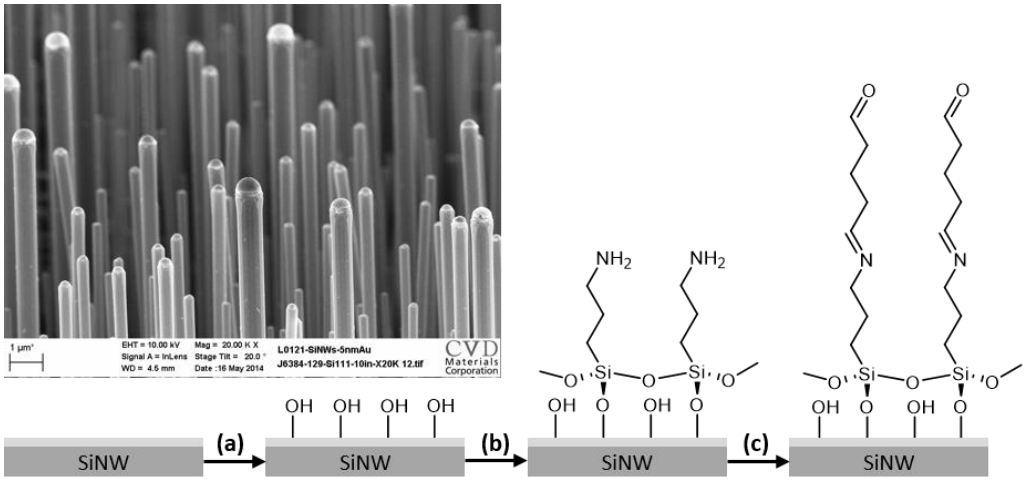

Figure 5: Hydroxylation (a) of the native SiO_x surface present on the SiNW surface, followed by a silanization reaction (b). (c) Additional step of functionalization with glutaraldehyde is presented here as an example for a modification of the surface with various functional groups. (Aswal et al. 2006) *Inset: scanning tunnelling microscope (SEM) image of SiNWs. Adapted with permission from CVD Equipment Corporation (www.cvdequipment.com)*

The 2D silicon monolayer can be also functionalized. The transformation from the nearly planar sp^2-hybridized silicene to the buckled and sp^3-hybridized silicane, also known as hydrogenated silicon nanosheets (SiNS-H), occurs after hydrogenation, forming a fully puckered layer of Si atoms decorated with H. (W. Wang et al. 2016; G Liu, X. L. Lei, et al. 2014) These Si-H bonds can be used for subsequent surface modification. Thus, radical-induced (Helbich, Lyuleeva, Höhlein, et al. 2016; Helbich, Lyuleeva, Ludwig, et al. 2016), or Pt-catalysed hydrosilylation reactions can be carried out (Nakano et al. 2012) with unsaturated compounds, providing both: protection from degradation and adjustment of the physical properties of the nanomaterial. Hydrogenated silicene (silicane) is predicted to have a non-zero band gap (Buscema et al. 2015), which can theoretically be adjusted *via*: surface functionalization (Oscar D Restrepo et al. 2014; Buscema et al. 2015; Zheng & Zhang 2012; Osborn et al. 2011), physical strain (F. Li et al. 2013), the influence of the substrate (Niu et al. 2014), or external electrical fields (Ni et al. 2014). This is one of the most fundamental advantages of silicanes over silicene and graphene. These SiNSs show consistent green photoluminescence (PL) at 510 nm (Helbich, Lyuleeva, Höhlein, et al. 2016). Additionally, it is predicted to exhibit outstanding electronic properties, according to theoretical calculations (Zheng & Zhang 2012; Nakano et al. 2006; Wu et al. 2014; Wei & Jacob 2013)

The functionalization can be used to control physical properties of the material for the desired application. However, successful functionalization also protects the treated nanomaterial and thus preserves its intrinsic properties for further use. The synthesis of hybrid materials and composites, as well as the fabrication of mixtures/blends enables facile treatment during the subsequent device fabrication steps. For the fabrication, the features of the embedding compound in the composite (Tobias Helbich et al. 2017), of the polymer in the blend (Helbich, Lyuleeva, Ludwig, et al. 2016) or the

molecule on the surface (Helbich, Lyuleeva, Höhlein, et al. 2016) can be used, which can be covalently, or non-covalently bound. As a result, *e.g.,* the melting temperature of the composite (due to the polymer, such as SiNS-polymer@polymer), the solubility of the blend (*e.g.,* SiNS-R/P3HT), or the homogeneity of the hybrid materials in general and with it the interaction of the sheets within the polymer can be achieved. This use of both materials properties is a valuable tool and a benefit for subsequent improvement of the device performance.

Hydrophobic and hydrophilic SINSs can be dispersed and used for further treatment and fabrication steps. Additionally, controlled dispersibility in various liquid environments ensures reproducibility during already well-known and established fabrication techniques, such as spray- (Abdellah & Abdelhalim 2013), spin- (Melzer et al. 2014), or dip-coating. (Harun et al. 2012) With these techniques, ordered structures and thin films can be prepared using dissolved, or dispersed composites/blends. (Xie et al. 2016) Inkjet printing is another powerful and easily accessible method, which enables access to a variety of patterns. These patterning techniques are applicable for sensing areas of the device and for electrodes printing. (Fiori et al. 2014; Torrisi et al. 2012)

Additionally, this fabrication technology can be applied to a number of various supporting substrates. Various substrates can be chosen for the device preparation, since these methods allow not only the treatment of rigid, but also uneven, flexible and deformable surfaces. This enables the fabrication of "wearables", such as on-skin electronics (Miyamoto et al. 2017; Yokota et al. 2016) and smart tattoos (Kao et al. 2016) which have become the subject of intense investigation. The ability to print conductive materials on skin, stretchable plastics, wires of cloths and even contact lenses requires high accuracy. (Stoppa & Chiolerio 2014) The primary basis for this utilizes a well-dispersed nanomaterial in a solvent, which can be easily and rapidly evaporated. However, it is important that these nanomaterials are biocompatible. (Ray et al. 2009)

As a result, these advances in sample preparation have led to the fabrication of new transistors (Gao et al. 2012; Oscar D. Restrepo, Mishra, et al. 2014), photodetectors (Koski & Cui 2013), photovoltaic solar cells (Okamoto et al. 2011) and lithium-ion batteries. (Kumai, Shirai, et al. 2011; Kumai, Kadoura, et al. 2011; Kumai & Nakano 2015)

1.2. THE RISE OF 2D SILICON NANOMATERIALS: SILICENE & SILICANE

1.2.1. Silicene – From Synthesis to Application

This work concentrates on silicon in its 2D form, which will be described and analyzed for (opto)electronic device application. Freestanding silicon nanosheets (SiNSs) represent one of the 2D form of silicon-based materials, while being only one atom layer thick. As already mentioned, 2D silicon was first mentioned by Takeda and Shiraishi in 1994 (Takeda & Shiraishi 1994) and then got forgotten for more than 10 years, until it was reinvestigated using theoretical studies by Guzmann-Verri *et al.* (Guzmán-Verri & Lew Yan Voon 2007) As they were able to show with a tight-binding Hamiltonian, silicene is expected to be a semi-metal. Once again, it is built of a sp^2-hybridized nearly planar monolayer of honeycomb structured silicon atoms, has a zero-band gap and additionally, the presence of Dirac cones has been for the first time demonstrated in 2007. (Guzmán-Verri & Lew Yan Voon 2007) Furthermore, it has an ambipolar Dirac charge transport, which was theoretically predicted by Kim *et al.* in 2009. (Kim et al. 2009)

However, without an experimental evidence of this so-called “new cousin of graphene” (Le Lay et al. 2016), the fundamental studies around it reached an impasse. After the first synthesis of silicon nanoribbons on a silver substrate Ag (110) using an ultrahigh vacuum deposition technique in 2009 (Kara et al. 2009), the successful synthesis of silicene on Ag (111) was shown. (Vogt et al. 2012; Lin et al. 2012; Feng et al. 2012; Chiappe et al. 2012) Additionally, silicene could also be considered for transparent and flexible electronics, as it is a monolayered material. Thus, the long-awaited first experimental success was achieved by Tao *et al.*, who proved the outstanding physical properties of silicene, after building the first silicene based FET in 2015. (Tao et al. 2015)

Nevertheless, to realize stable reliable application, the drawbacks need to be overcome, such as the already mentioned stability of the material. The Nobel laureate Roald Hoffmann has stated: “I don’t often say something categorical, but I will say that a pristine free-standing single layer sheet of silicene (or a Si nanotube) will not be made. Silicene exists and will be made only on a support of some sort, metal or semiconductor”. (Hoffmann 2004) So far, his prediction has not been proven wrong.

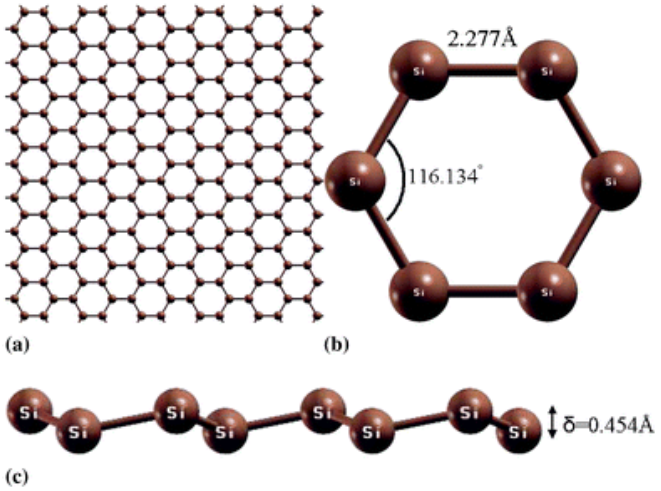

Figure 6: (a) Silicene plane image showing a honeycomb mesh of silicon atoms. Top-view (b) on a Si six-ring with lattice parameters and side-view (c) of a low-buckled silicon monolayer with a buckling height. Adapted from Peng et al. (Peng et al. 2013) *with permission of The Royal Society of Chemistry.*

The crystallographic thickness of silicene is 0.16 nm, as it was calculated from the atomic architecture. The experimentally measured thickness by H. Nakano (Nakano 2014), using atomic force microscopy (AFM) surface analysis technique, shows single layer thickness of about 0.4 nm. This difference to the theoretically predicted thickness is explained with the oxygen encapsulation, which takes place immediately after the material comes into contact with air.

Silicene was grown on rigid, mostly metallic substrates in UHV conditions. Hereby, only inert substrates with a negligible chemical reactivity, such as Ag(111), can be used, which is probably the most studied system, starting with reports in 2012. (Vogt et al. 2012; Grazianetti et al. 2016) The influence of the substrate is important, as it turns out to be an effective method to manipulate and thus shift the band gap of the as grown material. (Guo et al. 2015; Cahangirov et al. 2013; Guo et al. 2013) So far, aside from the already mentioned Ag support (Vogt et al. 2012; Lin et al. 2012), many substrates have been investigated for the experimental growth of silicene, such as ZrB_2 (Fleurence et al. 2012), Ir (Meng et al. 2013) and MoS_2 (Chiappe et al. 2014). In general, the influence of the substrates is strong enough to destroy the Dirac nature of monolayered materials (Spencer 2016), which needs to be prevented in the future and has been succesfully accomplished with the previously mentioned fabrication of the silicene based FET. (Tao et al. 2015) In their study, the silicon monolayer is covered by AlO_2 thin film and delaminated from the surface it was grown on, to get rid of the substrate's destructive influence. While measurements could be carried out, the material was still not stable enough for long-term operation of the device. This allows both, the advantages of the semiconducting properties of the nanomaterial and the initiated charge transitions between the valence and conductance bands with possible subsequent photon generations.

1.2.2. Silicane – Hydrogenated Silicon Monolayer as a Novel Representative of an sp^3-Hybridized Freestanding 2D Silicon

The decoration of silicene with hydrogen atoms leads to a transformation of the sp^2-hybridized monolayered material towards sp^3-hybridization, as shown in Figure 7. (W. Wang et al. 2016) Being fully hydrogenized, this new representative of a silicon-based 2D material, called silicane, can be suitable for the integration into novel electronics. It is predicted to have the preferable and thus more stable chair-like, or boat-like confirmation. (Trivedi et al. 2014) Nevertheless, it needs to be protected from ambient conditions as well. (Helbich, Lyuleeva, Höhlein, et al. 2016) The surface Si-H bonds can be used for the functionalization (Sugiyama, Okamoto, Mitsuoka, et al. 2010; Helbich, Lyuleeva, Höhlein, et al. 2016; Helbich, Lyuleeva, Ludwig, et al. 2016; Tobias Helbich et al. 2017) of the nanomaterial in the same way as the surface defects, which are present in graphene and were used for the immobilization for enzymes. (Hess et al. 2014)

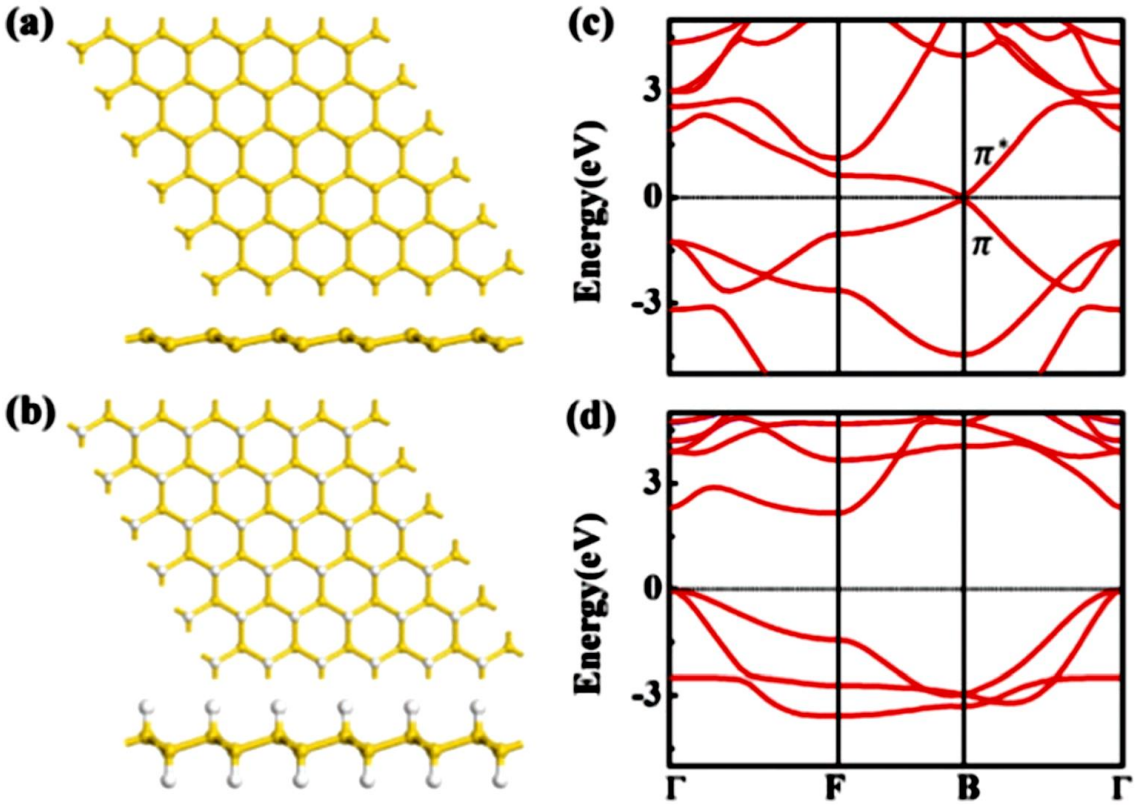

Figure 7: Sketch of the optimized geometric structures (top-view and side-view, H = white balls, Si = golden balls) for silicene (a) and silicane (b). Calculated band structures for silicene (c) with a zero-band gap and silicane (d) with an indirect band gap at the Γ point of 2.18 eV. Adapted from Li et al. (Li et al. 2017) *with permission of The Royal Society of Chemistry.*

The structural and electronic properties of silicane were first examined by Voon *et al.* in 2010 using the ab-initio density functional theory (DFT) computations. (Lew Yan Voon et al. 2010) It is predicted to have a non-zero band gap (Buscema et al. 2015), which should be adjustable *via* surface functionalization (Oscar D Restrepo et al. 2014; Buscema et al. 2015; Zheng & Zhang 2012; Osborn et al. 2011; Syaputra et al. 2015), physical strain (F. Li et al. 2013), the influence of the substrate (Niu et al. 2014; Zhang et al. 2014), and/or external electrical fields (Ni et al. 2014). As already stated, this is one of the most fundamental advantages of silicanes over the planar graphene and silicene. (Mohan et al. 2015) Furthermore, this nanomaterial shows green photoluminescence (PL) at 510 nm (Helbich, Lyuleeva, Höhlein, et al. 2016) and should also exhibit promising electronic properties according to theoretical calculations. (Zheng & Zhang 2012; Nakano et al. 2006; Wu et al. 2014; Wei & Jacob 2013) Upon hydrogenation, the buckling constant of the monolayered silicon increases from 0.45 Å to 0.72 Å, where the theoretical predictions show that the chair-like configuration is more energetically favored than the boat conformation. (Lew Yan Voon et al. 2010; Zhang et al. 2012) Upon hydrogenation the band gap is predicted to become indirect, with an energy of 2 - 3 eV, dependent on the calculation parameters (Table 1).

Table 1: Hydrogenated silicon monolayered material with calculated band gaps and configurations. Adapted from Spencer et al. (Spencer 2016)

Year	Author	Band gap (eV)	Direct/Indirect	Conformation
2010	Voon *et al.* (Lew Yan Voon et al. 2010)	≈ 2.0	indirect	chair-like
2011	Guzmán-Veri (Guzmán-Verri & Lew Yan Voon 2011)	2.2	indirect	-
2012	Zhang *et al.* (Zhang et al. 2012)	2.36/1.6	indirect/direct	chair-like/boat-like
2015	Wang *et al.* (R. Wang et al. 2015)	2.2	indirect	chair-like
2015	Rupp *et al.* (Rupp et al. 2015)	2.94	indirect	chair-like

For example, Trivedi *et al.* calculated an indirect band gap of around 2.3 eV for the 2D silicon after hydrogenation. (Trivedi et al. 2014) This step turns silicene to an indirect band gap semiconducting silicane. Li *et al.* predicted the band gap for layered polysilane monolayer to be 2.18 eV, as shown in Figure 7. (Li et al. 2017)

At the same time, Houssa *et al.* have shown in their DFT based calculations the possibility for both: boat- and chair-like configurations. Whereby, the chair configuration has an indirect band gap and the boat configuration of the material possesses a direct band gap. (Houssa et al. 2011) Although the indirect band gap is one of the main disadvantages of the material, it can still be used as an optically active nanomaterial, if the band gap is controlled and shifted. Huang *et al.* have shown that with the use of bilayer silicane, the band gap can be turned into a direct, or quasi-direct one with a promising application in LED industry. (Huang et al. 2013)

2. METHODS AND FABRICATION TECHNIQUES

2.1. GENERAL INFORMATION

All reactants and reagents were purchased from Sigma-Aldrich, Alfa Aesar or Wacker and used without further purification, if not stated otherwise. Toluene was dried prior to use with an *MBraun* solvent purification system *MB SPS-800* whereby argon 4.8 (99.998 %, *Westfalen AG*) was used as inert gas. Acetone was dried over molecular sieve, degassed *via* 3 freeze-pump-thaw cycles and stored under argon. For storage, the exfoliated SiNSs were placed in a glove box with argon 4.8 (99.998 %, *Westfalen AG*). Air or water sensitive reactions were executed under standard Schlenk techniques. The SiNS-substrate@polymer nanocomposites were compounded in a *MicroCompounder* (*DACA Instruments*). For oxygen and argon plasma, *Femto low-pressure plasma system* (plasma cleaner) was used with continuously adjustable radiofrequency generator (13.56 MHz; 0 - 300 W).

FTIR spectra were measured with a *Bruker Vertex 70 FTIR* using a *Platinum ATR* from *Bruker*. **TGA** measurements were executed with a *DSC 3+ Star system* from *Mettler Toledo* with heating rates of 10 K/min and nitrogen flow rates of 10 mL/min. **AFM** measurements (contact mode, *Asylum Research MFP-3D AFM* with an ARC controller) were performed after spin-coating (1500 rpm, 90 s) of the polymer and the blends, or drop/dip-coating on Si/SiO_2 substrates. **SEM** images were recorded with a *NVision 40* from *Carl Zeiss* (Germany) using an acceleration voltage of 1.0 kV beam energy.

2.2. SYNTHESIS AND FUNCTIONALIZATION OF SINSS

2.2.1. Synthesis of Silicane

In an argon atmosphere a mixture of calcium (Alfa Aesar, 99.5%) and silicon (Wacker, 99.99%) was pressed to a pellet and melted in an arc furnace. The chemical exfoliation was performed as published by Helbich *et al.* (Helbich, Lyuleeva, Höhlein, et al. 2016): $HCl_{conc.}$ (100 mL) was cooled in a Schlenk flask to -25 °C and $CaSi_2$ (1.00 g) was added under Ar. The reaction was carried out for 7 d at -25 °C. The resulting suspension was filtered under Schlenk conditions through a glass frit. The yellow residue was washed with degassed acetone and dried under vacuum. The obtained $(Si_6H_6)_n$ were stored under Ar atmosphere until further use.

2.2.2. Etching of Silicon Nanosheets (Helbich, Lyuleeva, Höhlein, et al. 2016)

In ethanol dispersed $(Si_6H_6)_n$ (0.090 g) were placed in an ultrasonic bath for 2 min. Water (2 mL) and aqueous $HF_{conc.}$(0.25 mL) were added and extracted with dichloromethane (3 × 5 mL) into PTFE

centrifuge tubes. Toluene (40 mL) was added to the dispersion, which was subsequently centrifuged (9000 rpm, 4 min). The SiNSs on the bottom of the tube were re-dispersed in acetone (2 mL) and centrifuged again. After washing with toluene (2 mL) and last centrifugation, the SiNSs were dispersed in toluene (for ThAc) or the neat substrate (for PhAc, 1-dodecene, ^{t}BMA) for further reactions.

2.2.3. Functionalization of SiNSs in the Microwave-reactor System

Reaction of SiNSs with dodecene and phenylacetylene was achieved in Schlenk conditions *via* mixing SiNSs with the substrate (2.5 mL) in a microwave (MW) tube. The used MW reactor was a *Discover-S* from *CEM* and was controlled by the software *Synergy 1.58.* The degassed (three times *via* freeze-pump-thaw) dispersion in a vessel was transferred into the MW reactor. After MW irradiation (2 h, 180 °C, no further cooling) with a different MW powers of up to 300 W, the mixture was transferred into a sealed PTFE centrifuge tube with Ar and centrifuged (9000 rpm, 4 min). The functionalized SiNSs were washed (3 x degassed acetonitrile$_{dry}$ (3 mL) and toluene (0.5 mL)) and centrifuged (9000 rpm, 4 min) again. After the dispersion of the SiNS-substrate in Et_2O, the product was dried under reduced pressure. For the functionalization with phenylacetylene (PhAc), the solid side product was dissolved in toluene and removed (*vide infra*). For the functionalization with 2-ethinyl-3-hexylthiophene (ThAc), the SiNSs were dispersed in toluene (2 mL) and the substrate (0.5 mL). For the alkyne functionalization, the cleaning step was extended by three washing steps with acetonitrile. SiNS-$C_{12}H_{25}$ (SiNS-Dodecene) was synthesized as yellow, SiNS-PhAc (SiNS-styrenyl) as orange-yellow and SiNS-ThAc (SiNS-thiopheneacethylene) as brown-bronze nanomaterial.

2.2.4. Functionalization of SiNS for humidity sensors:

The dispersion of SiNS-H in degassed toluene$_{dry}$ (12 mL, corresponds to 88 mg $(Si_6H_6)_n$) was mixed in a *Schlenk* tube with the monomer ^{t}BMA (3.3 g, 3 wt% of exfoliated $(Si_6H_6)_n$). The dispersion was degassed (3x freeze-pump-thaw cycles) and AIBN (20 mg) added to the mixture. After stirring for 16 h at 70 °C, the reaction mixture was diluted and centrifuged (9000 rpm, 4 min). The hybrid material was re-dispersed (3x) in toluene (0.5 mL), centrifuged and isolated by freeze-drying from benzene. FTIR spectroscopy measurements were taken after drop-deposition of the material on the target substrate.

2.2.5. Hydrolyzation reaction of ^{t}BMA functional groups for humidity sensor

After the functionalization with the *tert*-butyl group, the protecting group (*tert*-butyl) was removed by acid induced hydrolyzation reaction. The functionalized SiNS-^{t}BMA were dispersed in dichloromethane (2 mL) and trifluoromethansulfonic acid (5 drops) were added. The reaction mixture was stirred in the dark (20 min) and centrifuged after washing with toluene (5 mL). After removal of the centrifugate, the SiNSs residue was dispersed in ethanol (5 mL). Then, toluene (20 mL) was added and the suspension centrifuged again (9000 rpm, 4 min). The purified SiNSs were dispersed in ethanol

for further use. FTIR spectroscopy measurements were taken after drop-deposition of the material on the target substrate.

2.2.6. AIBN-initiated radical-induced functionalization reaction of SiNS-substrate@polymer

A dispersion of SiNS-H (corresponding to 0.088 g exfoliated $(Si_6H_6)_n$) in degassed $toluene_{dry}$ (or ethanol for AA) (12 mL) were mixed with 3 wt% (with regard to compound before etching) of the exfoliated $(Si_6H_6)_n$ substrate (3.30 g) in a Schlenk tube. AIBN (0.020 g) was added after degassing *(*3x freeze thaw pump cycles) and the reaction mixture stirred at 70 °C for 16 h.

For the isolation of SiNS-substrate@polymer, the reaction mixture was centrifuged (2 min, 9000 rpm) after precipitation in methanol (or toluene in the case of PAA). The solid was re-dispersed (2×), precipitated, and isolated by freeze-drying from benzene (or water in the case of SiNS-PAA@PAA).

For the isolation of SiNS-substrate, the reaction mixture was diluted and centrifuged (2 min, 9000 rpm), re-dispersed (3×) in the reaction solvent (0.5 mL), centrifuged, and freeze dried from benzene (or water for SiNS-PAA). Table 2 summarizes the materials used in the reaction.

Table 2: Substrates, which were used for the radical induced reactions and the corresponding solvents.

substrate	*M* *(g·mol^{-1})*	*m* *(g)*	*N* *(mmol)*	*solvent for reaction*	*solvent for precipitation*	*solvent for freeze drying*
styrene	*104.06*	*0.500*	*4.80*	*toluene*	*methanol*	*benzene*
MMA	*100.05*		*5.00*			
AA	*72.02*		*6.94*	*ethanol*	*toluene*	*water*

2.3. Photolithography and Metal Evaporation for Interdigital (IDE) Structure Patterning

The substrate (Si^{++}/SiO_2 wafer, or Kapton with 75 µm thickness) was cleaned and pre-heated at 110 °C for 2 min. The Photoresist (AZ5214E) was coated on the substrate surface *via* spin-coating deposition technique (100 rpm, 2.8 s; 3000 rpm, 20 s; 1000 rpm, 20 s; 6000 rpm, 6 s). Pre-baking of the photoresist was carried out at 110 °C for 60 s. The coated wafer/Kapton film with the photoresist was then exposed through the mask with the desired integrated finger structure to an Hg-lamp for photoresist

exposure (1.7 s) of the uncovered parts. Reversal baking step of the covered surfaces was carried out on a hotplate at 125 °C (2 min), followed by the flood exposure step with Hg-lamp (> 200 mJ/cm^2, 1 min). The treated thin-film on the substrate was exposed to a developer solution (AZ400K : water, 1 : 4, 20-25 s) to remove the soluble parts of the photoresist. The resulting structure on substrate is shown in Figure 8, first left image.

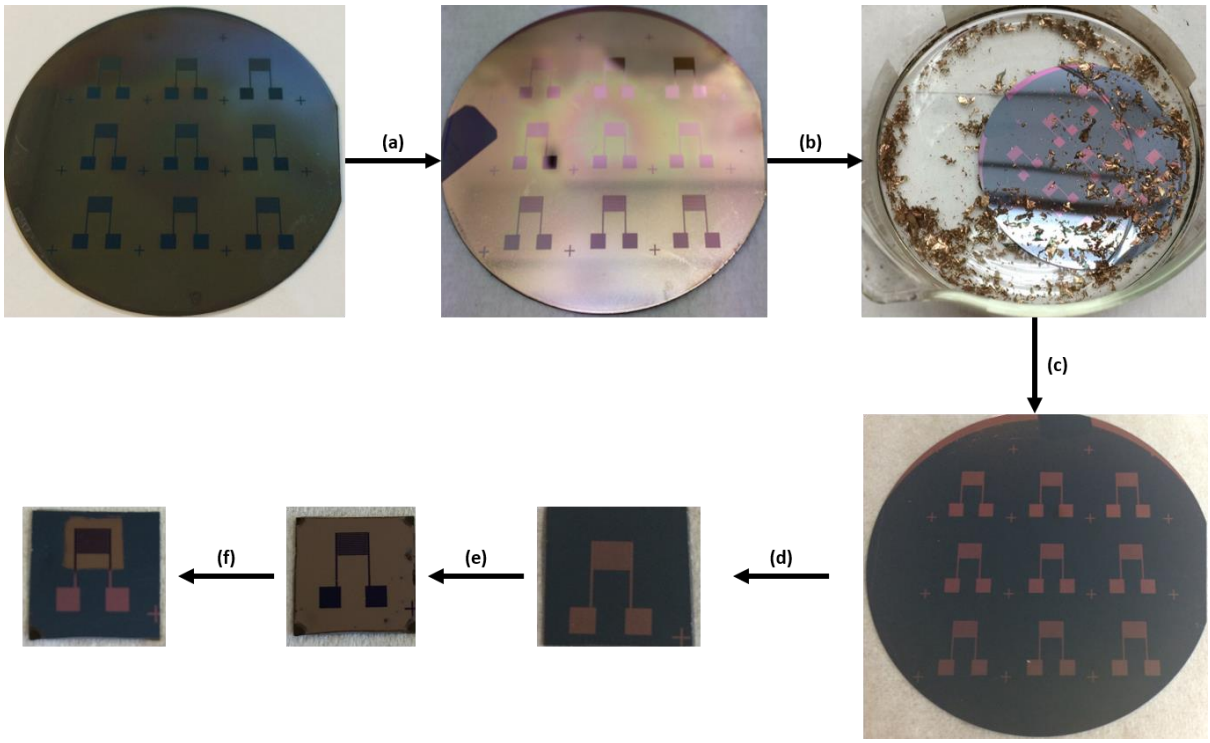

Figure 8: IDE structure patterning on Si^{++}/SiO_2 substrate after photolithography fabrication step. (a) With photo lack prepatterned Si^{++}/SiO_2 surface is placed in an evaporation chamber for subsequent chromium (5 nm) and gold (40 nm) evaporation. (b) Lift-off fabrication step, in which the photo lack with the deposited metals is removed from the surface using acetone and isopropanol. (c) After washing in acetone and isopropanol, the surface is dried resulting in a clean substrate with Cr/Au pattern. (d) Cutting of the substrate in adjusted sizes of the sample (ca. 1 x 1 cm). (e) Deposition of the polymer P3HT, or the SiNS-substrate/P3HT blend via spin-coating. (f) Removing of the polymer, or the blend from the contact areas with acetone.

Using metal vapor deposition technique, chrome (5 nm) and gold (40 nm) metals were evaporated on the substrate at high vacuum conditions (Figure 8a). During the Lift-off procedure (Figure 8b) the parts with Cr/Au metals on the photoresist were washed off and the desired Cr/Au pattern of the finger structure with source and drain elements (5 nm chromium, 40 nm gold, channel length 50 mm, W/L ¼ 900) remained on the substrate. Subsequent cleaning and treatment with argon plasma (0.4 bar, 70%, 5 min) and subsequently oxygen plasma (0.3 bar, 50%, 60 s) were carried out (Figure 8c). The substrate was cut into samples with desired sizes for further use (Figure 8d). The quality of the pattern structures was examined under an optical microscope.

2.4. SGFET FABRICATION AND CHARACTERIZATION

2.4.1. SGFET fabrication:

P3HT was dissolved in a chosen solvent (*1,2,*-dichlorobenzene, Figure 9a) and stirred overnight at 60 °C in a glovebox. The functionalized SiNSs (specific wt% of the P3HT-solution, Figure 9b) were dispersed in the dissolved P3HT polymer.

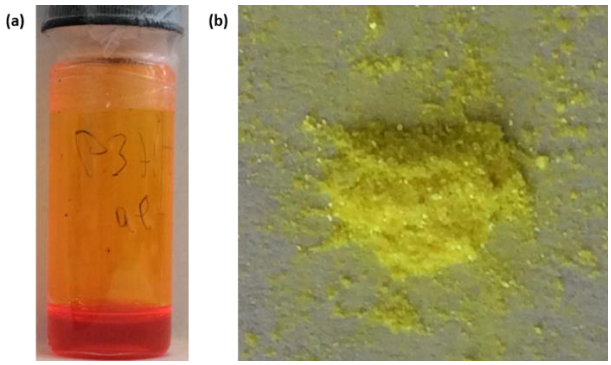

Figure 9: (a) Image of the semiconducting polymer P3HT dissolved in 1,2-DCB. (b) SiNS-$C_{12}H_{25}$ powder after freeze-drying from benzene.

A drop of the prepared dispersions of P3HT and SiNS-substrate/P3HT blends was placed on the middle of the pre-patterned and pre-cut Si^{++}/SiO_2 wafer or Kapton (polyimide, Figure 10 (a)) and spin coated (1500 rpm, 90 s). Subsequently, it was annealed at 120 °C for 10 min (Figure 8e). The resulting polymer and blend films (Figure 10 (b)) were approximately 50 to 70 nm thick.

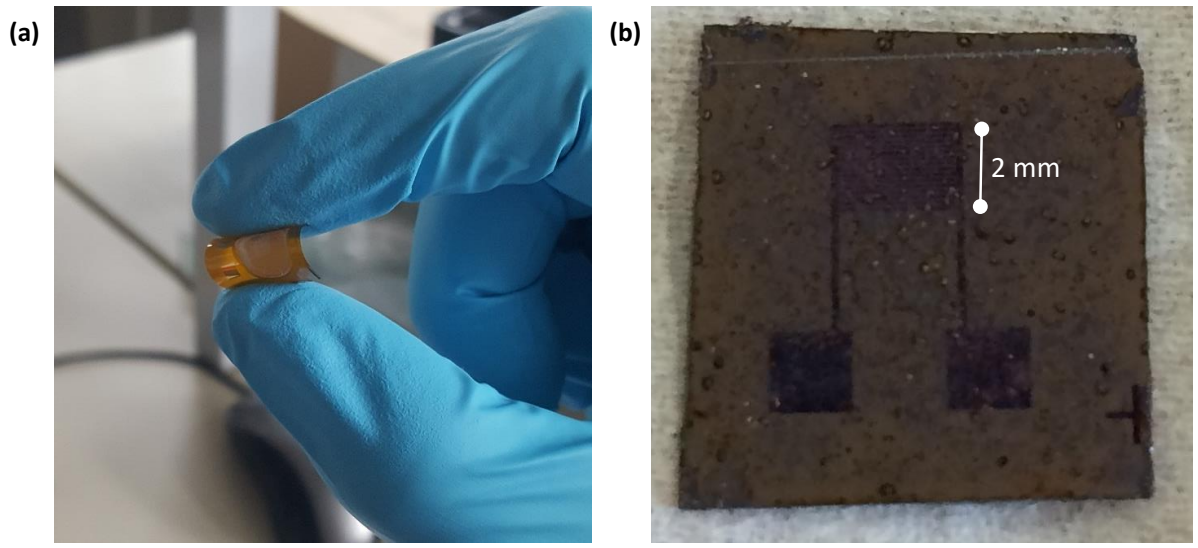

Figure 10: (a) Flexible Kapton foil with the pre-patterned IDE structure and the drop-deposited functionalized SiNSs. (b) With SiNS-$C_{12}H_{25}$/P3HT coated SI^{++}/SiO_2 surface, the IDE structure with the thin film on top of it is visible with bar eyes.

2.4.2. Electrical Characterization

Electrical characterization of the fabricated devices was carried out using a *Keithley* source meter (*System 2636A*).

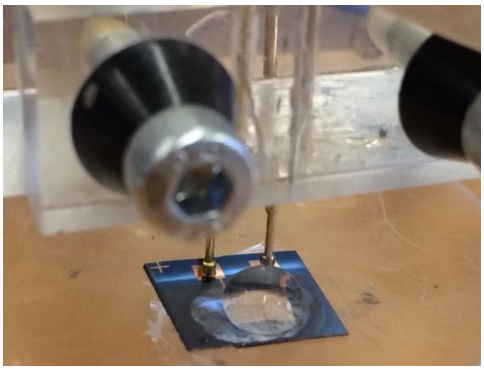

Figure 11: Image of an IDE structure on Si^{++}/SiO_2 substrate contacted by Au electrodes. Functionalized SiNSs from toluene solution are drop-deposited on the surface and a water droplet placed on top.

The thin film was removed from the source and the drain contact areas, which is shown in Figure 8f. The Au electrodes of the set-up were connected to the source and the drain parts of the patterned IDE structure (IDES) and one drop of deionized water is placed onto the IDES area, which is shown in Figure 11. With the measurement apparatus contacted Pt-wire was dipped into the liquid, connecting the semiconductor surface and the gate electrode (Figure 12). The measurements were carried out under an aluminum cover to ensure constant measurement in dark conditions.

Transfer curves of drain current (I_D) *vs.* gate voltage (V_G), (drain voltage V_D = constant) were recorded at different gate voltages (V_G). Gate potential was applied to the Pt-gate-electrode, immersed in freshly prepared deionized water varying between V_G = 0.8 V and -0.8 V with a sweep rate of 0.001 Vs^{-1}. For the output curves I_D was recorded at different V_D from -0.8 V to 0.8 V at constant V_G values (V_G = -0.8 V to 0.8 V in 0.2 V steps). The Figure 12 shows images of the SGFET measurement setup from the top (Figure 12b) and the side view (Figure 12a).

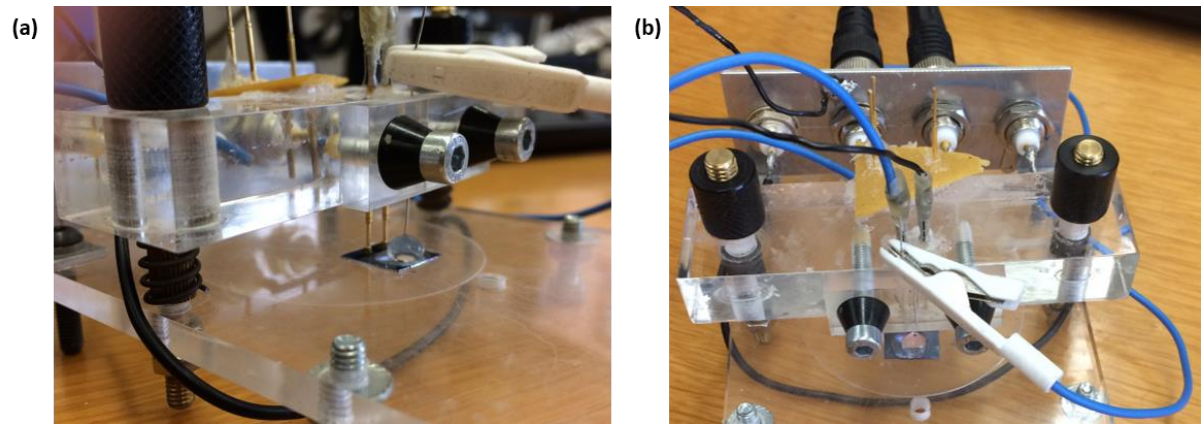

Figure 12: SGFET measurement set-up from the side (a) and the top (b) view. The Au contacts of the IDE structure are physically and electrically connected to the source and the drain electrodes (Au) of the current measurement set-up. The gate is a Pt-wire, which is in contact with the water droplet on the top of the sensitive surface on the "finger-pattern" of the IDE structure. It is physically and electrically connected to the potentiostat via an electrical clamp.

2.4.3. Electron Paramagnetic Resonance (EPR) studies

The measurements were carried out at temperatures of T = 5 K (T = -268.15 °C) in a *JEOL* continuous wave X-band spectrometer. Lock-in detection with magnetic field modulation at 100 kHz and a helium flow cryostat were used. The g-factor was calibrated using a di(phenyl)-(2,4,6-trinitrophenyl)iminoazanium (DPPH) reference spectrum. The EPR samples for a hybrid thin film were prepared to imitate the SGFET device conditions. P3HT was dissolved in chloroform (1 wt%) and stirred overnight. SiNS-substrate were dispersed in the prepared P3HT solution, achieving a ratio of P3HT : SiNS-substrate with 2 wt% : 1 wt%. The suspended mixture (0.1 mL) was filled into a transparent EPR quartz tube and the solvent removed under reduced pressure at room temperature. The tube was sealed with epoxide glue and measured with the measurement apparatus. All sample preparations were prepared in Ar conditions.

2.5. HUMIDITY SENSOR FABRICATION

2.5.1. Device Fabrication

The procedure of IDE structure (5 nm chromium, 40 nm gold, channel length 50 mm, W/L ¼ 900) patterning is described in chapter 2.3. The Au pre-patterned Si^{++}/SiO_2 and polyimide (Kapton HN, 75 µm thickness) substrates were exposed to Ar plasma (0.4 bar, 70%, 5 min) and then O_2 plasma (0.3 bar, 50%, 60 s). The dispersions of functionalized SiNSs (15 mg in 1 mL toluene) were drop-casted precisely onto the channels area of the IDE structure and dried (125 °C, 10 min) in a glovebox.

2.5.2. Device Characterization

A *SMA* (*SubMiniature* version A) male connector was connected with Ag-paint to the electrodes ends points. The automated (*LabVIEW 2016*) electrical measurements were carried out with control over an impedance analyzer (*Keysight E4990A*) with an impedance probe kit (*4294A1*) for the sensor readout. The excitation voltage applied in all measurements was direct-current voltage (V_{DC} = 0) and alternating current voltage (V_{AC} = 500 mV) in the frequency range from 1 kHz to 10 MHz. A prior calibration was carried out to compensate the parasitic elements. The sensor was placed in a climatic chamber (*VLC4006*) with temperature and humidity control. The monitoring was performed over the climatic chamber sensor system. For the RH sensing, the moisture content was ramped up in 10% steps and held for 1 h to ensure a stable value in the whole chamber volume. Similar approach accounts for the temperature sensing with 5 °C steps for 1 h.

2.6. PHOTONIC SENSOR FABRICATION

2.6.1. SiNS-substrate@polymer Sensor Analysis and Fabrication

For the photonic sensor fabrication, the dispersion of SiNS-^{t}BMA (30 mg) in toluene$_{dry}$ (2 mL) was drop-deposited onto pre-patterned Au/Cr contacts (40/5 nm) on Si^{++}/SiO_2 substrate in a glovebox. Prior to that, the surface was cleaned with Ar plasma (0.3 mbar, 70% power, 1 min). The deposited material was dried at 115 °C for 10 min.

The SiNS-substrate@polymer nanocomposites were compounded in a *MicroCompounder* (*DACA Instruments*) at 100 rpm and 220 °C under N_2 atmosphere. The composite was cut into small pieces, placed and melted on top of the area of the surface with already deposited SiNS-^{t}BMA material, while heating at 125 °C. The SiNS-X@Polymer was pressed onto the surface. The device was allowed to cool very slowly to room temperature immediately after deposition.

For AFM Analysis of the SiNS-^{t}BMA hybrid material, spray-coating was performed with an air atomizing nozzle from a commercially available air brush (*Gabbert Triplex*). The dispersed material was sprayed onto the substrate, which was heated on a hotplate during the deposition. The deposited material was then analyzed with AFM tapping mode technique.

2.6.2. Electrical Device Characterization

I_D (A) *vs.* time *t* (ms) measurements were recorded at constant drain (transfer characteristics) and gate (output characteristics) voltages (V_G = 1 V, 1.2 V, …, 2 V) using a source meter (*Keithley model 2636A*).

Output curves (I_{SD} *vs.* V_D) were taken by sweeping V_D = −5 V to 5 V. The device was illuminated with a commercially available energy-saving lamp (9 W, 2500 K, 50 - 60 Hz, 60% light in 100 s).

2.7. MATERIAL PREPARATION FOR THE TIPL AND TRPL MEASUREMENTS

2.7.1. Measurements in solution

The material in solid state (SiNS-substrate powder, or SiNS-substrate@polymer composite) is dispersed in $toluene_{dry}$ and transferred in a sealed quartz cuvette. The dispersion is reset *via* shaking of the cuvette before each new measurement, except PL *vs.* time studies.

2.7.2. Measurements in solid state

The material (ca. 500 µm thickness) is drop-casted from toluene dispersion on a non-fluorescent glass plate (1 mm thickness). The measurements of the composites are carried out after melting (125 °C) the SiNS-substrate@polymer on a non-fluorescent glass substrate.

2.8. TIME-INTEGRATED PL (TIPL) AND TIME-RESOLVED PL (TRPL) MEASUREMENTS

The measurements were carried out within the ATUMS collaboration at the University of Alberta in Edmonton (Canada) together with the group of Prof. Frank Hegmann. SiNSs-substrate in the corresponding solvent was transferred into a cuvette and measured at room temperature.

For the samples in solid state, the UV-fused quartz glass with drop-deposited material was placed on the copper finger with a whole in the middle of an optical microscopy cryostat (*Cryo Industries*) and measured in ambient conditions. Then it was measured in vacuum ($p = 2.2 \times 10^{-7}$ mbar). Then, the cryostat with the sample was cooled by free-flowing liquid nitrogen (LN_2) with the aid of a temperature controller (*Lakeshore 335*) and the data recorded in 10 °C steps. Low temperature compatible *Apeizon* grease was used to adhere the edges of the quartz glass onto the copper sample holder. An 800 nm Ti:Sapphire ultrafast laser (*Coherent RegA 900*) with 65 fs pulse width and 250 kHz repetition rate was used to optically excite the samples at 400 nm *via* second harmonic signal generation from a *BBO* crystal. All measurements were carried out at an average of 435 ± 5 µW excitation power. The PL was collected by an objective (20x *Mitutoyi M Plan Apo*) and filtered by a 435 nm long pass filter (*Edmund Optics*). The TIPL was measured for 0.5 seconds by a CCD (*Princeton Instruments Acton Spectrometer*) with a resolution of ± 1.28 nm at 200 µm slit. For the nanosecond timescale TRPL, a time-correlated single photon counting (TCSPC) technique was employed, which consists of a single-photon avalanche

photodiode connected to a TCSPC module (*PicoHarp 300, Picoquant*). The instrument response, determined from the convolution fit to Gaussian function, provides a time resolution of 35 ± 1 ps, where $g(t)=G \times exp\left(-\frac{4ln(2)\cdot(t-t_0)^2}{w^2}\right)$ and *f(t)* are the Gaussian and inverse power law functions, respectively. The convolution $(f*g)(t)=\int f(t-\tau)\, g(\tau)\, d\tau$ provides the width of the Gaussian, *w*, corresponding to the width of the instrument's impulse response.

During the TRPL measurements, low probability of registering more than one photon per cycle must be maintained. For that, number of counts that is less than 10% of the laser repetition rate (25 kHz) is kept constant in order to maintain a relative statistical error of less than σ = 10%. (Prasankumar & Taylor 2011) Counts per min of less than 10,000 were maintained. The samples were cooled for at least 10 min before each TRPL measurement. The TRPL data were fitted from 0.1 ns to prevent contribution of the instrument response, until the baseline which is the average of the dark counts. For measurements of the µs lifetime component, a Si-avalanche photodetector (*Thorlabs APD130A*, 20 ns time resolution) and a fast oscilloscope (*Tektronix DPO 2024B*, 200 MHz) were used instead.

2.9. TRANSMITTANCE MEASUREMENTS

The External Quantum Efficiency (EQE) is measured, using a xenon arc lamp (300 W, 77 Hz) chopped at 77 Hz through an *Oriel Cornerstone 260 ¼ m* monochromator (*Newport Corporation, Irvine, CA, USA*) and an *Oriel Merlin* digital lock-in amplifier (*Newport Corporation, Irvine, CA, USA*).

3. Results and Discussion

3.1. Synthesis, Functionalization and Characterization

The synthesis of freestanding silicane (SiNSs) is mainly carried out *via* chemical exfoliation starting from the Zintl-phase calcium disilicide ($CaSi_2$). (Nakano et al. 2006) The product after the soft chemical deintercalation of calcium atoms can be the layered polysilane (Si_6H_6) and siloxene ($Si_6H_3(OH)_3$) (Dahn et al. 1993), depending on the reaction conditions. Both materials have a backbone of puckered silicon 2D layers similar to the (111) planes of the bulk silicon. (P. Wang et al. 2016) The slightly buckled Si layers are separated by Ca^{2+} planar monolayers (Figure 13a).

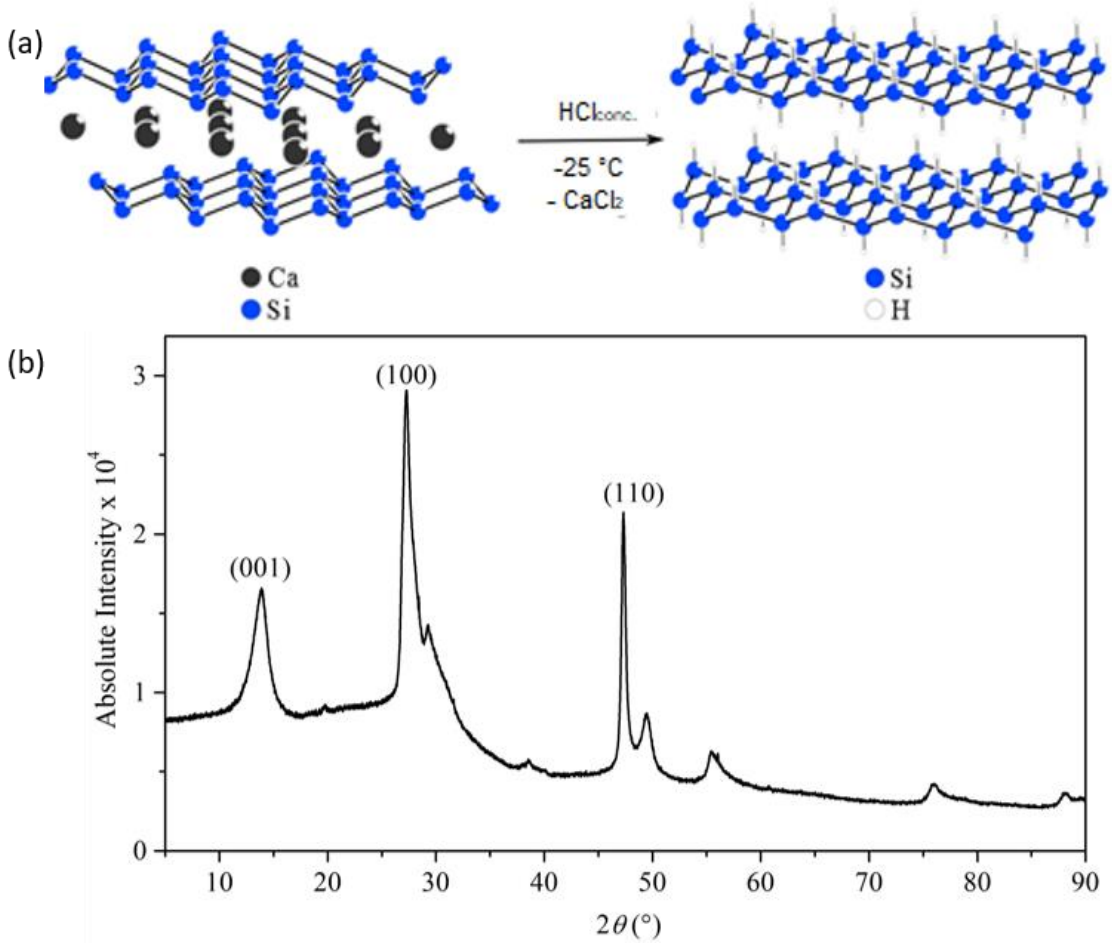

Figure 13: (a) Synthesis of 2D layered polysilane (silicane) from $CaSi_2$ with $HCl_{conc.}$ at -25°C. (b) X-ray powder diffraction pattern of freshly synthesized SiNSs showing (001), (100) and (110) peaks of Si. Adapted from Helbich et al.(Helbich, Lyuleeva, Ludwig, et al. 2016) *with permission of John Wiley and Sons.*

During the deintercalation of calcium cations from the layered structure with concentrated hydrochloric acid at -25 to -35°C, the crystalline structure of $CaSi_2$ collapses, which results in the

liberation of freestanding silicon nanosheets (SiNSs). As already mentioned, also full hydrogenation (Sugiyama, Okamoto & Nakano 2010; Helbich, Lyuleeva, Höhlein, et al. 2016), or hydrogenation rendered with hydroxylation (Dahn et al. 1993; Yamanaka et al. 1996) of the material takes place during the process, depending on the temperature of this reaction step. The sketch of the reaction and the power diffraction pattern of the freshly synthesized silicane (SiNS-H) is shown in Figure 13. $CaCl_2$ is formed as a by-product during the reaction and can be easily washed away during the work-up procedure.

Right after the deintercalation of the Ca^{2+} ions, the SiNSs do not show any visible PL. However, after the etching step of the nanomaterial with concentrated hydrofluoric acid, a green PL peaking at 510 nm could be observed. Figure 14 shows the emission (%) *vs.* wavelength (nm) spectrum of SiNS-H sheets dispersed in toluene.

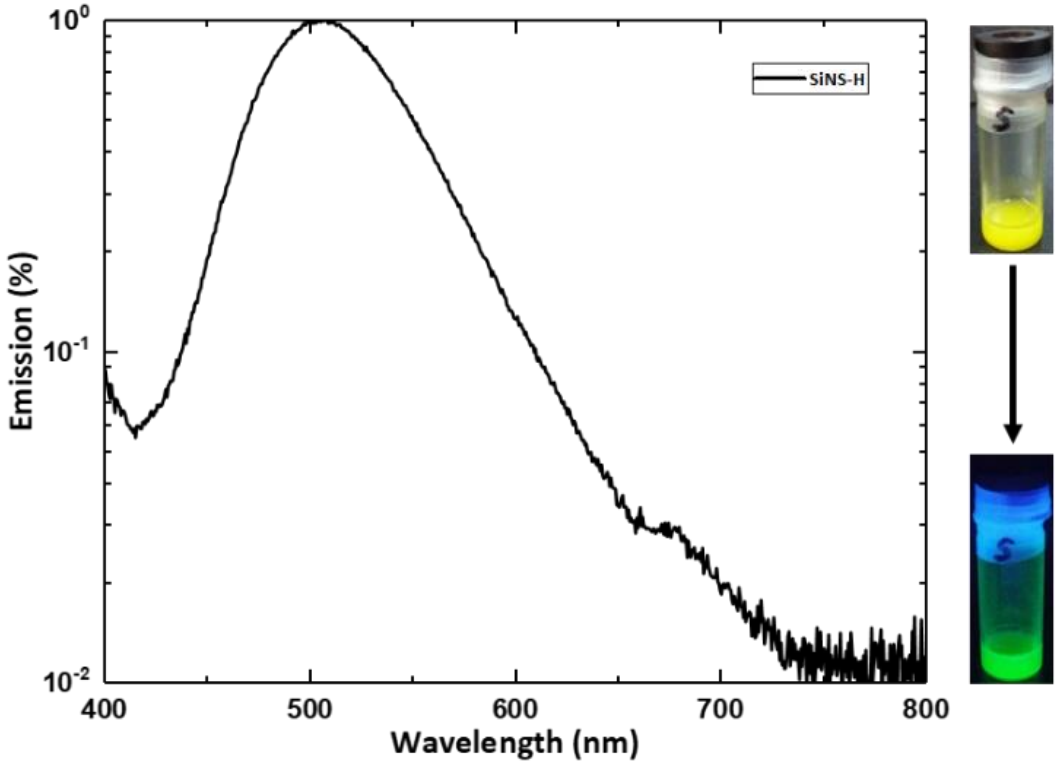

Figure 14: PL spectrum showing emission (%) vs. wavelength (nm) of the as prepared UV (λ = 365 nm) irradiated SiNS-H dispersed in toluene.

Using the sp^3-character of silicane, the surface of the layered material can be modified, aiming for multifunctional hybrid materials and composites. The radical hydrosilylation reaction is the modification method of choice in this work. It can be initiated not only through temperature assisted activation, but also with radical starters such as azobis(isobutyronitril) (AIBN) (Helbich, Lyuleeva, Ludwig, et al. 2016), diazonium salts (*e.g.,* 1,2-DDB) (Helbich, Lyuleeva, Höhlein, et al. 2016), lewis-acid

assisted reaction (*e.g.,* with BH_3, or BF_3) (Tobias Helbich et al. 2017), diaryliodoniumsalts (*e.g.,* bis(4-tert-butyl- phenyl)iodonium hexafluorophosphate (BIP) (T. Helbich et al. 2017)) and microwave energy. (Lyuleeva, Philipp Holzmüller, Helbich, Stutzmann, et al. 2017) However, the basic compound is still a molecule with an unsaturated double bond, of which one electron pair can be split in two radicals, or be involved in an initiator assisted radical hydrosilylation reaction. Figure 15 summarizes some of the functionalization reactions, which were carried out within our groups.

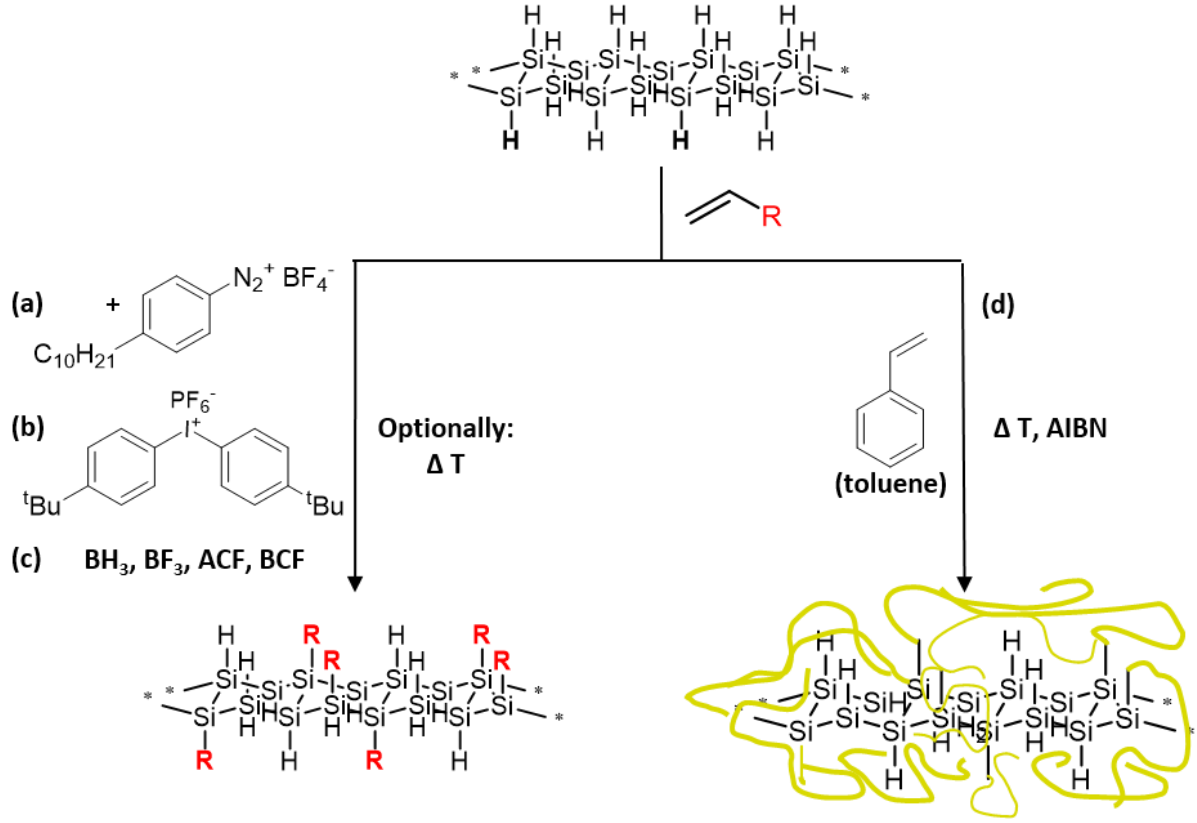

Figure 15: Functionalization reactions of SiNS-H at different conditions. (a) Diazonium salt 4-decylbenzene diazonium tetrafluoroborate (4-DDB) initiated hydrosilylation reaction; temperature was additionally used for the initiation. (b) Diaryliodonium salt bis(4-tert-butyl- phenyl)iodonium hexafluorophosphate (BIP) was used for the radical hydrosilylation reaction, no additional temperature was used for the synthesis. (c) Lewis acid as radical initiator for subsequent surface modification, no additional temperature is necessary. (d) AIBN initiated hydrosilylation reaction of SiNSs surface for SiNS-PS@PS composite synthesis.

Previously, also other groups investigated the modification of SiNS-H to prevent their degradation and to enable the control over the properties of this nanomaterial. Since 2006, Nakano *et al.* carried out a variety of organic surface modification approaches, such as hydrosilylation, aminization and phenylation. (Okamoto et al. 2011; Nakano et al. 2012; Okamoto et al. 2010; Sugiyama, Okamoto, Mitsuoka, et al. 2010) The group has shown that the functionalized SiNSs have a blue-shifted absorption onset of 4.2 eV (Nakano et al. 2012; Okamoto et al. 2010), which is in good agreement with

our results presented in Figure 16. The non-functionalized SiNS-H show absorption (lowest transmittance values) starting from 305 nm (4.01 eV) and the composite SINS-PS@PS even at lower wavelengths, starting from 297 nm (4.17 eV).

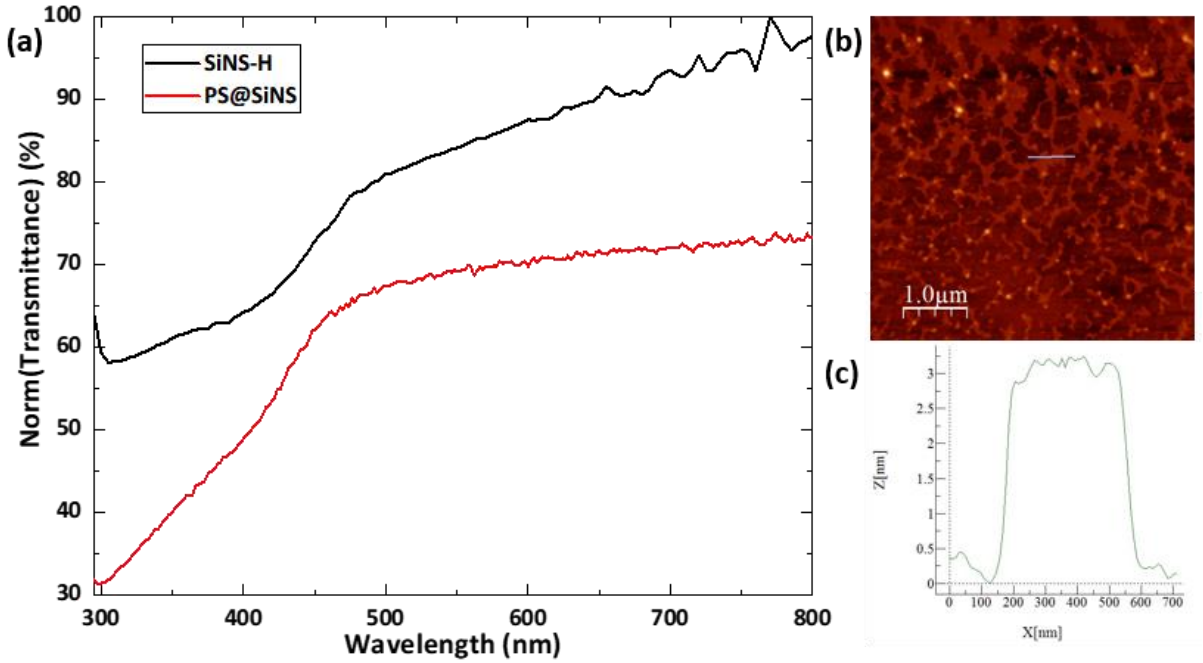

Figure 16: (a) Transmission (%) vs. wavelength (nm) spectrum of etched SINS-H and SiNS-PS@PS composite. An absorption onset can be observed starting from 4.01 and 4.17 eV for SiNS-H and SiNS-PS@PS respectively. (b) AFM image of spin-deposited SiNS-$C_{12}H_{25}$ hybrid material from 1,2-dichlorobenzene (1,2-DCB) and the corresponding height profile z (nm) along the blue line in the AFM image.

Nonetheless, the type of the transition cannot be specified only from the plots, when comparing the center wavelength energy E_{cw} from the PL spectra and with the plots estimated optical band edge E_g. The onset of the absorption is within the PL spectra with no dramatic Stokes shift, which can be observed with the Tauc's plots with $(\alpha h\nu)^2$ for direct and $(\alpha h\nu)^{0.5}$ for indirect transition, calculated from the PL spectra. The differences between the PL peak energies and estimated band gaps are around 0.03 eV, in the order of thermal energy at room temperature, which can also derived from the broad PL peaks (ΔE_{PL} = 0.330 – 0.375 eV, unlike PL from bulk crystalline semiconductor of around 0.047 eV (1.8 k_BT) at room temperature). (Lyuleeva, Mary A B Narreto, Helbich, Veinot, et al. 2017)

With these results, it is possible to consider fully hydrogenated and especially, due to the greater stability, functionalized SiNSs for the use of this nanomaterial in optoelectronic applications. (Wei & Jacob 2013; Hussain et al. 2014; G Liu, X. Lei, et al. 2014) Based on these considerations, our group succeeded in the fabrication of a first prototyped photonic sensor, which can be used in ambient conditions. The fabrication technique and the analysis will be discussed in Chapter 4.2.

3.2. PL AND TRPL STUDIES OF HYDROGENATED AND FUNCTIONALIZED SINSS.

As already mentioned, freshly synthesized and etched SiNSs exhibit green PL. The PL can be described as relaxation of the electrons after their excitation with high energy light, during which photons are emitted. The green PL of the functionalized SiNS is one of their remarkable properties, which origin is still not completely understood. Most of the nanomaterials obey the phenomenon of quantum confinement. (Delley & Steigmeier 1993; Delerue et al. 1993; Öğüt et al. 1997) It was also observed in low-dimensional silicon, such as porous silicon (Canham 1990), silicon nanoparticles (Kabashin & Meunier 2003), silicon nanocrystals (Takagi et al. 1990) and Si/SiO_2 superlattices. (Vinciguerra et al. 2000) Nevertheless, not only quantum confinement, but also other effects such as interface states (Wang et al. 2005; Luppi & Ossicini 2005), luminescent defects states (Kanemitsu 2002) and oxygen vacancy states (Degoli & Ossicini 2000) at the Si/SiO_2 interface were found to be the reason for the emitted PL in *e.g.,* SiNCs. However, the quantum confinement is still found by Derr *et al.* to be the main reason for the PL in SiNCs. (Derr et al. 2009)

In this work, the PL of the differently functionalized SiNSs is analyzed and discussed. The chemical treatment of the surface could influence its physical features, as it was shown in other various silicon-based nanomaterials. (Spencer et al. 2013; Brennan, Morishita & Michelle J S Spencer 2016; Dasog et al. 2014) With functional groups, it might be possible to push or pull the electrons towards and from the surface respectively and thus shift the HOMO and LUMO edges of the gap. Also siloxane, being functionalized not only with hydrogen atoms, but also hydroxy groups, was reported by Hengge *et al.* in 1964 (Hengge & Grupe 1964) to have differences in the fluorescence dependent on the functionalization. Nevertheless, SiNSs have a very broad (relatively high ΔE_{PL}) green PL at around 510 nm, which does not shift in a controlled way: neither with different lateral sizes of the nanomaterial, nor with various functional molecules covalently attached to the surface, which was previously predicted by theoretical calculations. (Gao et al. 2012; Ding & Wang 2012) Freestanding 2D SiNSs are consistently emitting green PL at 510 – 517 nm (around 2.40 - 2.45 eV, Figure 21b). This is close to the value of *e.g.,* the HF-treated layered polysilanes, reported by Nishimura *et al.*, with the PL_{max} at around 2.3 eV (540 nm). (Nishimura et al. 1996) Also the density functional theory (DFT) calculations by Gang *et al.* confirm a band gap energy of about 2.4 eV. Thereby, the group studied the influence of strain and electric field on the properties of the material. (Gang et al. 2013)

The broad PL spectral linewidth may be caused by the inhomogeneity of the surface, either coming from the material itself, or from influences of the functional groups on the surface. Another reason could be the broad variety of the lateral sizes of the sheets together with packed agglomerates in dispersion. The lateral size can render from hundreds of nanometers up to several micrometers. Since

all particles can be excited and thus contribute to the emitted light, it may also cause broadening of the PL. For example, Kim *et al.* studied 2D silicon-based material, which was grown on a substrate with the CVD technique. The group has shown a clear PL_{max} dependence on the lateral size and thickness of their nano-sized material. Although the nature of the by Kim and his co-workers presented sheets is different, compared to the one of our layered material, it can provide a hint for understanding about the dependence of the broadening of the PL linewidth on the size variety. (H. J. Kim et al. 2011) Nevertheless, due to the difference in structure, it is very likely to have also a different behavior with varying sizes, which will be confirmed in the following.

The stacking structure of the sheets and with it arising influences of the layers on each other should also be considered as an impact on the PL. As discussed in our previous results (Helbich, Lyuleeva, Höhlein, et al. 2016), SiNSs tend to easily agglomerate. These stacking structures form multi-layer SiNSs systems, in which the single silicon monolayers may influence each other in terms of their symmetry, lateral straightening and order. For example, Spencer *et al.* have demonstrated that the stacked phenylated silicene can render its band gap with the distances between the sheets, going from the infinite, over minimum to the compressed-like distances. (Spencer et al. 2013) Furthermore, diluted dispersions of the functionalized sheets lead to a small blue shift of the PL_{max} (Lyuleeva, Tobias Helbich, Rieger & Lugli 2017), which confirms its additional dependence on the agglomerates formation. Agglomerates tend to form in more concentrated dispersions.

Being a potential additional reason for PL broadening, we could show that the tailing in the band gap obeys the Urbach rule. As it will be described in more detail later in this chapter, it even turned out to be the most important effect, observed with the PL broadening. Comparable to our results, also siloxene show the Urbach-edge slope as the distribution of the size of the band gap, which was described by Rosenbauer *et al.* in 1993. (Rosenbauer et al. 1993) But before we come to the understanding of the origin of the PL, its behavior with time and during the irradiation will be analyzed.

To check the length of the emission time, PL intensity *vs.* time studies applying SiNS-$C_{12}H_{25}$ (SiNS-Dodecene) were carried out. The readily functionalized material (SiNS-$C_{12}H_{25}$ dispersed in toluene) was chosen, due to the enhanced stability in air. Figure 17 shows PL intensity *vs.* wavelength spectrum of the SiNS-$C_{12}H_{25}$ (dispersed in toluene). Fast decrease in the intensity is already observed after 2 min of irradiation with the laser beam.

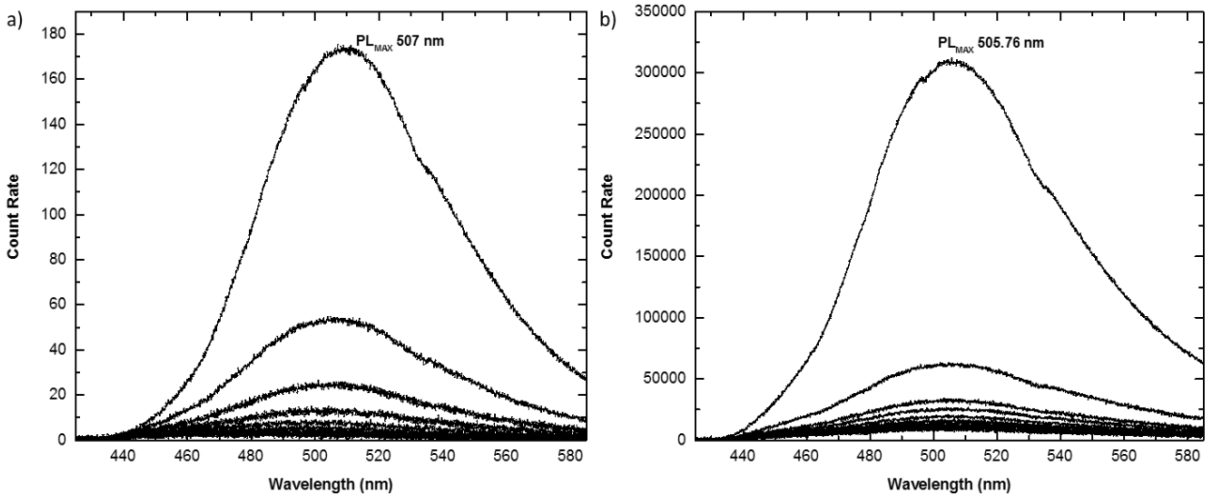

Figure 17. *PL count rate vs. wavelength (nm) of a) in toluene dispersed SiNS-$C_{12}H_{25}$ and b) drop-casted SiNS-$C_{12}H_{25}$ on thin quartz plate measured in 2 min steps for 20 min.*

The fast degradation is caused by the UV light, which the material is exposed to, resulting in the formation of SiO and SiO_2 particles. (Helbich, Lyuleeva, Ludwig, et al. 2016)

After each re-shaking of the dispersion, the initial luminescence intensity can be reached. Hence, the fast precipitation of the illuminating sheets in toluene seems to mainly contribute to the observed decay. Additionally, a small blue shift of the PL_{max} from 506 nm to 501 nm could be detected after 4 min (see Figure 18a).

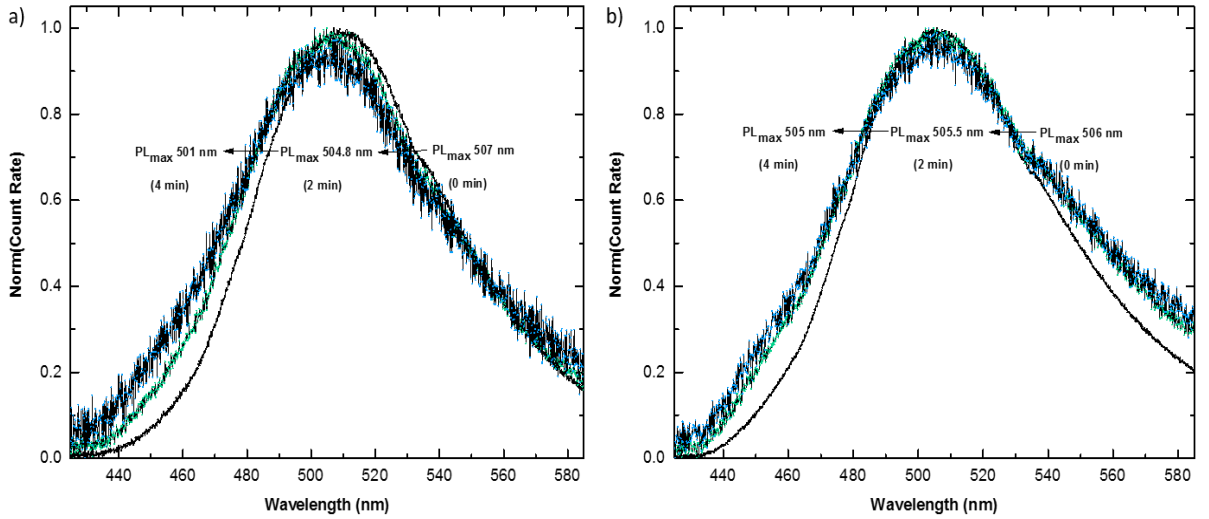

Figure 18. *Normalized PL count rate vs. wavelength of SiNS-$C_{12}H_{25}$ a) dispersed in toluene and b) drop casted on quartz plate measured in air. PL_{max} blue shift could be observed in toluene dispersed SiNS-$C_{12}H_{25}$ already after 4 minutes during the measurement.*

Due to the precipitation of the material on the bottom of the cuvette, a natural de*via*tion of the bigger and smaller particles is taking place. As already mentioned, the value of the band gap is expected to

be in direct connection with the particle size in case of *e.g.,* by Kim *et al.* synthesized and studied 2D SiNSs. (U. Kim et al. 2011) Nevertheless, quantum confinement effect could not be observed for our material. Therefore, minor solvent effect on the nanomaterial could be possibly present, where the solvent molecules have a physical interaction with the dispersed nanomaterial. (Intartaglia et al. 2012) It might be detected when low concentration of the dispersed material is irradiated and mainly their PL collected with the detector.

To further understand, where the loss of the PL comes from, measurements in solid state were carried out. For these experiments the dispersed materials were drop-casted on a quartz plate, dried from solvent and exposed directly onto the laser. The PL was measured with the same set up. However, the decrease in its intensity was faster than the one of the particles in toluene. There is no possibility for the material to move around and to replace the already degraded particles with the still unbroken ones. Intense and concentrated irradiation of a single spot of the drop-casted sample is most likely the reason. Figure 19b shows the PL intensity *vs.* wavelength of drop-deposited SiNSs-$C_{12}H_{25}$, measured in 2 min steps. In this case, the PL_{max} shift is very small (around 1 nm) compared to the sample in solution (Figure 19a). This confirms the possible solvent effect on the nanomaterial.

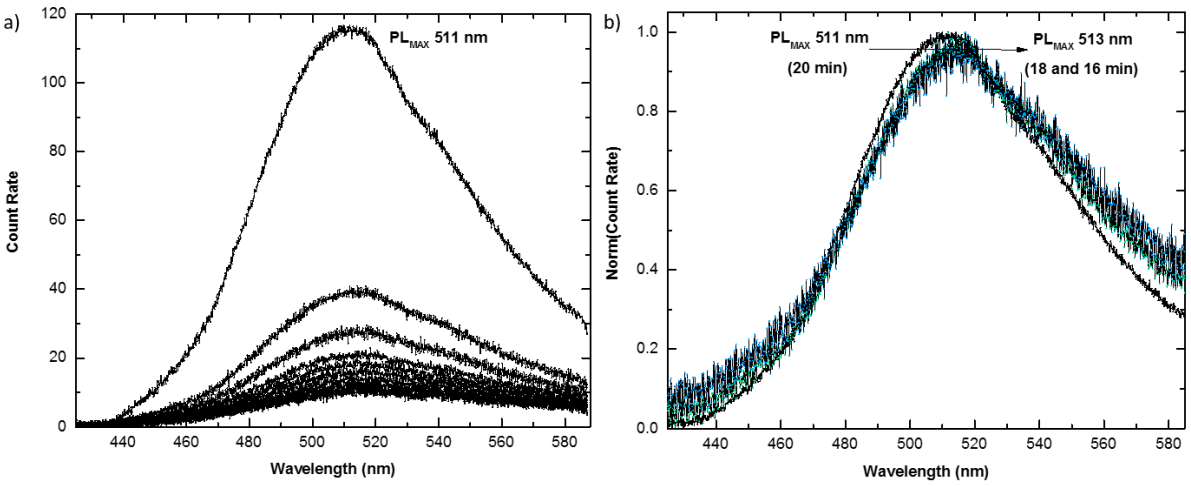

Figure 19: Drop-casted SiNS-Dodecene (solid) PL count rate vs. wavelength in 2 min steps over 20 min measured in vacuum (a) and normalized PL count rate vs. wavelength (b). Red shift of around 2 nm within the first four minutes could be observed.

Air oxygen could have an influence on the PL as well, as it was observed in other silicon-based nanoparticles. (Fuchs et al. 1992; Salh 2011) Two different conditions for functionalized and in polymer matrix embedded SiNSs were chosen: PL measurements in air and in vacuum. PL of the SiNS-$C_{12}H_{25}$ film measured in air slightly blue shifts with time. In vacuum, the PL is still present and shows high intensity at t = 0 min. Nevertheless, the measurements in vacuum show a redshift of around 2 nm within the first 4 min (normalized spectrum, Figure 19b).

At this point it is important to mention the difficulty in comparing the PL intensity results of different measurements. Every single irradiated sample and every spot has a non-consistent number of excited particles. Nevertheless, the loss of the luminescence still takes place. The red shift, which can be observed with the measurements in vacuum, might arise from the Si-Si bond formation between the sheets in z-direction, after Si-radicals have been formed *via* UV-light caused bond cleavage. New bond formations were also observed in germanium nanosystems, such as germanium nanosheets by Veinot and his group. Thus, bigger nanoparticles are formed, which would lead to a different PL_{max}. The corresponding manuscript is currently under preparation.
At the same time, residual oxygen might still be present in the SiNS-$C_{12}H_{25}$ network. This might lead to partial oxidation and thus to a visible redshift of the PL due to oxidized porous silicon formation, as reported by Wolkin *et al.* (Wolkin et al. 1999)

To examine the PL as closely related to the electronic band gap characteristic behavior of the material, we studied the ability to tune the PL and shift it towards different wavelengths. Brennan *et al.* calculated that the functionalization of 2D-sheets with aromatic molecules may influence the electronic structure and thus also the band gap of the material. (Brennan, Morishita & Michelle J S Spencer 2016) Regarding to their results, those organic molecules can tune the size of the band gap. In this connection, we referred to the already mentioned functionalizations of SiNSs and synthesis of SiNS-substrate@polymer based composites (Figure 15d) as a possible approach for precise band gap tuning.

The PL of the SiNS-substrate@polymer (polymer = polystyrene, polyacrylic acid) based composites was studied in more detail. (Helbich, Lyuleeva, Ludwig, et al. 2016) Styrene acts as a monomer for the synthesis for in the following analyzed SiNS-polystyrene@polystyrene (SiNS-PS@PS) hybrid material. The polymer forms a matrix, embedding the SiNSs. At the same time, it is covalently bound to the surface of the nanomaterial. It is conceivable that attaching these molecules directly to the surface would lead to a change in the PL_{max} position of the irradiated composite. On one hand, the electronic pushing or pulling effects, coming from the molecules on the inorganic underlying surface could have an influence. On the other hand, also the already mentioned buckling and thus disorder of the sheets caused by the stacking of the organic functional groups in x/y-direction, could be a potential factor for additional influence. However, as it will be shown once again, these buckling influences seem not to be strong enough for an obvious PL_{max} shift. But it has certainly an influence on the behavior of the excited electrons and their de-excitation, which will be discussed in more detail with the TIPL and TRPL analysis.

SiNS-PS@PS shows a PL_{max} at around 507 nm in vacuum and about 503 nm in air, presented in Figure 20. Thus, the expected obvious PL_{max} shift due to the influence of the surrounding polymer-network could not be clearly observed. Even though, slight shifts towards higher wavelengths could be detected, these should be examined carefully. Nevertheless, in the herein described measurements we can observe and characterize qualitatively the corresponding PL changes, while varying the conditions during the measurements of the same sample.

As expected, the PL intensity in air of SiNS-PS@PS has a less dramatic drop, compared to the one of the dodecene (-$C_{12}H_{25}$) functionalized samples. (Helbich, Lyuleeva, Ludwig, et al. 2016) It is due to the protection of the sheets from rapid oxidation of the material, supported by the UV irradiation. Herein, a slight blue shift of the PL_{max} with the time takes place, which can be seen in Figure 20a.

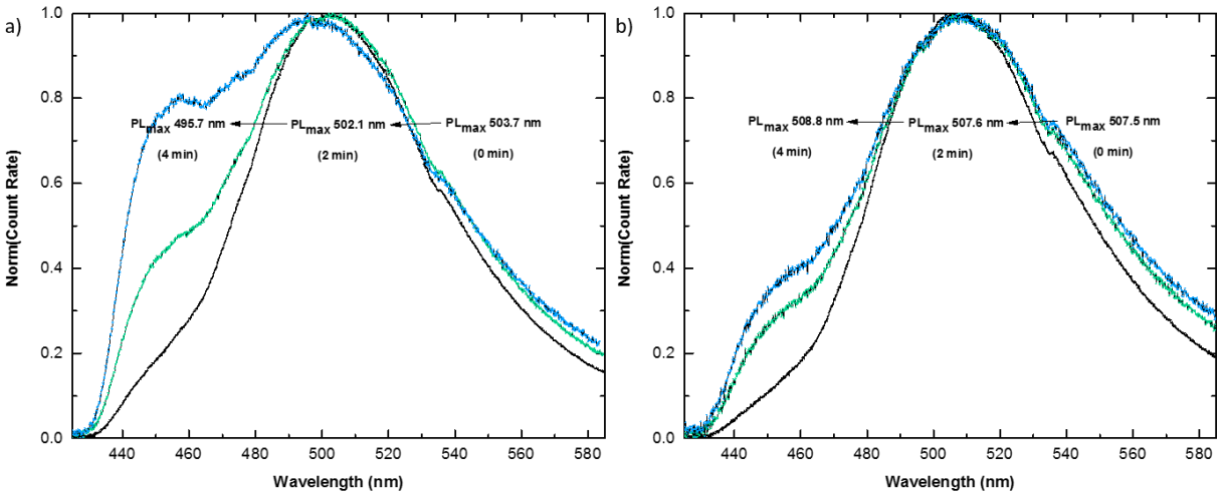

Figure 20: Normalized PL count rate vs. wavelength of SiNS-PS@PS measured a) in air and b) in vacuum. PL_{max} blue shift could be observed for the measurements in air already after 4 min measurement time.

For the irradiation of the SiNS-PS@PS sample in vacuum, no PL_{max} change in any direction was detected. However, the already mentioned redshift, which was observed for the drop-casted material SiNS-$C_{12}H_{25}$ (solid) (Figure 19b), was not expected here. The nanosheets embedded in the polymer matrix are partly connected to each other, forming a conductive network within the polymer matrix. They do not form ordered stacking layers as they could do within the agglomerates and therefore cannot lead to the already assumed bigger Si-nanomaterials formation, or tuning of the band gap *via* mutual influencing. Furthermore, the oxidation which was assumed to also cause a redshift, is suppressed by the protection of the embedded sheets from the ambient conditions.

In both cases, the loss of the PL intensity could be observed. Si-radicals are formed and react directly with the surrounding atmosphere. The polymer matrix embedded sheets are more stable even under

direct irradiation, due to bigger possibility of the recombination reaction of two Si-radicals forming again a Si-Si covalent bond.

These results confirm that the functional groups, which are directly bound to the SiNSs, have no influence on the PL_{max}, which could be detected. Nevertheless, it is still possible to approach and to understand the behavior of the electrons within the hybrid materials during their excitation and relaxation processes, using for example TRPL measurement techniques. The detailed studies and description can be additionally found in the manuscript by Lyuleeva *et al.* (Lyuleeva, Mary A B Narreto, Helbich, Veinot, et al. 2017), which is currently under preparation.

This additional information about the PL can not only help to eliminate any distracting influences, but also provide a possibility to eventually be able to tune the PL. It could be shifted to the desired range *via e.g.,* direct modification of the surface. The PL dynamics and behavior of other silicon-based nanomaterials were studied by many groups in the last decade. (Nakano et al. 2005; Nakano et al. 2006; Okamoto et al. 2010; Okamoto et al. 2011; Okamoto et al. 2015; Ohshita et al. 2016) The measurements can give information not only about the general composition, but also about the carrier dynamics within the material and towards its interface to the surrounding system.

TRPL and TIPL spectroscopy are powerful techniques. In this connection, TRPL measurements were carried out of the differently functionalized SiNS-substrate and SiNS-substrate@polymer composites. The decay of the excited electrons could be detected and shows a nanosecond lifetime decay rate (shown in Figure 21 (a)) for all functionalized SiNSs. The fit has the power law function and is universal for every SiNSs based hybrid material studied in this work. The fit can be described with the equation (1).

$$I(t) = I_0 + \frac{A}{(bt+1)^c} \quad \textbf{(1)}$$

A and *b* are constants, *c* is the power law exponent, *t* is time and I_0 is the offset accounting for the dark counts of the TRPL measurements. At longer times ($t >> 1$), $I(t) \approx t^{-c}$.

The value of the power law exponent *c* gives insight into the recombination processes of electrons right after their excitation. Thus, for example $c = 2$ can be accounted to bio-molecular, or band-to-band recombination processes. (Jonscher & De Polignac 1984; Pelant & Valenta 2012) $2 > c > 1$ would represent hopping mechanisms *via* multi-trapping of carriers. (Scher et al. 2008; Tiedje & Rose 1980) $1.5 > c > 0.95$ would stand for the tunneling processes: *e.g.,* electron traps, or random distribution of recombination centers, whereby temperature has no effect on the system. (Huntley 2006)

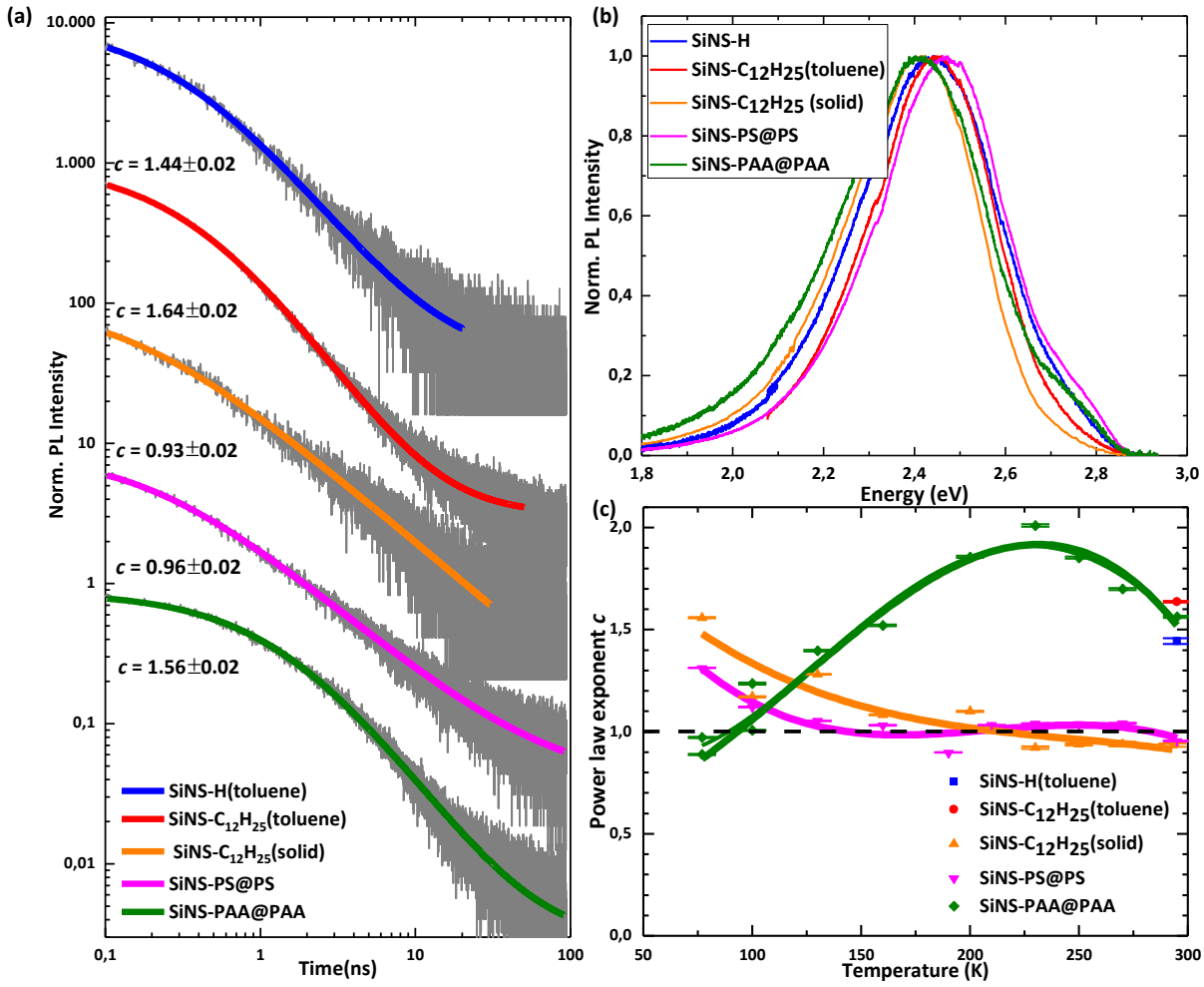

Figure 21: a) TRPL spectrum (log-log plot) of SiNS-substrate and SiNS-substrate@polymer measured at room temperature. The solid lines represent the fit to Equation 1. b) PL of differently functionalized SiNSs measured at room temperature after excitation with ultraviolet laser (λ = 400 nm). c) Powel law exponent c vs. temperature T of differently functionalized SiNSs. The horizontal dashed line serves as guide to eye at c = 1. The green dashed line is the extrapolation of the c vs. T curve for SiNS-PAA@PAA. Adapted from Lyuleeva et al. (Lyuleeva, Mary A B Narreto, Helbich, Veinot, et al. 2017)

As already mentioned, universal fit of the decay spectra could be found, which confirms the PL of the SiNSs coming from the band-tail recombination. The band-tail states in SiNSs are dominated by static structural disorder of the nanomaterial. In this connection, the deviation of the power law exponent *c* from the value *c* = 2 represents the grade of the disorder within the 2D structure. This disorder can be caused by several aspects starting from the deintercalation of Ca^{2+} ions from the crystalline $CaSi_2$ structure. Thus, already the liberation at low temperatures leading to free-standing sheets in solution and the etching step can cause damages to the sheets and lead to defects, holes and disorder formations. Additionally, the subsequent functionalization of the nanomaterial is carried out at different conditions with a variety of functional groups. Every modification aspect, such as reactivity of the unsaturated compound and of the initiator for the hydrosilylation reaction; the value and the nature of initiating energy, applied during the reaction; additionally, the influence of the attached

molecule itself on the 2D structure, due to interactions between functional groups, have impact on the morphology of the SiNSs. Regarding the latter, covalently attached molecules can stack forming *e.g.,* hydrogen bonds in case of the acrylic acid groups of the PAA functionalization, or π-π interactions in case of styrene functional groups. In this connection, also the power law component c in our examples is in direct relation to different functionalizations. Thus, SiNS-H is the least disordered material, followed by $–C_{12}H_{25}$, –PAA and then -PS functionalization in increasing distortion order. This can be also related to the increasing *c* value, calculated from the fits of the decays. The bare material SiNS-H (c = 1.44) and the functionalized SiNS-$C_{12}H_{25}$ (c = 1.64) in solution show *c* values close to c = 2. SiNS-PAA@PAA has the *c* value of c = 1.56 and SiNS-PS@PS composite of $c \approx 1$, indicating the highest disorder of the SiNSs surface. Figure 22a shows the sketch of SiNSs, indicating the changes in disorder of the surface with functionalization and the corresponding energy diagrams (b, c) of the electron tunneling processes after excitation.

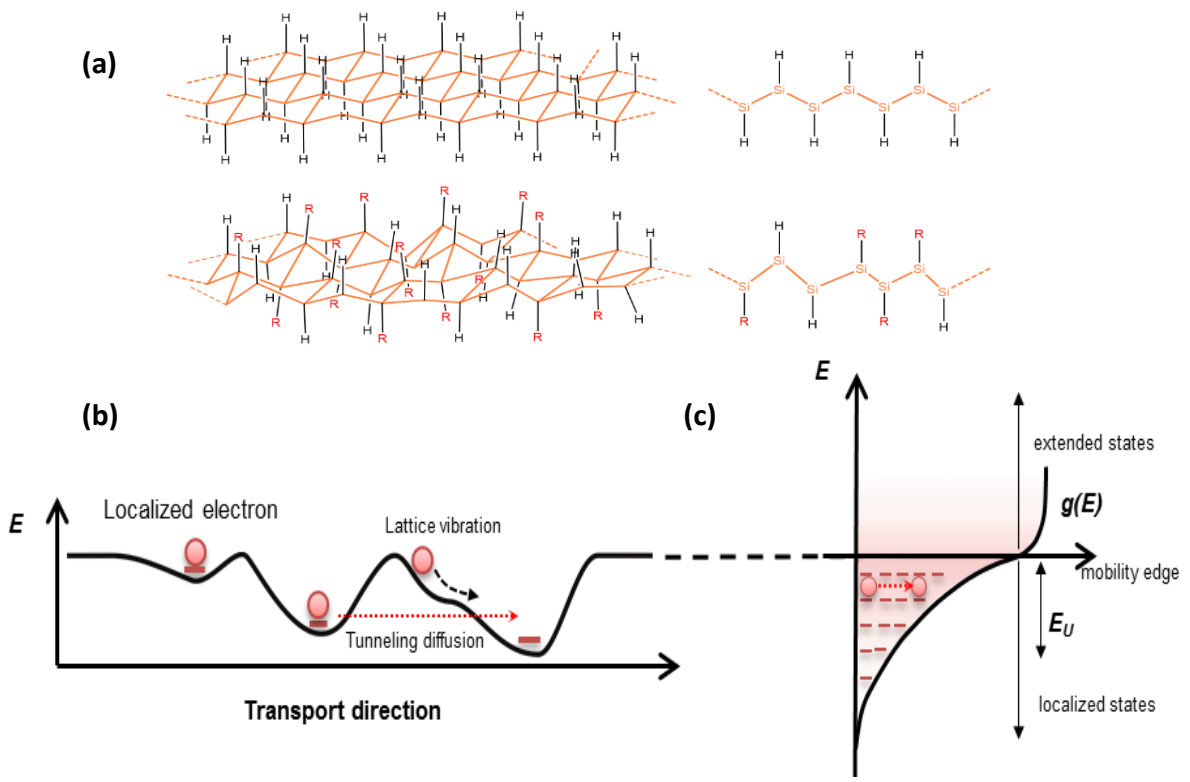

Figure 22: (a) Top picture shows relatively ordered SiNS-H sheet with side view. Introduction of disorder in with –R (R = $C_{12}H_{25}$; PAA, PS) functionalized SiNSs with side view presented in the bottom picture of (a). (b) The energy landscape is distorted due to buckling of the nanosheets. Processes of de-excitation of the electrons after the illumination with high energy light (λ = 400 nm) is shown in transport direction. The corresponding band structure is shown in (c), which has broad distribution of shallow localized band tale states below the conduction band.

The broad PL of the sheets is the dominant contributing factor to the band tail states, which comes through the herein described disorder in the nanomaterial. Its relatively constant PL_{max} only varies

from E = 2.40 eV to 2.47 eV (λ = 502 – 516 nm) regardless of the surface functionalization and is characterized as band-like, due to the band gap opening. It is originating from the 2D Si back-bone of the material and has broad exponential tails, attributed to the broad localized band tail states. At low temperatures, TRPL represents tunneling charge transport and an improvement in carrier diffusion. The rise of the PL intensity is the result.

In summary, the nature of the charge carrier transport can be well compared with the analogous disordered semiconductors. Once again, this strengthens the ability of SiNSs to be used for incorporation into the already established (opto)electronics in industry, which are so far based on amorphous Si.

4. Application of SiNSs in Nanoelectronics

4.1. Modified Silicon Nanosheets based Solution-gated Field-effect Transistor (SGFET)

As described in previous chapters, due to the sp^3-hybridization and the Si-H termination, SiNSs possess a band gap and can be functionalized according to the subsequent needs for fabrication. This surface modification step makes the sheets suitable for industrial processing techniques. Incorporation in nanocomposites and application in novel nano-silicon-based technology can be achieved.

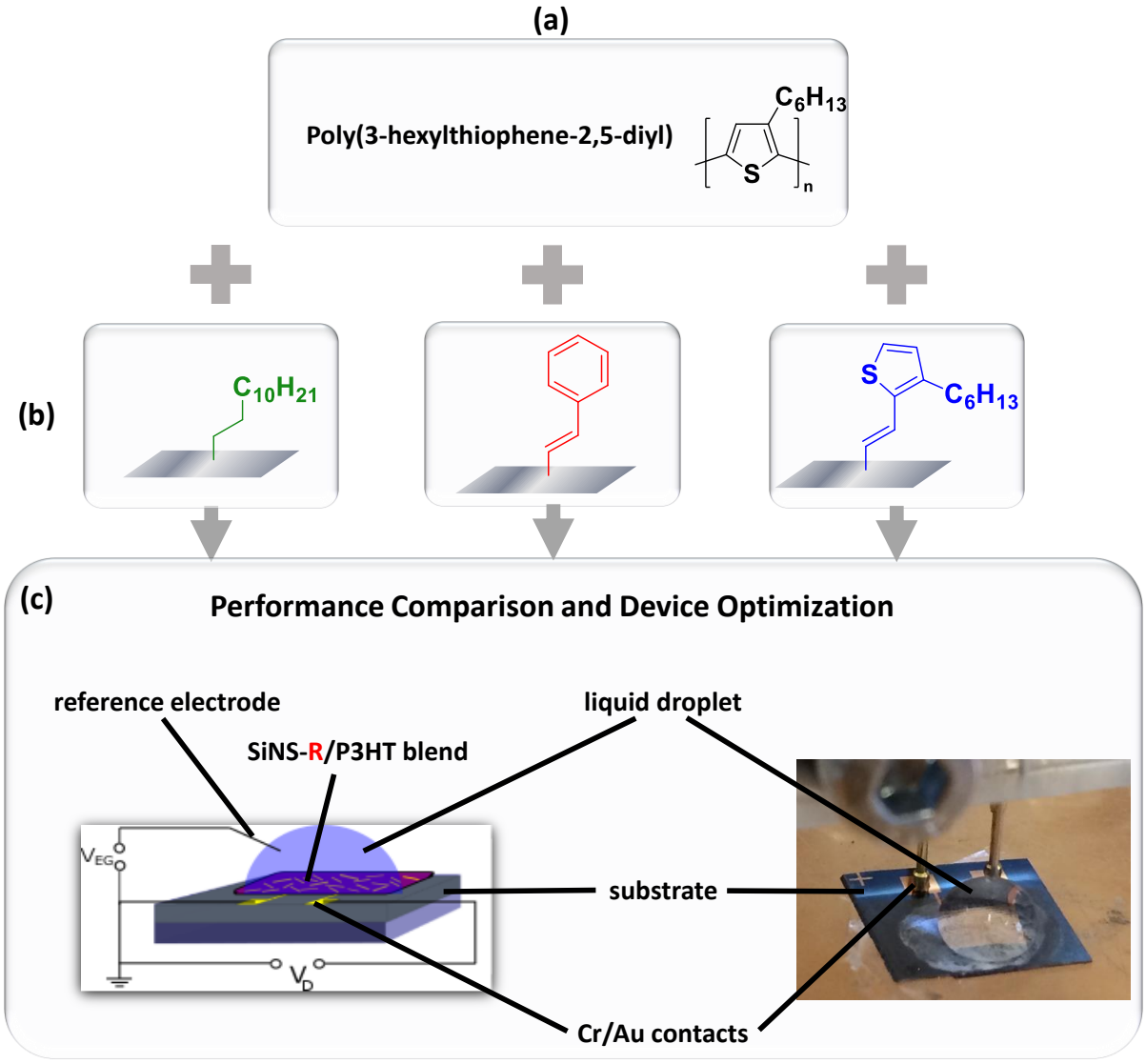

Figure 23: Structural formula for poly(3-hexylthiophene-2,5-diyl) (a) and SiNS-R (R = dodecane, phenyl acetylene, thiophene acetylene) (b) based solution-gated field-effect transistor (c). Schematic image (c, left) and picture of the fabricated device in the measurement set-up (c, right).

The results described in this chapter, can also be found in the corresponding submitted manuscript by Lyuleeva *et al.* (Lyuleeva, Philipp Holzmüller, Helbich, Stutzmann, et al. 2017) This chapter presents the modification of the silicane surface with specific functional groups. These organic molecules can be covalently attached to the silicanes using a microwave-reactor system *via* reproducible radical-induced hydrosilylation reaction. Subsequently, the synthesized hybrid materials are blended with the semiconducting workhorse polymer poly(3-hexylthiophene) (P3HT), building the basis for the solution-gated field-effect transistors (SGFETs) fabrication. To adjust the surface of the inorganic sheets to the characteristics of the polymer for homogeneous blend formation, thiophene based conjugated substrates are grafted on the SiNSs for improved electrical performance of the SGFETs.

4.1.1. State of the Art and Aim

Research on nanomaterials has provided an impetus for the sensing technologies on a chemical and biomolecular level. (Kelley et al. 2014; Erickson et al. 2008; Turner 2013) In addition, FETs are a promising tool for highly sensitive and widely applicable detection of *e.g.,* substrates or molecules in biological systems. (Huang et al. 2012; Liu & Guo 2012; Noor & Krull 2014) The general, mechanism of the FET-based detection is the change in electrical conductivity of the sensitive film, induced by charge carrier density variations or even charge transitions between the sensitive material and the approaching molecules, which need to be detected. (Barreda et al. 2017) These occur directly on, or near the functionalized channels of the transistor in the form of functional polarity change resulting from external influences (Hess et al. 2014) or bond splitting/formation during chemical reactions. (Kergoat et al. 2012; Whitener 2014) Both effects have a direct influence on the sensitivity of the material and lead to a direct change in current, which can subsequently be detected. Additionally, transistors provide a label free detection of surrounding targeted molecules and could be implemented to form faster and lower-cost biomolecules detecting devices. (Leyden et al. 2010) Or, referring to the proposed definition from the International Union of Pure and Applied Chemistry: “A biosensor is a self-contained integrated device, which is capable of providing specific quantitative or semi-quantitative analytical information using a biological recognition element (biochemical receptor) which is in direct spatial contact with a transducer element”. (Ronkainen et al. 2010)

For successful applications in biological systems, the requirements such as accuracy and a high sensitivity of the measurement need to be ensured. Furthermore, biological compatibility and work ability of a sensor in aqueous solutions are another major aspects that must be considered when selecting materials for use in biological sensors. In this context, the control of the materials’ properties, which are used in the sensing system, becomes once again high priority.

Nanomaterial-based FETs have been widely investigated. For example CNTs (Allen et al. 2007), graphene, SiNWs (Barreda et al. 2017; Patolsky et al. 2006), TMDCs (Chow et al. 2017) and black phosphorus (Li et al. 2014; Du et al. 2014; Yue et al. 2016) based FETs all use the capabilities that arise when the dimensions are reduced to the nanoscale. These materials have the same goal: precisely controlled detection and high sensitivity, based on preferably a biocompatible material, which can be fabricated reproducibly and with low costs on even flexible substrates. However, regarding two-dimensionality, silicon has the potential to provide all the required properties and conditions for fabrication of a FET that is flexible, biocompatible, sensitive and controllable. Graphene, as the most popular 2D material, provides a good foundation for consideration of 2D materials as an alternative for post-silicon electronics. (Hess et al. 2011; Novoselov et al. 2004; Sui & Appenzeller 2009) It is highly sensitive to its environment, allowing for the creation of a new label-free immuno-sensitive graphene FET, which was demonstrated by Ohno *et al.* (Ohno et al. 2010) Nevertheless, the main issue in graphene-based electronics arises - the intrinsic lack of a band gap. (Novoselov et al. 2004) Silicon is an established industrial work-horse, put to use extensively in the electronics industry. Therefore, having a 2D silicon-based FET would be a highly attractive solution for these limitations that arise in bulk silicon. (Lu et al. 2012) However, as already mentioned, 2D silicon such as silicene and layered polysilane, lack stability, due to the ability to easily undergo oxidation reactions that form a glass-like α-SiO_x phase (Dahn et al. 1993) under ambient conditions and influence of UV light. (Helbich, Lyuleeva, Höhlein, et al. 2016; Helbich, Lyuleeva, Ludwig, et al. 2016) This requires encapsulation, using either composite synthesis, or covalent functionalization, which was already described in chapter 1.2. Additionally, the already mentioned ease of fabrication and assured sensing performance needs to be established. Resulting from that, P3HT as a well-known semiconducting polymer (Liao & Yan 2013) was considered for the use in combination with 2D SiNSs. One of the main advantages of the blend formation is the ease of the subsequent thin film fabrication, which becomes a well-controlled and reproducible fabrication step. Furthermore, blends also allow for non-destructive combination of both materials' properties, which eventually lead to the improvement in the performance of the device. The implementation of a nanomaterial such as CNTs (Rubin et al. 2002) or graphene (Sun & Wang 2007) within the active area of the device was shown to lead to a significant improvement of its sensitivity. The combination of functionalized SiNSs with P3HT was not only used to embed the inorganic nanomaterial and thus increase its stability, but it also facilitated the fabrication and improved the sensitivity of the desired FETs as well.

4.1.2. Results and Discussion

As the first approach to demonstrate promising potential of SiNSs in electronic application, the functionalized SiNSs were used for SiNS-substrate/P3HT based SGFETs fabrication. The improvement of the operating thin-film transistor was achieved by preparing P3HT with SiNS-substrate blends, whereby the following substrates were chosen: dodecene, phenylacetylene and 2-ethinyl-3-hexylthiophene. The choice of the substrate was based on the nature of the molecules that would be attached to the inorganic material's surface. To increase the homogeneity of the blends, surface treatments *via* chemical functionalization needed to be undertaken, which would improve the miscibility of the inorganic material in the organic semiconducting polymer. (Musumeci et al. 2007)

Dodecene was chosen as a substrate due to its C-chain, which is comparable with the residue, present on each repeating molecule within the polymer chains. Phenylacetylene includes the increase in the system of the conjugated electrons, since this aromatic molecule possesses a 6-ring with delocalized π-electrons. Providing additional π-π stacking interaction of the orbitals with the thiophene rings of the polymer, possible improvement in the arrangement of the sheets can be achieved together with the enhancement of the charge transfer during the device operation. And finally, 2-ethinyl-3-hexylthiophene is a functional group, which combines both mentioned molecule characteristics. In general, exhibiting an even higher structural similarity to P3HT, it promises to show the best miscibility results, leading to the most promising FETs improvement. In the Figure 24 AFM images and sketches for the described hybrid systems can be observed. Differences in the film morphology can already be seen without magnification, but also AFM measurements confirm that the SiNS-2-(3-hexylthiophene-2-yl)vinyl/P3HT (SiNS-ThAc/P3HT) blends (Figure 24c) provide the most homogeneous films with heights of around 50 – 70 nm.

During the preparation, no chemical reactions with new bond formations or cleavage occur, leading to a preservation of both materials' properties. This interaction with the P3HT is one of the main impacts on the electrical performance of the blend based FETs. The high impact of the 2-ethinyl-3-hexylthiophene molecules modified SiNSs on the polymer will therefore be confirmed by the transistor characterization, but also EPR measurements (*vide infra*) will be conducted.

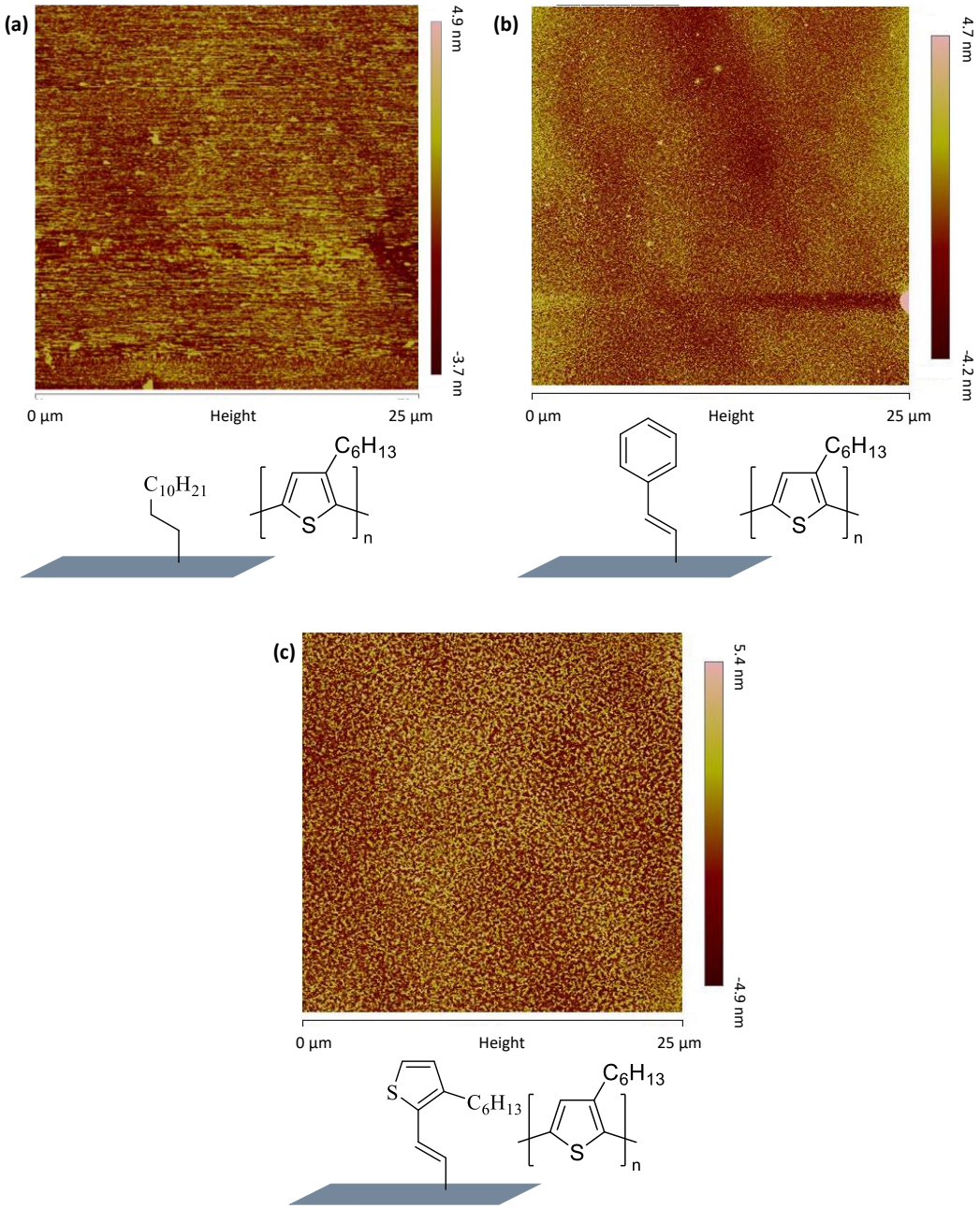

Figure 24: AFM images (size: 25 µm²) for SiNS-$C_{12}H_{25}$/P3HT (a), SiNS-styrenyl (SiNS-PhAc) (b) and SiNS-2-(3-hexylthiophene-2-yl)vinyl (SiNS-ThAc) (c) with sketches for the corresponding molecular structures under below.

The predicted electrical conductivity of the SiNSs and the p-doped behavior of the P3HT polymer enables the device to operate as a FET. (Skrypnychuk et al. 2015) Their semiconductivity allows the device to be switched ON and OFF with the applied gate voltage (Lambert 2005; Sudo et al. 1999), which is an important feature, when energy of the power supply needs to be preserved while the device is not in operation. Adding the inorganic sheets to the semiconducting polymer, increases the drain currents when the transistor is switched ON (at $V_G \leq 0$ V). This effect was thought to arise from the improved connection between the crystalline regions within the polymer film (Sun et al. 2005) and the decreased overall distance

between the source and the drain. With the decrease in distance, the resistance is lowered simultaneously, facilitating the charge carrier mobility in the blend. This influence was already described by Bo *et al.* in the pickup stick transistors, which used single-walled CNTs (SWCNTs) to reduce the source-drain distance. (Bo et al. 2005)

Nevertheless, for a better understanding of the exact influences of the covalently attached functional groups and the SiNSs on the performance of the SGFETs, SiNS-substrate/P3HT based SGFETs were fabricated and electrical measurements carried out. FETs based on four different spin-coated materials were compared: P3HT, SiNS-$C_{12}H_{25}$/P3HT, SiNS-styrenyl/P3HT (SiNS-PhAc/P3HT) and SiNS-2-(3-hexylthiophene-2-yl)vinyl/P3HT (SiNS-ThAc/P3HT) hybrid films. The transistor characteristics are shown in Figure 25a.

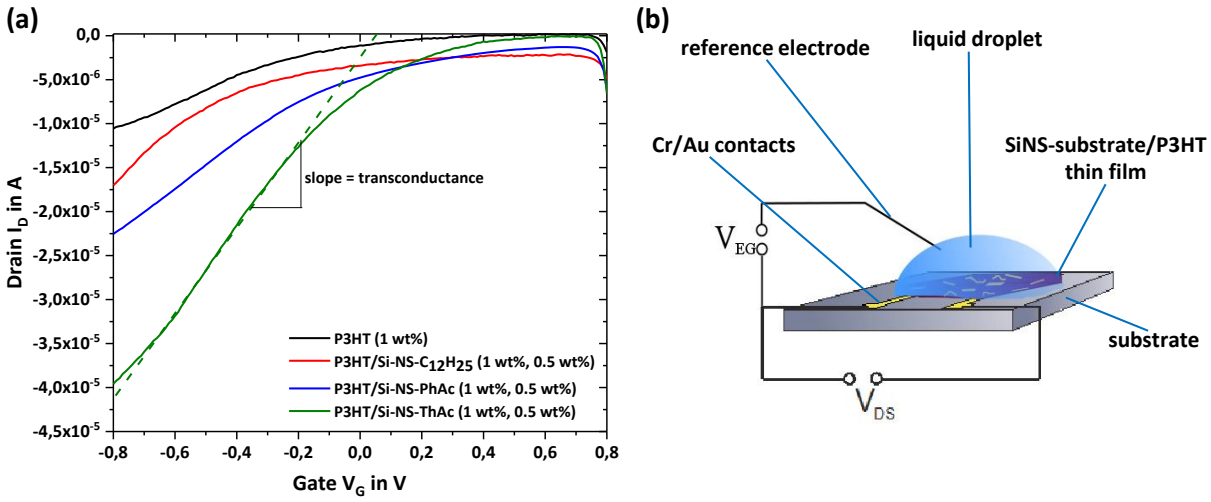

Figure 25: (a) Transfer characteristics of P3HT (1 wt%), SiNS-$C_{12}H_{25}$/P3HT (0.5 wt%/1 wt%), SiNS-PhAc/P3HT (0.5 wt%/1 wt%) and SiNS-ThAc/P3HT (0.5 wt%/1 wt%) thin-film based SGFETs. The slope of the dashed line indicates the transconductance of the SiNS-ThAc/P3HT as the best performing blend. The drain voltage is V_D = -0.1 V. (b) Sketch of a SGFET based on SiNS-substrate/P3HT blended thin film. The reference electrode is herein the gate electrode, through which V_G is applied.

The sensitivity of the SGFETs is characterized by measuring transfer curves with I_D *vs.* V_G at a constant drain voltage V_D. Here, V_D = -0.1 V was chosen to demonstrate the sensitivity of the performing device at even low voltages. The maximum drain current ($I_{D,max}$) at V_G = -0.8 V depends strongly on several influences during the blends and further FET fabrication steps, such as spin-coating and annealing of the thin films. However, even storage and measurement conditions like temperature and light are further factors (Manceau et al. 2011), which have impact on the performance of the transistor. The conditions for the comparison of the devices, such as prepared batch of the dissolved P3HT polymer or the temperature, were kept as constant as possible, to exclude any interference with the obtained results. In this work, $I_{D,max}$ = I_{ON}, since the transistor is defined to be "switched ON" at the highest value of the drain current. Thus, for example the P3HT based device (black solid line in Figure 25a) in the presented measurement is reaching $I_{D,max}$ values of -10 µA.

After adding the SiNS-substrate to the polymer, the resulting SGFETs show significantly increased drain currents. As already discussed and expected, with the influence of the functionalization this increase in current shows the following order, going from the least to the best performing blend: SiNS-$C_{12}H_{25}$ (I_{ON} = 17.5 µA) < SiNS-PhAc (I_{ON} = 22.5 µA) < SiNS-ThAc (I_{ON} = 40 µA). The dodecene functionalized nanosheets could introduce disorder into the polymeric system, which is less likely present in the blend with the ThAc functionalized sheets (for further analysis see Grazing-Incidence Wide-Angle X-Ray Scattering (GIWAXS) Measurements in the appendix). In addition, the dodecene chains do not form stacking structures with the aromatic rings of the P3HT polymer, which might be useful for the charge transfer and thus increase the mobility in the film. (Urien et al. 2007; Brinkmann & Rannou 2007; Machui 2014) Another issue, arising with the SiNS-$C_{12}H_{25}$ blends, is the increased OFF current (I_{OFF}) at gate voltages of about $V_G \geq 0.4$ V. While the ON current is increased, the OFF current is also significantly shifted towards higher values. This effect lowers the ON/OFF ratio of the device and thus the sensitivity of its performance. Also, the SiNS-PhAc based blends show comparable shift of the I_{OFF}, resulting in the ON/OFF ratio of I_{ON}/I_{OFF} = 17.4. The reason could be either the inhomogeneity of the film, or the agglomerates of the sheets, which might form due to insufficient mixing with the polymer and subsequent accumulation of the sheets on the bottom of the thin film. These stacking structures can build occasional parts in the channel with lower resistances, allowing currents to flow even when the transistor is turned OFF. As already mentioned, keeping the OFF current as low as possible when the device is not in operation, is valuable when it comes to the extension of the lifetime of the power supply and use in low-power applications.

Finally, the best performing blend is based on SiNS-ThAc mixed with P3HT. The OFF currents in this device were kept in the range of bare P3HT, at the same time I_{ON} reaches nearly 4 times higher values. (Figure 26a) The transconductance (g_m) of the device is defined by the slope of the I_D/V_G curve and reaches the value of $4.98 \cdot 10^{-5}$ A/V being automatically enhanced. This improvement is directly related to the sensitivity of the device, since it shows how much current change can occur at a certain change of the voltage. These measurements show that the ThAc functionalization evokes the best characteristics of the herby presented p-type transistors. For that reason, also the output characteristics were performed to complete the characterization of a transistor, showing for a p-semiconductor typical shape of the curves, while negative voltages were applied (Figure 26b). These results confirm the miscibility influence on the device performance and can pave the way towards new and promising solutions, which can help to face related issues in surface engineering and charge interaction control of the material.

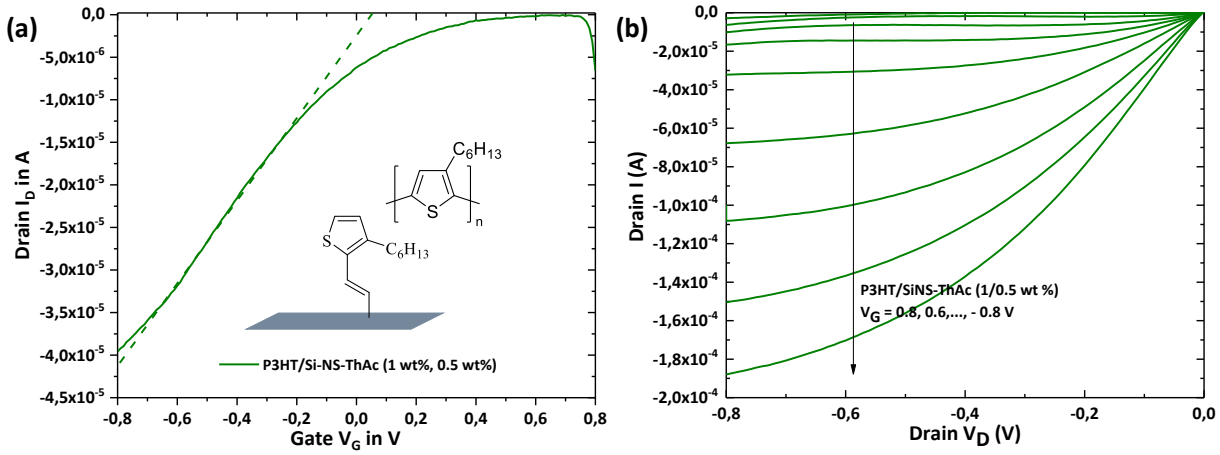

Figure 26: Transfer characteristics at V_D = -0.1 V (a) and output characteristics with constant V_G values from 0 V to -0.8 V in 0.2 V steps (b) of the SiNS-ThAc/P3HT (0.5 wt%/1 wt%) based SGFET. The measurements were taken right after the device fabrication and under absence of light in ambient conditions. The inset shows molecular structures of both materials (inorganic SiNS-ThAc and organic P3HT) present in the blend.

However, coming back to the output curve of the herein discussed device (Figure 26b), all the blends show deformed shapes. The I_D values are increased, starting with drain voltage values V_D = - 0.6 V at constant gate voltages of V_G = 0.8 V to V_G = 0 V in 0.2 V increments. SiNS-ThAc/P3HT based devices show a deformation in the output curve, which can be observed in Figure 27a. At positive drain voltages, the charge carriers in the p-doped semiconducting material should ideally not be in motion, causing current to flow between the drain and the source electrodes. However, this is not the case with the SiNS-substrate blends. When the loading of the polymer with inorganic sheets is higher (for example going up to 2 wt%), this phenomenon is even more prominent. On one hand, this can be related to the nature of the 2D silicon. For example in silicene, ambipolar Dirac transport was predicted, which reacts with a current flow to both positive and negative drain voltages. (Quhe et al. 2015; Tao et al. 2015) Additionally, silicane sheets embedded in the polymer, which will be presented in more detail in the next chapter, also demonstrate current flow between the source and the drain electrodes. Thus, the 2D silicon should still be able to provide charge carriers, even if the drain voltage is set to positive values.

On the other hand, the inorganic material could simply dope the organic polymer *via* charge transfer effects within the blend, which was also observed for the SiNCs/P3HT hybrid materials and led to the conclusion that SiNCs can be used for photovoltaic applications. (Dietmueller et al. 2009)

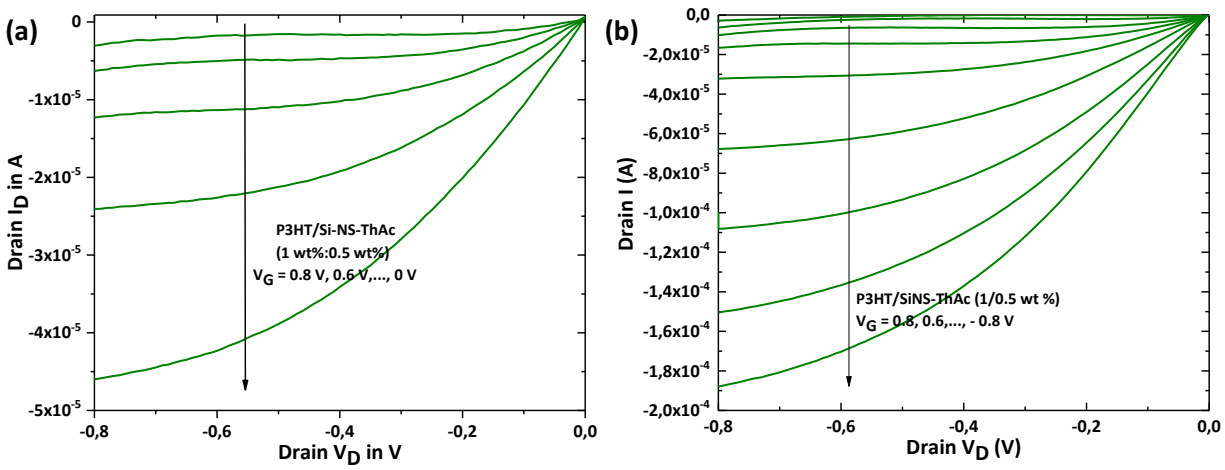

Figure 27: Output characteristics containing I_D vs. V_D curves for SiNS-ThAc/P3HT (0.5/1 wt%) at V_G = 0.8 V to 0 V in 0.2 V steps (a) and V_G = 0.8 V to -0.8 V in 0.2 V steps (b).

In summary, further studies on blend properties and the interaction between SiNSs and P3HT show that not only the source-drain distance and the electrical properties of the SiNSs are responsible for the improvement of the transistor performance. Additional doping effects of the semiconducting polymer caused by the inorganic nanomaterial, have significant influence on the properties of the blend. To better understand these effects, EPR measurements were carried out, which allow to investigate and understand the behavior of unpaired electrons in the measured material. These electrons might interact with the materials in a hybrid system, which could offer some insight into the processes, occurring during the measurement. (Weil & Bolton 1994)

Using EPR analysis, the hereby studied thin films were investigated. The aim was to find the mechanism responsible for the differences in performance when used in a hybrid material. Thus, possible influences of the differently functionalized SiNSs on P3HT were compared. Table 3 summarizes the results of the EPR analysis.

Table 3: EPR analysis of thin films at 5 K. The signal characteristics as origins of the respective paramagnetic states with corresponding g-factor and the line widths (ΔH_{pp}) are shown. The g-factors are corrected by the correlation to the standard DPPH.

thin film	EPR signal	g-factor	ΔH_{pp} (G)
P3HT	P^+	2.0038	7.3
SiNS-$C_{12}H_{25}$	Si-db	2.0037	10.8
SiNS-$C_{12}H_{25}$/P3HT	P^+	2.0022	3.0
SiNS-$C_{12}H_{25}$/P3HT	SiNS-$C_{12}H_{25}^-$	2.0056	4.9

SiNS-ThAc	$SiNS\text{-}ThAc^-$	2.0044	5.7
SiNS-ThAc	$SiNS\text{-}ThAc^+$	2.0019	9.0
SiNS-ThAc/P3HT	P^+	2.0019	2.8
SiNS-ThAc/P3HT	$SiNS\text{-}ThAc^-$	2.0048	4.1
SiNS-ThAc/P3HT	$SiNS\text{-}ThAc^{*-}$	2.0027	1.9

After the exposure to microwave radiation, the EPR signals were detected with an external magnetic field. Already the P3HT shows a weak signal, which is most probably caused by the impurities in the material and the fact that P3HT is paramagnetic (long lived polaron p^+). These impurities most likely come from the polymer itself, which is controlled by the supplier. In addition, also the solvent can cause contamination of the polymer. (Ceuster et al. 2001) Therefore, the signal does not completely match with the values, found in literature. (Ceuster et al. 2001; Al-Ibrahim et al. 2005) This is, why the hereby presented samples are always prepared from the same batch of the P3HT solution before the subsequent comparison between the blends.

To assure the right identification of the EPR signals, the bare functionalized SiNSs-substrate were measured. 2-ethinyl-3-hexylthiophene functionalization showed the most promising results.

Under microwave irradiation one could assume that charge can be separated in SiNS-ThAc hybrid materials, which would lead to the production of $SiNS\text{-}ThAc^+$ and $SiNS\text{-}ThAc^-$ species. Only here these signals could be observed, but not in the example of $SiNS\text{-}C_{12}H_{25}$. The $SiNS\text{-}ThAc^+$ and $SiNS\text{-}ThAc^-$ signals are comparable with other Si based compounds (Dietmueller et al. 2009; Apeloig et al. 2000; Wadsworth et al. 1985) and thiophene values (Shiotani et al. 1983), found in literature. The signal is asymmetric, which might be the result of electrons in the inorganic sheets interacting with the ThAc functionalization. Further signals indicating charge transfer doping within the mixed material can be observed in the form of a new paramagnetic resonance. (Additional analysis with Light-induced EPR measurements can be found in the appendix)

The analysis of the signals in comparison to the values found in literature let us suggest specific processes/mechanisms for p^+ transportation within the SiNS-ThAc/P3HT hybrid system. Figure 28 shows a possible model for p^+ transport. The mechanism includes four main charge transport steps: (1) polaron p^+ hopping from P3HT onto the thiophene group of SiNS-ThAc and further to the silicon of the SiNSs, acting as the transport medium for charge; (2) charge

transport occurs on one side of the SiNS, improving the transport between the P3HT chains; (3) polaron transport through the silicon sheet from one side of the inorganic layer to the other, enhancing the charge hopping in the alkyl stacking direction of the P3HT and finally the π-π hopping of the charge carriers *via* interaction/stacking of thiophene rings with the P3HT polymer chains (4).

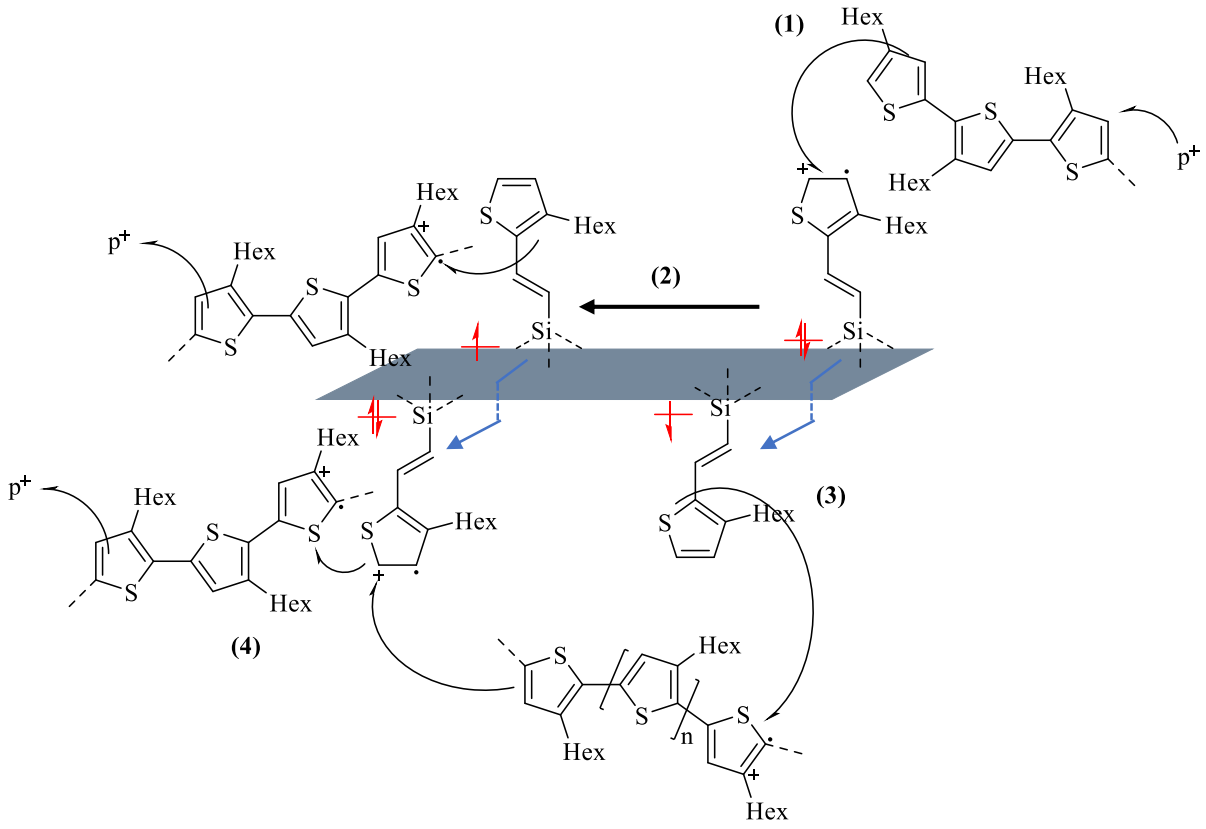

Figure 28: Charge transfer mechanism within the blends. Four steps are present. (1) polaron hopping from P3HT to thiophene group of SiNS-ThAc. (2) Horizontal transport on one side of the sheet by σ-conductivity. (3) Charge transport through the SINS from one side to the other in vertical direction. (4) Interaction via charge transfer between P3HT and the thiophene molecules accompanied by π-π stacking.

All transport steps are most likely accompanied by charge separation within the SiNS-ThAc, leading to SiNS-ThAc^{*+} and SiNS-ThAc^{-}. A similar process could occur in SiNS-$C_{12}H_{25}$/P3HT blends. Nevertheless, the fairly long chains of the dodecene molecules are expected to disable efficient charge transfer due to the insulation of the sheets from the polymer, which results in lower SGFET performance.

4.1.3. Summary

SGFETs based on thin films of hybrid blends were prepared and analyzed. A strong enhancement in the transistor performance was observed as soon as the organic semiconducting polymer P3HT was mixed with the inorganic functionalized SiNSs. The functionalization itself not only improved the miscibility and thus homogeneity of the spin-coated thin films, but in addition to that the charge transfer became more efficient, and so an increase in performance of the operating transistor was witnessed. The best performing blend was found to be SiNS-ThAc/P3HT, with OFF currents of $4.7 \cdot 10^{-8}$ A comparable to the values of the bare polymer ($1.5 \cdot 10^{-7}$ A) and 4 times increased ON currents, leading to the ON/OFF ratio of $8.3 \cdot 10^{2}$. The EPR analysis showed that charge transfer occurs in a four-step fashion, which confirms the predicted interaction of the P3HT chains with the sheets *via* π-π stacking and the electrical nature of the functional groups, which are similar to the ones of P3HT repeating part. Polaron hopping, horizontal and vertical transport within the SiNSs and charge transfer due to π-π stacking are believed to be present in the blend. Overall, the so-called charge transfer doping of the P3HT by the inorganic functionalized sheets can contribute to the mobility and thus provide sufficient charge transfer within the sensing thin film in a SGFET. Furthermore, the ambipolar Dirac charge transfer of the 2D silicon (Tao et al. 2015) can potentially enable an additional source of charge carriers which would result in the improved performances of SGFETs.

4.2. SiNS-Polystyrene@Polystyrene Multifunctional Composite for Photonic Sensor Application

Another application for the 2D layered silicon is their use for a photonic sensor fabrication. The work, presented in this section, is substantially reproduced with permission from previously published manuscript (Lyuleeva, Tobias Helbich, Rieger & Lugli 2017),

As discussed in chapter 1.2.2., many calculations and first experimental studies have been carried out to highlight the properties of the buckled silicon nanosheets. However, no implementation into industrial application could have been achieved until now.

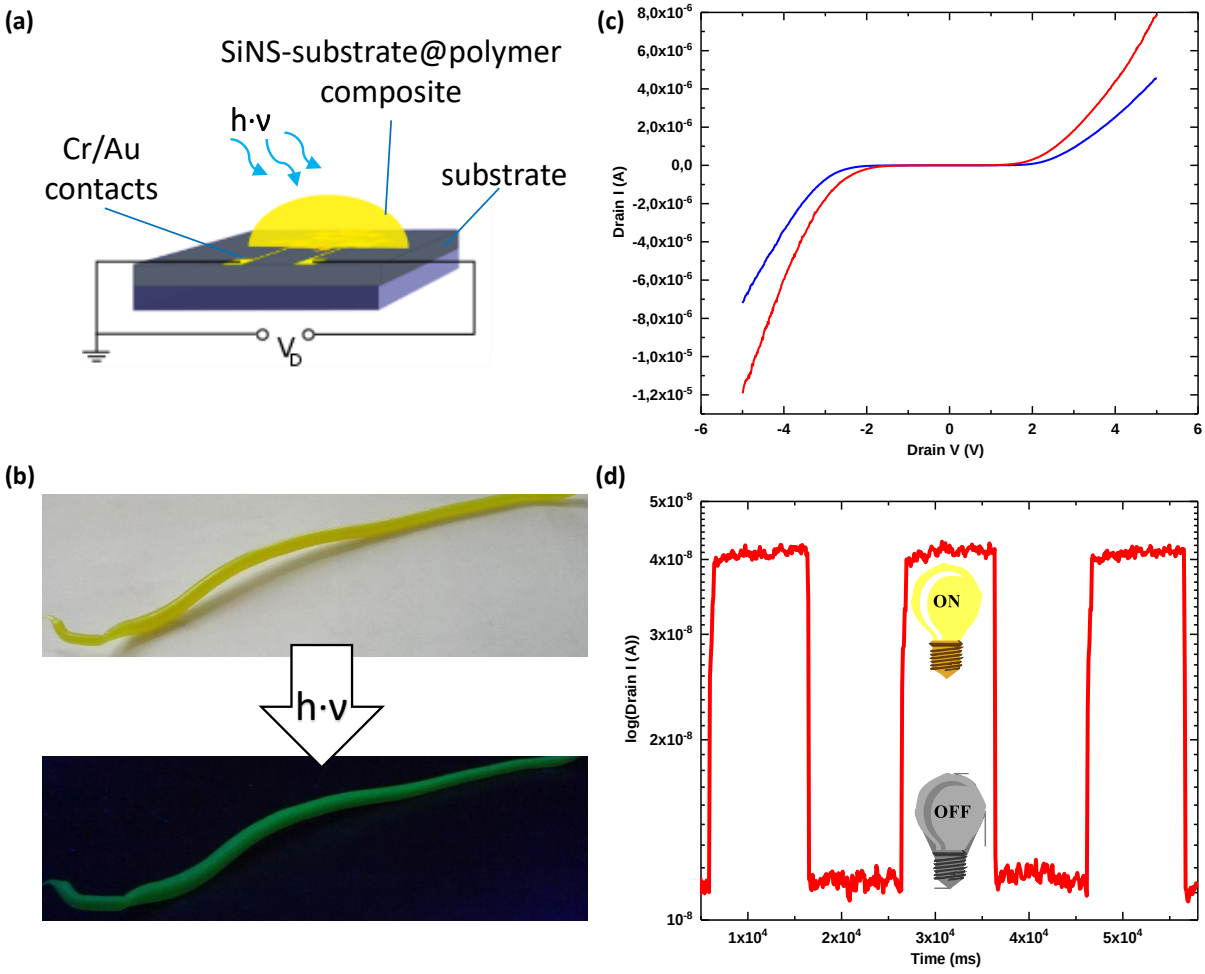

Figure 29: (a) Set-up for photo-detection measurements with the SiNS-substrate@polymer based composite, placed on Au/Cr pre-patterned IDE structure. (b) SiNS-PS@PS composite before and during irradiation with UV light. (c) I_D (A) vs. V_D (V) characteristics of the built device, which was measured at V_G = 0 V while sweeping the V_D from 5 V to -5 V. Blue line denotes the measurement in darkness and red light the measurement under light radiation. (d) I_D (A) detection with the logarithmic scale vs. time (ms) showing immediate current change with switching on and off an illuminating light source.

As already mentioned, SiNSs are promising candidates for nanoelectronic devices and flexible electronics. In this chapter examples for the application of functionalized SiNS based composites are presented. In a polymer matrix embedded sheets act as active material for photonic sensors. The implementation of inorganic SiNSs in a nanocomposite *via* covalent binding improves not only their stability, but also the ease of the subsequent device fabrication. Thus, the hybrid material can be used in a straightforward setup preparation procedure. The hereby described modification and encapsulation of the silicane not only opens a new field of photosensitive application, but additionally improves the stability and processability of the material.

4.2.1. State of the Art and Aim

Optoelectronic nanotechnology is one of the major fields in electrical engineering research with the aim to cover a wide range of industrial goals. One particular interest is highly sensitive, robust and conductive materials that are needed for the fabrication of novel (opto)electronic devices. Together with the aim of making devices smarter, cheaper and mostly long-living for application in wearable electronics, new properties need to be discovered. 2D nanomaterials offer a wide variety of features, which could potentially satisfy these demands. Alongside the properties demanded by industry, flexibility, high transparency, quantum confinement, luminescence, and ease in fabrication are offered by this new class of materials.

For the optoelectronics industry, materials, which are sensitive to light, are of particular interest. Based on these considerations, silicon is one of the dominating ones. It is preferred for the ease of integration into established standards. Nevertheless, there are certain limitations of silicon as a light-absorbing material. These limitations prompted research into alternatives with the goal of achieving enhanced sensitivity of photodetectors by, for example, reducing the dimensionality of the material. Improved performance in terms of efficiency (Barkelid & Zwiller 2013), speed, wavelength tunability, flexibility (Sun & Wang 2007) and transparency (Li et al. 2014) have been seen, proving that lower-dimensional nanomaterials can yield greater photosensitivity compared to their bulk counterparts. (Sun & Wang 2007) In general, novel systems in the so called flatland show photosensitive response, which was reported for example, in graphene and TMDC based sheets. (Wilson, J. A.; Yoffe 1969) MoS_2 or $MoSe_2$ were demonstrated by Velusamy *et al.* to show a highly sensitive band-selective photonic response. (Velusamy et al. 2015) Broad photodetection range was achieved using composites consisting of sensitive nanosheets and polymers. Thus, different combinations were shown to lead to the detection of several wavelength regions together with the ability to fabricate a flexible device. Hu

et al. succeeded in building a photonic sensor based on 2D materials, namely GaS nanosheets. (Hu et al. 2013) Their device was placed on a rigid Si^{++}/SiO_2 substrate and can be used for the detection across UV and visible regions. All together, these achievements encourage research in silicon-based science to find a suitable approach for the fabrication of 2D silicon-based photonic sensors.

This is where 2D SiNSs have much to offer. Sugiyama *et al.* confirmed in 2010 that 2D silicon is suitable for photonic sensor applications after detecting light-induced photocurrent using a three-electrode photo-electrochemical cell. (Sugiyama, Okamoto, Mitsuoka, et al. 2010) After modification of the nanomaterial, a current could be generated. For example, modifying the SiNSs with phenyl groups produced wavelength-dependent currents which could be generated using wavelengths below 410 nm. (Sugiyama, Okamoto, Mitsuoka, et al. 2010) This indicates photo-excited current generation *via* a band gap transition. (Koski & Cui 2013; Ohshita et al. 2016)

Nevertheless, despite these successful results, Sugiyama and co-workers demonstrated a lack of stability of freestanding SiNSs, which are sensitive to external influences such as oxygen in air. Our work also confirmed this instability. (Helbich, Lyuleeva, Höhlein, et al. 2016) Additionally, as already mentioned, SiNSs possess a high surface-to-volume ratio and thus tend to agglomerate easily, which requires additional modification to ensure dispersion in organic solvents. (Sugiyama, Okamoto, Mitsuoka, et al. 2010) Therefore, the stabilization *via* surface modification plays a significant role and as it will be demonstrated in the following section that covalently bound composites can be synthesized, which preserve both materials properties. Thus, with this nanocomposite the processing properties of the polymers with the (opto)electronic characteristics of the SiNSs were combined for the fabrication of a light-sensitive device.

4.2.2. Results and Discussion

As already mentioned, the herein studied silicane sheets have a band gap of about 2.4 – 2.45 eV, which leads to a green PL at around 510 nm of the material. (Tao et al. 2015; Nakano 2014; Niu et al. 2014) The sheets can be illuminated with UV light, which forces the charge carriers to jump into excited states and subsequently return to their original energy value by emitting photons. This causes photoluminescence, which in the case of SiNSs is in the visible range. Additionally, to confirm once again, the SiNSs have a height of about 5 nm, whereby stacking layers can be detected with the AFM imaging. An AFM image of freshly exfoliated SiNSs is shown in Figure 30.

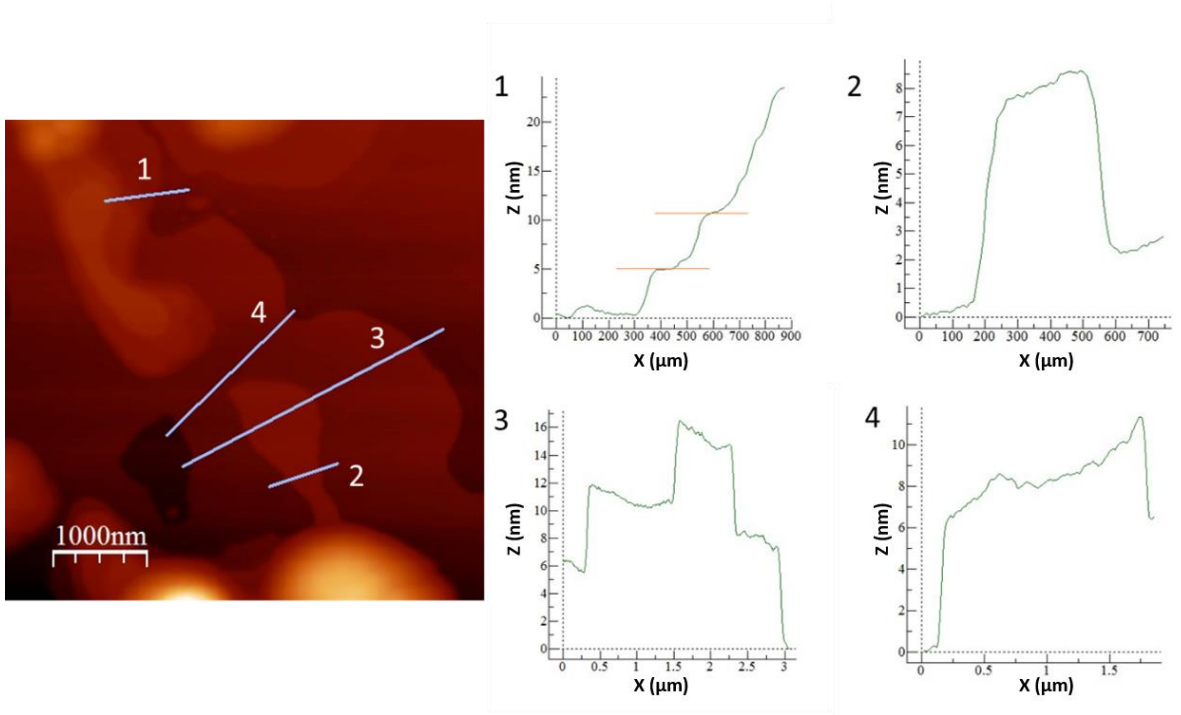

Figure 30: AFM image (left) of hydrogenated SINS on SI^{++}/SiO_2 substrate with corresponding height profiles 1 to 4 along the blue lines.

Many theoretical and experimental studies were performed to show the great potential of 2D silicon for (opto)electronic application. It was shown that SiNSs exhibit these exceptional (opto)electronic features because of their unique buckled 2D structure. (Mohan et al. 2013; Roome & Carey 2014; Vogt et al. 2012; Scalise et al. 2014) Especially transparent and flexible optoelectronics can be targeted. Nevertheless, no groups have succeeded in the actual fabrication of a working photonic sensor so far. In this chapter, one possible modification of the 2D silicon-based nanomaterial will be presented, which covers all the above-mentioned requirements for photonic sensor application.

For the fabrication of an (opto)electronic device, the SiNSs need to be modified to preserve their properties as semiconducting, freestanding and photoluminescent material. As such, SiNSs were combined with an organic polymer for covalent nanocomposite synthesis. The composite (SiNS-substrate@polymer; polymer = polystyrene (PS), poly(acrylic acid) (PAA)) can be synthesized in a simple one-step reaction, which involves the inorganic sheets with the monomer as reactant and a radical starter, such as for example AIBN, or thermal energy. It is a straightforward procedure, which leads to modification of SiNSs with selected organic components. The combination of both materials properties and improvement of the stability of the sheets allows not only the fabrication of novel devices, but also facilitates the subsequent processing steps. (Niu et al. 2014; Hess et al. 2011; Chimene et al. 2015)

In this work, SiNS were synthesized using chemical exfoliation from $CaSi_2$. The deintercalation of Ca^+ ions allows the crystal structure to collapse and the sheets to freely move in the dispersion of the

solvent used. After etching with HF, the readily hydrogenated sheets can be covalently functionalized, as already described for the fabrication of SGFETs. In this case, the reaction is most likely not limited to the functionalization of single molecules, or oligomers on the surface, but is expanded to polymerization of brushes from the SiNSs, which is initiated by the radical starter AIBN. As a result, the 2D sheets can be covalently covered by the polymer of choice and an additional polymer matrix can be formed simultaneously surrounding, separating and stabilizing the SiNSs. The SiNS-substrate@polymer composite is the resulting product, which can be deformed *via* melting after heating the polymer matrix to a temperature (125 °C) just above the melting point of the polymer. Additionally, it still shows green PL of the sheets after excitation. The reaction mechanism is shown in Figure 31. The hereby presented synthesis is based on styrene, resulting in SiNS-polystyrene@polystyrene (SiNS-PS@PS) composite.

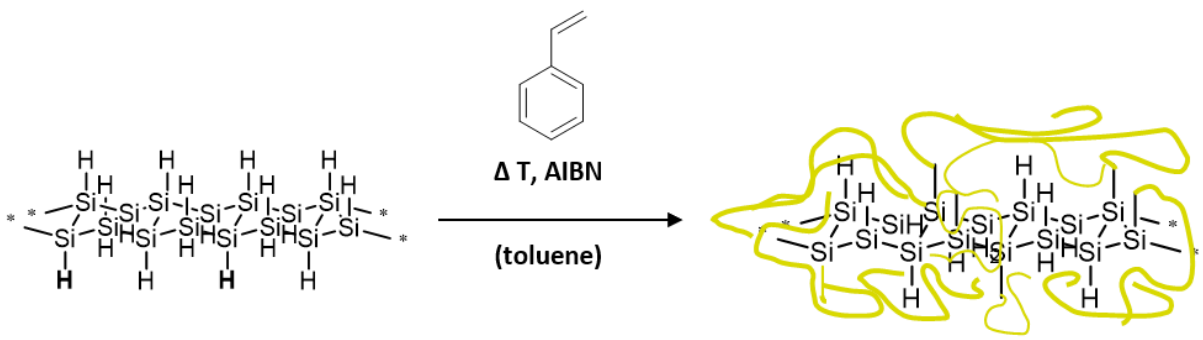

Figure 31: SiNS-PS@PS composite synthesis. AIBN serves as radical initiator together with temperature as energy supply. Toluene is the solvent of choice for dissolution of styrene. The yellow lines indicate polystyrene, which was covalently grafted on the SINSs' surface. The reaction mixture is stirred to achieve a better homogeneity.

The green PL, which is present even after functionalization, shows that the SiNSs are still present in the composite. Raman spectroscopy (Helbich, Lyuleeva, Ludwig, et al. 2016) and energy-dispersive X-ray spectroscopy (EDX) (Lyuleeva, Tobias Helbich, Rieger & Lugli 2017) show clear evidence of the sheets. The composite has a yellow color, which demonstrates the preservation of the inorganic material's properties and could be the first hint that the material should absorb in the high-frequency range of visible light quoted by Okamoto *et al.* (Okamoto et al. 2015) The organic matrix serves not only as a stabilizing support, which stops the modified sheets from moving around the hybrid material during the device operation, but also as protection against external influences, such as oxygen and light. The lifetime of the sheets was increased significantly (Helbich, Lyuleeva, Ludwig, et al. 2016), which enables the storage of the new material for several months even in ambient conditions. Furthermore, it can be treated with solvents, in which the polymer can be dissolved, and heat can be applied for its deformation. The special benefit of these new features is the facilitation of the subsequent fabrication steps. Sensing devices and a photonic sensor can be prepared with the pre-

existing techniques, such as spray-coating, spin-coating, and even simple deformation by melting of the substrate on a hotplate.

SiNS-PS@PS shows absorption at wavelengths lower than 450 nm, which strengthens and confirms the current generation studies of Sugiyama *et al.* (Sugiyama, Okamoto, Mitsuoka, et al. 2010; Koski & Cui 2013) This can be observed once again with the absorbance *vs.* wavelength spectrum in chapter 3. The lower transmittance values for the composite (SiNS-PS@PS, Figure 16) may come from the greater thickness of the composite and the partial absorbance of the light by polystyrene. (Sangawar & Golchha 2013) Furthermore, the current measurements of the material with the wavelength, which are shown in Figure 32, confirm the measurements of Sugiyama and coworkers. (Sugiyama, Okamoto, Mitsuoka, et al. 2010) They show increased current generation at wavelengths starting from around λ = 330 nm (3.75 eV) and peaking at around λ = 435 nm (2.85 eV).

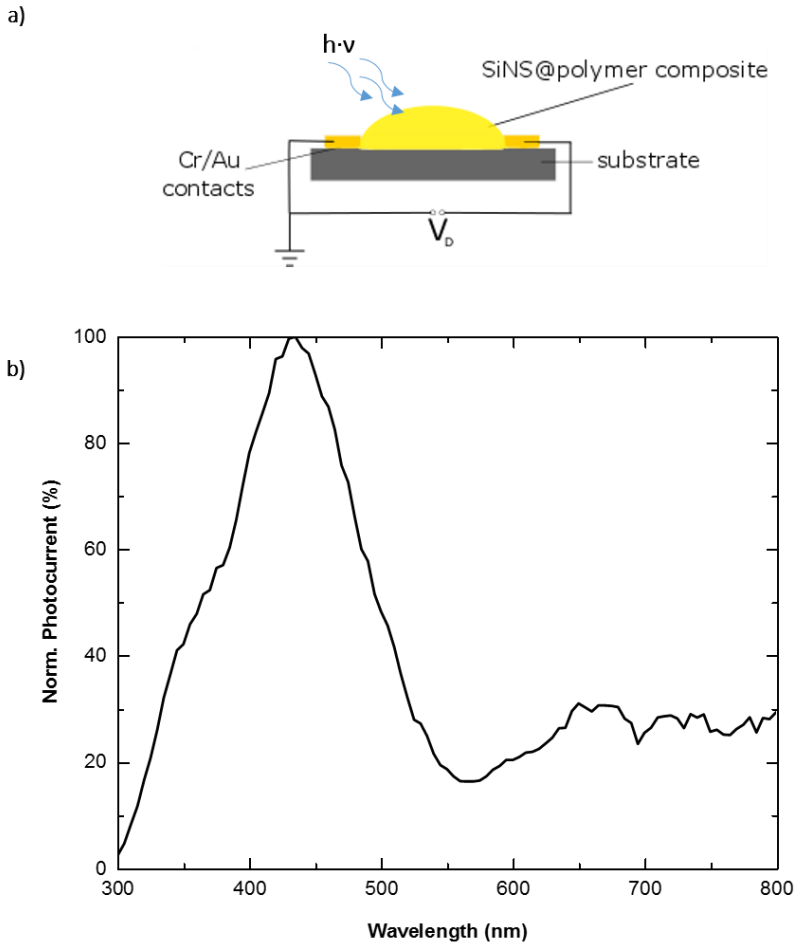

Figure 32: (a) SiNS-PS@PS (SiNS@polymer) composite based photonic sensor and its normalized Photocurrent (%) vs. wavelength (nm) spectrum (b).

Another absorption onset at 3.7 eV was calculated by Wei *et al.*, who considered excitonic effects, which may affect the optoelectronic properties of the studied nanomaterial. (Wei & Jacob 2013) In addition, this onset is comparable with the results shown in Figure 33. This leads again to the studies

of the PL of the synthesized composite, which appears to be at around the same wavelength as the non-functionalized material. The shoulder at around 680 nm corresponds to the already mentioned 2D nanomaterial siloxene, which has H- as well as OH-termination. (Dahn et al. 1993; Kautsky & Herzberg 1925; Kautsky 1952; Wöhler 1863; Böhm, J.; Hassel 1927) This was first reported by Wohler *et. al.* in 1863 (Wöhler 1863) and was revisited by Fuchs and Stutzmann *et al.* in 1992. (Fuchs et al. 1992) The revived material seems to be partly present in the hereby studied composite. The appearance of siloxene can be explained with the oxidation of the nanomaterial during the synthesis, or the PL measurements. The synthesis itself is strictly dependent on the reaction conditions, which leads to formation of different materials and might be the case here as well. As Dahn *et al.* presented, pure siloxane layers as well as a mixture of siloxane and layered polysilane layers can be synthesized from $CaSi_2$ by varying the temperature. (Dahn et al. 1993)

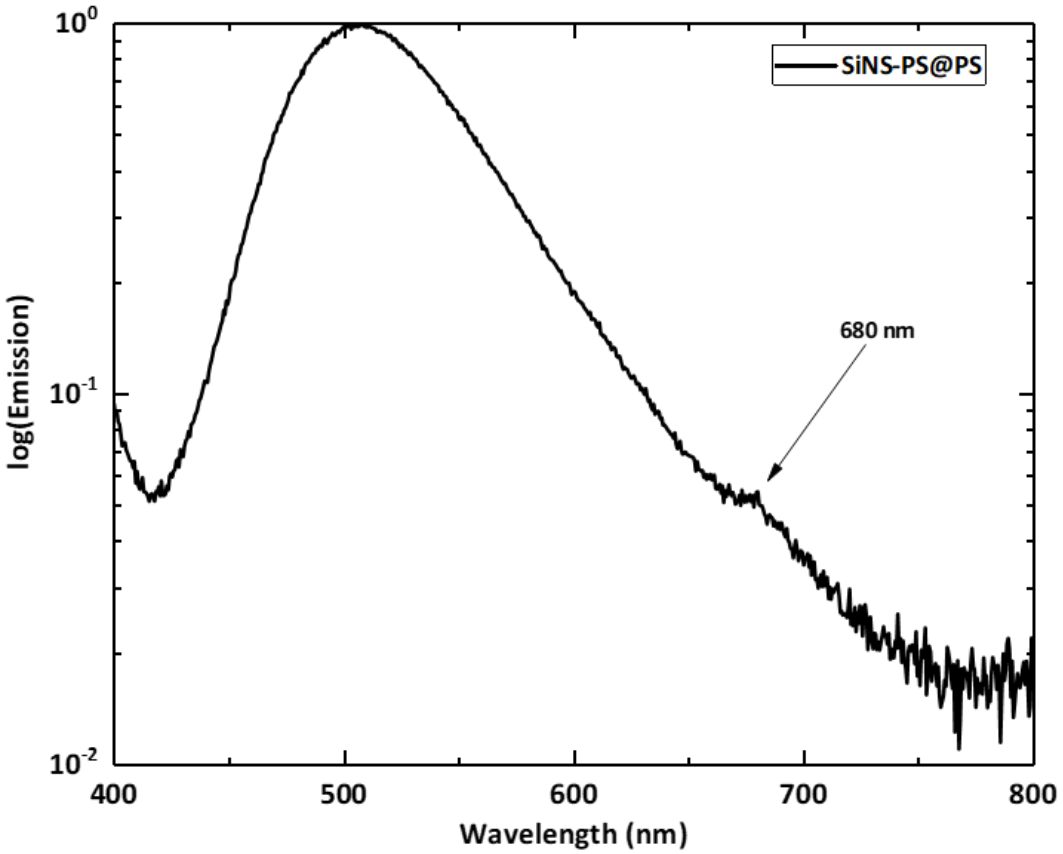

Figure 33: Logarithmic scale of the PL measurements with time of the SiNS-PS@PS composite. The peak at 680 nm indicates the partial formation of siloxane layers in the composite material.

Together with the already discussed PL and TRPL studies, hereby non-existent PL shift strengthens our conclusion about the band-to-band recombination, which might take place after the excitation. These considerations were also reported by Koski *et al.* (Koski & Cui 2013)

With it, we illustrated that SiNSs exhibit photosensitive properties, which can be used for the fabrication of photonic sensors. Due to that, illumination-dependent current response of the sheets was studied. Polystyrene embedded SiNSs were used to assure not only the increased lifetime, but also subsequent facilitated fabrication of the material. The fabricated photonic sensor is shown in Figure 34.

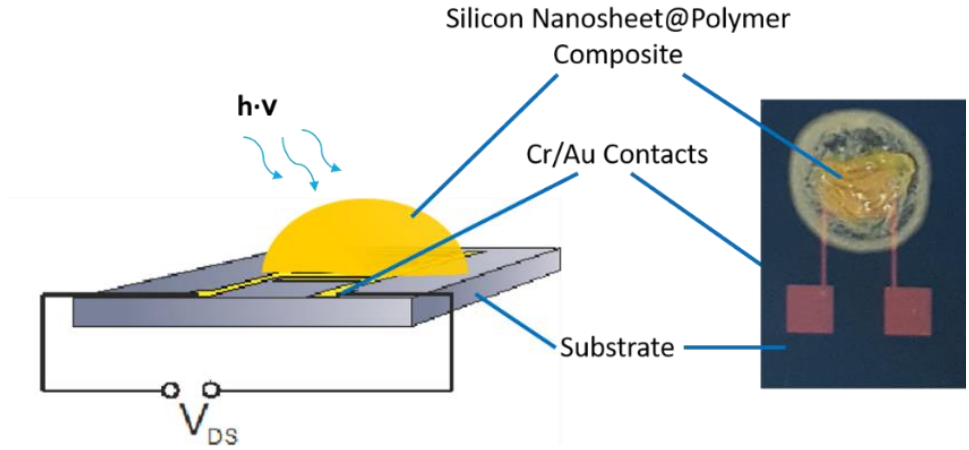

Figure 34: Sketch (left) and image (right) of the photonic sensor set-up based on SiNS-PS@PS composite melted on drop-deposited SiNS-^{t}BMA.

For the fabrication of the SiNS-PS@PS based photonic sensor, the SiNS-PS@PS composite was melted at the temperature T = 125 °C, which is just above the melting point of the polystyrene (T_m(polystyrene) = 103 °C), on spray-deposited SiNS-^{t}BMA. This temperature was chosen, in order to make sure that the material does not become liquid. At temperatures well above the melting point, the sheets and polymer chains move freely within the composite. This would subsequently lead to an uncontrolled composite deposition and with it a lower probability of a secured percolating path for successful photoinduced current generation, since polymer chains could form an insulating layer between the sheets and the electrodes. In addition, the barely flexible composite was carefully pressed on the substrate. Additionally, force was applied to prevent the formation of the insulating layer. The additional step of SiNS-^{t}BMA deposition was carried out to assure the connection of the embedded SiNSs with the Au/Cr contacts on the substrate. The functionalization with ^{t}BMA functional groups was chosen due to the hydrophobic property of the molecule, which is also one of the characteristics of the polystyrene based polymer matrix. Homogeneous deposition was assured *via* the air-brush spray-coating technique. (Abdellah et al. 2009) For that, the nanomaterial was dispersed in toluene. Hereby, homogeneous deposition is one of the critical steps, which are important for the reproducibility of the device fabrication. A further advantage is the possibility to scale up the fabrication process, due to low-cost static spray deposition, which is shown in Figure 36b. (Abdellah &

Abdelhalim 2013) Additionally, this technique can be applied for the material distribution on various surfaces, such as flexible substrates like polyimide (Kapton) films.

The characteristics of the operating device of the SiNS-PS@PS based photonic sensor are shown in Figure 35.

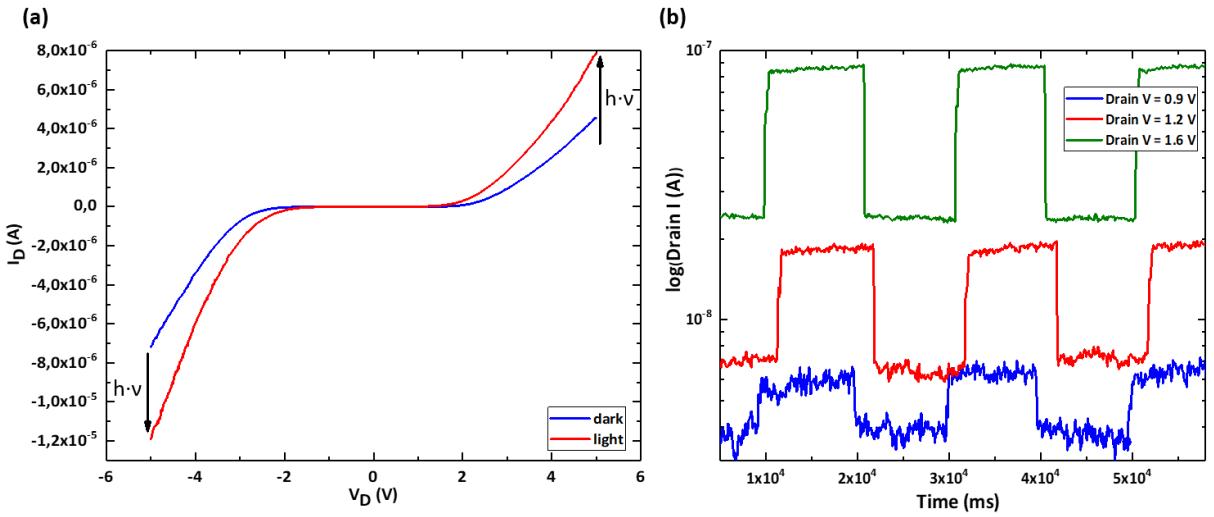

Figure 35: (a) Drain current (A) vs. drain voltage (V) of the SiNS-PS@PS based photonic sensor at constant gate voltage V_G = 0V. (b) Drain current (A) vs. time (ms) at different gate voltages V_G = 0.9 V, 1.2 V, and 1.6 V, which were chosen as an example.

As soon as the connection was established, increased current flow could be observed during the irradiation of the material with light (red line, Figure 35a). For the current dependence studies, a commercially available light bulb (9 W, 2700 K, 50/60 Hz) was used (Figure 35b). An increase in the irradiation intensity could also be observed with the fabricated device. The drain current was measured in darkness and under irradiation. The output characteristics in Figure 35a show the corresponding I_D (A) *vs.* V_D (V) curves. As soon as the device is irradiated, a significant increase in current can be observed. This impact is even higher with increasing drain voltage values. Thus, the current increases exponentially when V_D exceeds ± 2 V. The I_D/V_D curve shows diode like behavior. The device can be nearly switched OFF ($I_D = 7 \cdot 10^{-11}$ A) at drain voltage values around 0 V and turned on again, when V_D is increased again in negative or positive direction. Therefore, the sensitivity of the device allows clearly visible detection of current change with V_D values greater than ± 0.5 V.

Additionally, measurements with only SiNS-^{t}BMA deposited substrate were performed to assure that the light sensitive results in Figure 35 were generated by the composite and not by the deposited

underlying material. Figure 36a shows the corresponding drain current *vs*. drain voltage measurements.

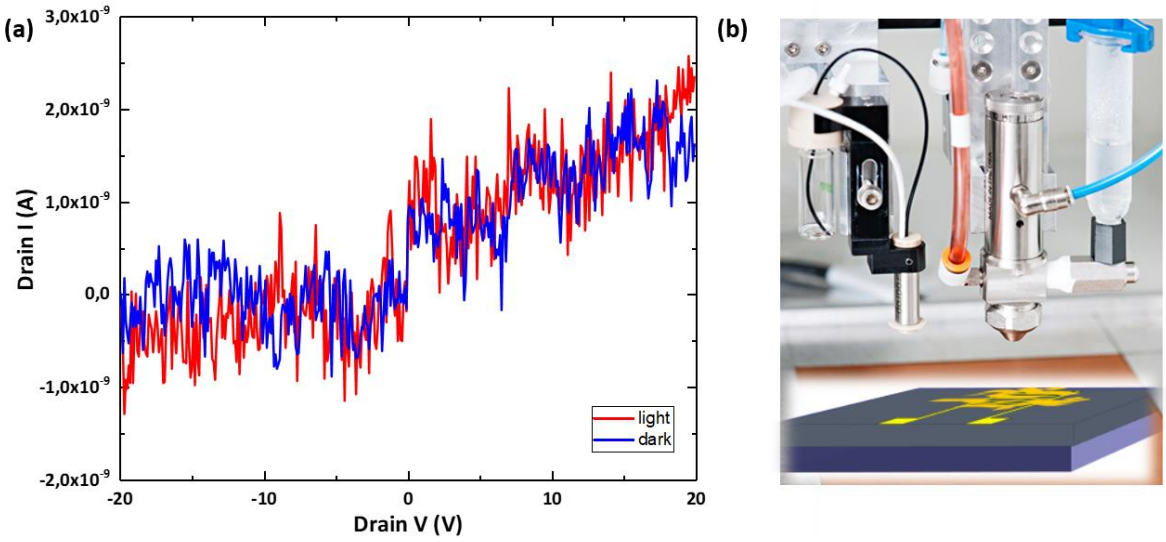

Figure 36: (a) I_D vs. V_D measurements of SiNS-^{t}BMA on Si^{++}/SiO_2 surface. (b) Static spray-deposition set-up for nanomaterials dispersions.

The electrical measurements of the SiNS-^{t}BMA, which were deposited on Au/Cr contacts on Si^{++}/SiO_2 substrate do not show any significant change in current with light irradiation. In general, only very low currents were observed. The reason could be the lack of stability of the sheets under ambient conditions, especially when voltage is applied. Furthermore, the not-established conductive network of the sheets, which is crucial for successful device operation, could be another reason. The arrangement, stacking and connection of the deposited SiNSs with the powder-like deposited material is poorly performed in comparison to the 3D network with the homogeneously implemented inorganic SiNSs.

4.2.3. Summary

With these studies, experimental application in a photosensitive device based on a 2D silicon nanomaterial was performed for the first time. The application for the use of the material as a photonic sensor was theoretically predicted by many researchers. Nevertheless, no successful fabrication of a working device based on 2D SiNSs was presented so far. A one-step synthesis of the composite was established, which allows successful nanocomposite fabrication *via* radical hydrosilylation reaction on the SiNSs surface together with the polymerization of the styrene monomer, leading to a formation of a 3D matrix. (Helbich, Lyuleeva, Ludwig, et al. 2016) As a result, a

multifunctional composite was synthesized, which possesses both materials properties, allowing its deformation with increased temperatures and showing light dependent conductivity.

These studies lay the foundation for further fabrication approaches of sensing 2D nanosilicon-based devices. Additionally, the theoretical studies, which predicted outstanding properties of the layered polysilane, are herewith reinforced and their already remarkable value of sensitivity and conductivity increased.

4.3. TUNING THE HYDROPHILICITY OF SiNSs SURFACE FOR CAPACITIVE HUMIDITY SENSOR FABRICATION

Previously, we have already shown that the well-established surface chemistry, which introduces covalent attachment of various functional groups to the surface, can be used to form hybrid materials with properties of both, the inorganic sheets and the organic molecules attached. So far that functionalization step has also been used for the protection of the SiNSs against external influences, to keep the properties of the inorganic sheets for subsequent application in FETs and photonic sensors. However, with the work described in this chapter, we go beyond the classic approach of SiNSs' functionalization and incorporation into the already well-known fabrication techniques: we concentrate on the application possibilities of the oxidized SiNSs, which synthesis was by now rather avoided than intended. The oxidation of SiNSs leads to a highly porous material, which shows remarkable sensitivity towards humidity. The additional functionalization with hydrophilic molecules enables precise engineering of the surface. It allows the surrounding water molecules to approach and interact with the sensitive material directly at the interface and within the pores, yielding in highly sensitive response to humidity and temperature changes. The results described in this chapter can also be found in the corresponding submitted manuscript by Lyuleeva *et al.* (Lyuleeva, Tobias Helbich, Bobbinger, Rieger, et al. 2017)

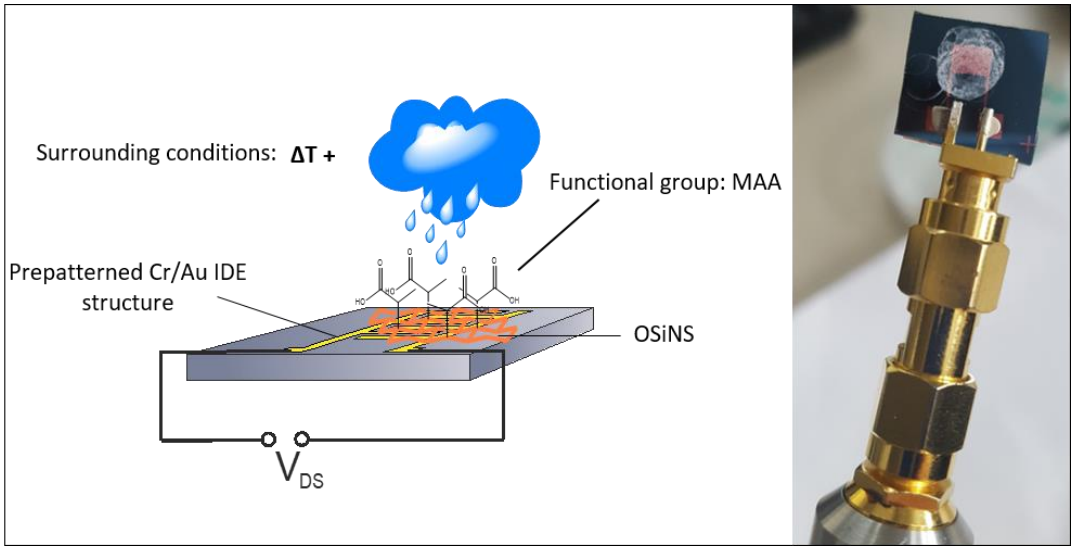

Figure 37: Schematic (left) and photographic (right) image of the humidity sensing set-up based on porous OSiNS-MAA deposited material on a rigid (e.g. Si/SiO_2), or flexible (e.g. Kapton) substrate. The set-up is placed in a climatic chamber and measured with time in varying humidity and constant temperature, or varying temperature and constant humidity conditions.

4.3.1. State of the Art and Aim

Water is one of the most common molecules in the environment. Its ratio in atmosphere has a significant impact on our everyday-life and therefore needs to be controlled, in order to prevent unexpected results especially in industrial processing. (Traversa 1995) The manufacturer needs to rely on the reproducibility of the product, just as the customer relies on the quality, stability and durability of the purchased device. This reproducibility can be harmed by the amount of water vapor present during the device fabrication in *e.g.,* semiconductor industry. The food industry relies on the shelf life of the product, which can only be guaranteed if the absence of water is assured. (Mathlouthi 2001) That value may be monitored and strictly traced by humidity sensing devices. (Chen & Lu 2005) In summary, water vapor control provokes a wide interest in materials science and electrical engineering. Since the industry is constantly chasing after cheaper and smarter solutions, research must find new ways to use the physics of not only natal materials, but also synthetically made ones. Furthermore, experimental and fundamental research encompasses nanoscopic materials for the satisfaction of the industrial needs. Once again, the class of 2D materials such as graphene (Novoselov et al. 2004), MoS_2 (Mak et al. 2010), germanene and silicene (Chowdhury & Jana 2016) provide interesting possibilities due to their already mentioned outstanding properties. Thus, for example, in direct-gap or indirect-gap semiconductors (Yamanaka et al. 1996; Bianco et al. 2013; Jiang et al. 2014; Xu et al. 2013; Dettlaff-Weglikowska et al. 1997), conductivity, or semiconductivity (Matthes et al. 2014) and further features, coming with for example quantum confinement (Wilcoxon et al. 1999), while lowering the size of the material, spark interest. Two important aspects for an innovative electronics industry, which arises with smaller size and dimensionality, are transparency and flexibility of the considered materials. On one hand it allows the fabrication of invisible electronics, which is desired from an esthetical prospective and provides water level control without distracting the perception of the average customer. On the other hand, it makes the fabrication of highly flexible and even stretchable devices for atmospheric conditions possible, which is required for the comfort factor of the wearables, manufactured from these low-dimensionality materials.

For the humidity control, the amount of water in gas needs to be determined. (Roger et al. 2016) The ratio of the partial pressure of water in gas to the saturation vapor pressure of a gas at a given temperature (Chen & Lu 2005), is one of the most commonly used values for high humidity ranges and is referred to as relative humidity (RH). The following materials were reported to be suitable for humidity sensitive measurements: ceramics, such as Al_2O_3 (Chakraborty et al. 1999), TiO_2 (Morimoto et al. 1969; McCafferty & Zettlemoyer 1971), SiO_2 (Lin et al. 1993; D'apuzzo et al. 2000; Kong et al. 1997), spinel compounds, modified polyelectrolytes (Rauen et al. 1993; Sakai et al. 1996; M. S. Gong

et al. 2002; M.-S. Gong et al. 2002; Lee et al. 2013) and conductive polymers. (Macdiarmid 1987) However, also 2D materials were used in recording ambient humidity. In the 2D world, graphene is a trendsetter for the application of novel 2D structures and proved to be useful in form of graphene oxide films. Its capacitance can be influenced by the surrounding water molecules, which was shown by Borini *et al.* with their graphene oxide thin films. These were used for low cost transparent and flexible sensor fabrication with response accuracies of up to 90%. (Borini et al. 2013)

Nevertheless, coming back to the mainly silicon-based sensors and electronics industry (Schulz 1999), SiNSs have become very useful. The previously described goal in this work was focused on encapsulation and protection of freestanding SiNSs (Helbich, Lyuleeva, Höhlein, et al. 2016; Helbich, Lyuleeva, Ludwig, et al. 2016; T. Helbich et al. 2017) for semiconducting device fabrication purposes. (Lyuleeva, Tobias Helbich, Rieger & Lugli 2017; Tobias Helbich et al. 2017; Lyuleeva, Philipp Holzmüller, Helbich, Stutzmann, et al. 2017) Covalent hydrosilylation reactions for hybrid materials and composites were carried out to embed the sheets chemically in a layer, or matrix of organic molecules. However, for the detection of humidity and with it the fabrication of a capacitive humidity sensor, dielectricity is desired over conductivity. The dielectric constant of the material can easily be tuned by ad- or chemisorption of molecules on the surface. For that, the values of the dielectric constants of the active layer and the approaching molecules, which need to be detected, need to be different. This is true for the interaction of oxidized silicon (with a fairly low dielectric constant) and the surrounding water molecules (which have a high dielectric constant). (Y. Wang et al. 2010) This effect may vary with the value of relative permittivity, which can be used for detection purposes.

Additionally, as the example of porous silicon (p-Si) shows, high surface to volume ratio can be a good basis for the fabrication of capacitive humidity sensors. (Y. Wang et al. 2010) The porosity is an important aspect for a fast detection. (Sun et al. 1995) The interface physics and with it the interaction of the molecules with the sensitive material plays a crucial role not only for the sensitivity of the device, but also or the recovery of the material resulting in a fast response which is useful for sensor applications. With facile adsorption-chemisorption and capillary processes of water at an interface, fast humidity change response can be guaranteed. (Adamson & Gast 1997) All these factors can be ensured with the use of oxidized silicon nanosheets (OSiNSs), which were fabricated for nanomaterial based humidity sensing purposes. As already mentioned in chapter 1.2., 2D silicon has a very high surface-to-volume ratio, since (owing to its low dimensionality) this material consists of only surface molecules. (Helbich, Lyuleeva, Ludwig, et al. 2016) This property also leads to the agglomeration of the sheets, which was prevented so far with chemical modification of the surface and subsequent dispersion in different solvents. These stable dispersions can then be used in subsequent fabrication steps. However, this property to easily agglomerate is beneficial for this case, since the agglomeration

leads to stacked structures of 2D silicon layers, which combined with oxidation lead to highly porous packed silicon structures. (Okamoto et al. 2011; Helbich, Lyuleeva, Höhlein, et al. 2016) Additionally, to ensure good interaction with the surface as well as the penetration of the water molecules into the surface of the dielectric material, the physical properties of the interface can be adjusted. In our work, chemical treatment of the nanomaterial gives rise to the functionalization of the SiNSs which was proven to be useful. Hydrophilic groups can be attached to the inorganic material prior to oxidation, enhancing sensitivity, since sensitivity of the devices rises with the hydrophilicity of the surface. (Y. Wang et al. 2010)

4.3.2. Results and Discussion

For the fabrication of an OSiNS-based humidity sensor, SiNSs were synthesized the same way as the SiNSs that were used for the fabrication of the previously discussed SGFETs and photonic sensor (Chapter 4.1. and 4.2.). Sensing devices on both, rigid Si^{++}/SiO_2 as well as flexible polyimide foil (Kapton) were fabricated and characterized. The hereby presented results are also described in the submitted manuscript by Lyuleeva *et al.* (Lyuleeva, Tobias Helbich, Bobbinger, Rieger, et al. 2017) Pictures in Figure 38b and 38c show two examples of two fabricated humidity sensors.

For the fabrication of humidity sensitive material, the surface needed to be chemically modified, in order to assure good interaction with the water molecules during the measurement. Therefore, the synthesized SiNSs have been functionalized with ^{t}BMA molecules, which can easily be covalently bound to the surface of the nanomaterial *via* a radical hydrosilylation reaction with *e.g.,* AIBN as radical initiator. (Lyuleeva, Tobias Helbich, Rieger & Lugli 2017) The SiNS-^{t}BMA hybrid material can then be treated with trifluoromethansulfonic acid to undergo a hydrolyzation reaction, or through so-called saponification. This step allows the synthesis of carboxylic groups and with it of the hybrid material SiNS-methacrylic acid (SiNS-MAA). MAA termination makes the surface hydrophilic and thus accessible to water molecules. Well-defined surface properties and engineering are the key to successful humidity sensitivity of the hereby presented devices, as it will be shown with the comparison of both OSiNS-^{t}BMA and OSiNS-MAA based sensors.

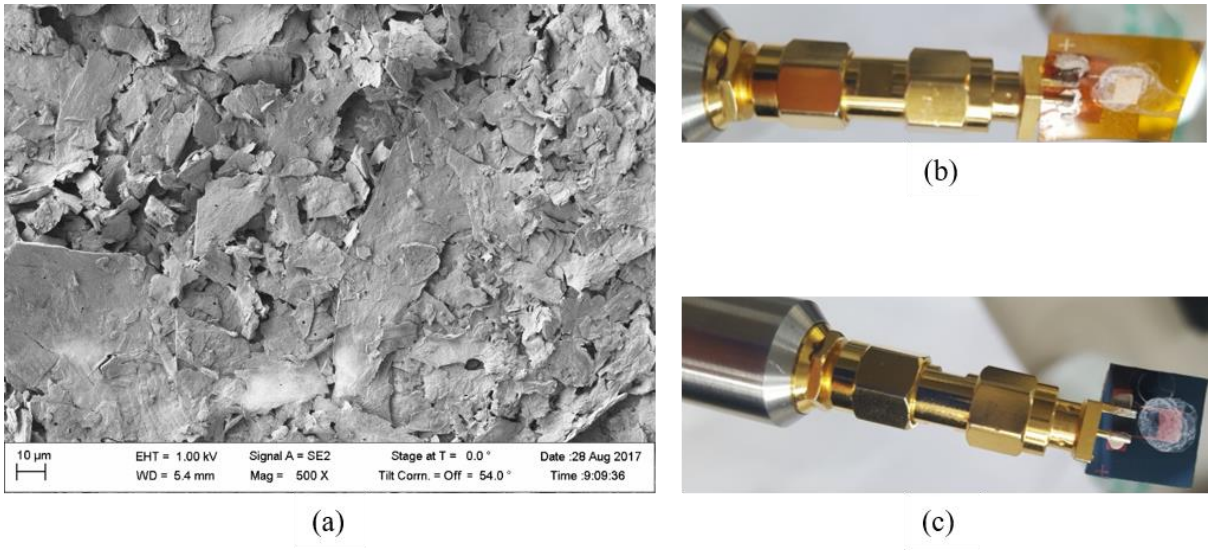

Figure 38. *(a) SEM image of drop-deposited OSiNS-MAA (thickness ≈ 100 nm); (b) OSiNS-MAA drop-casted on IDE Au/Cr (40/5 nm) structure, patterned on polyimide (Kapton, 75 µm) film. Humidity sensing device connected to the measurement set-up and (c) device on Si^{++}/SiO_2 substrate connected to the characterization set-up. Adapted from Lyuleeva et al.* (Lyuleeva, Tobias Helbich, Bobbinger, Rieger, et al. 2017)

For the oxidation of the functionalized SiNSs, the fabricated sensors were placed in the climatic chamber and exposed to several consecutive measurement cycles with elevated temperatures and varying relative humidity (RH) from 20 RH% to 85 RH%. The varying capacitance (nF) *vs.* RH% at a constant temperature and capacitance *vs.* temperature (T) at constant humidity values were recorded until the detected values stabilized and the material turned to a white layer. This color change indicates a successful formation of oxidized silicon. (Y. Wang et al. 2015)

To better understand the surface characteristics of the oxidized matrix, SEM images were taken. These allow the study of the morphology of the oxidized SiNS-^{t}BMA, drop-casted on a supporting surface. Figure 39 shows some examples of these images.

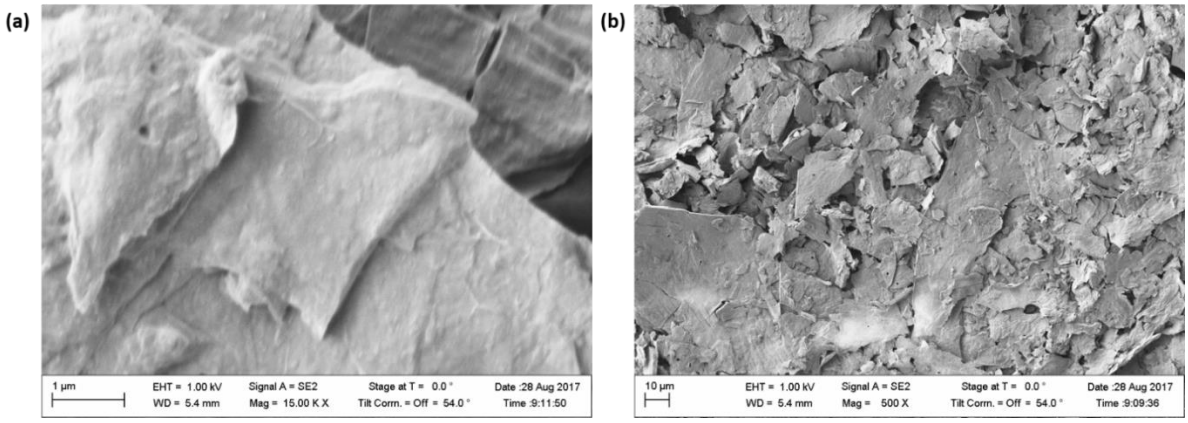

Figure 39: Scanning Electron Microscopy (SEM) images (zoomed in: a) of OSiNS-MAA after consequent measurement cycles. Fully oxidized matrix of stacked silicon layers is the sensitive material of the hereby presented humidity sensor.

As the images show, the oxidized SiNSs are randomly distributed in agglomerated stacks after the drop-deposition on a surface. To assure the reproducibility of the fabrication, exactly 50 µL of the same concentration of the dispersed sheets were used for the drop-deposition. The material was drop-deposited directly precisely on the pre-patterned Cr/Au electrodes in a form of a finger-IDE structure with 50 µm channel length. For the evaporation of the solvent after the deposition, temperatures slightly above the evaporation point of the corresponding solvent were chosen. This careful treatment is necessary to prevent additional local stress on the sheets due to the immediate change of the aggregate state of the solvent, in the presence of large temperatures. The readily fabricated humidity sensing devices are shown in Figure 40. Figure 40a presents OSiNSs deposited on Si^{++}/SiO_2 and incorporated into the set-up, whereas Figure 40b shows OSiNSs on a flexible Kapton substrate. On both images white powder can be clearly seen, indicating the oxidized material.

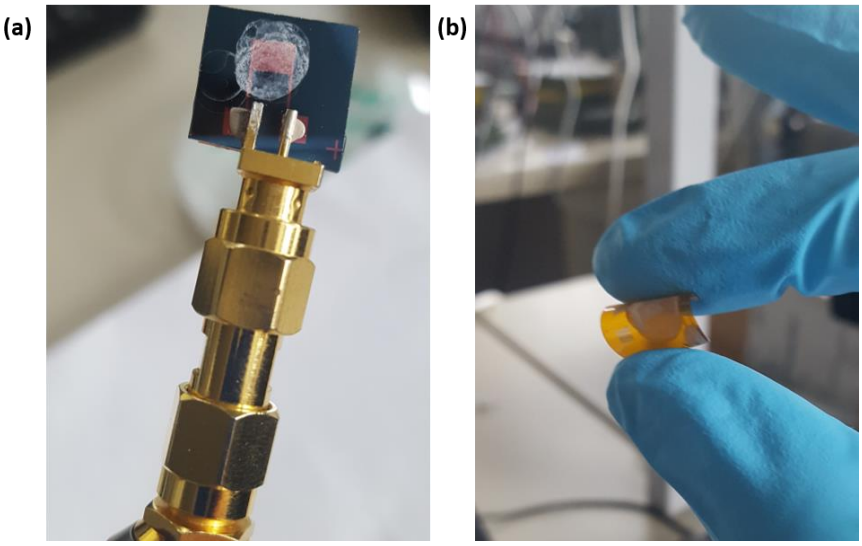

Figure 40: Humidity sensing devices based on OSiNS-MAA drop-deposited on Si^{++}/SiO_2 (a) and flexible Kapton (b) substrate. The as fabricated device can be directly attached to the contacts of the humidity measurement set-up of the climatic chamber, which is shown in figure (a).

Nevertheless, to verify the high porosity of the sheets, AFM images of the as synthesized and oxidized SiNSs were taken (Figure 41).

The image in Figure 41 clearly indicates the difference of plane SiNS-R surface (a) of one sheet with a height of around 4 nm, whereas the oxidized surface of the sheet (b) is rough, containing many holes. In this case, SiNS-$C_{12}H_{25}$ was chosen to verify the general behavior of the differently functionalized sheets towards the oxidation. The AFM images of the hereby studied OSiNS-MAA nanomaterial can be seen in Figure 42.

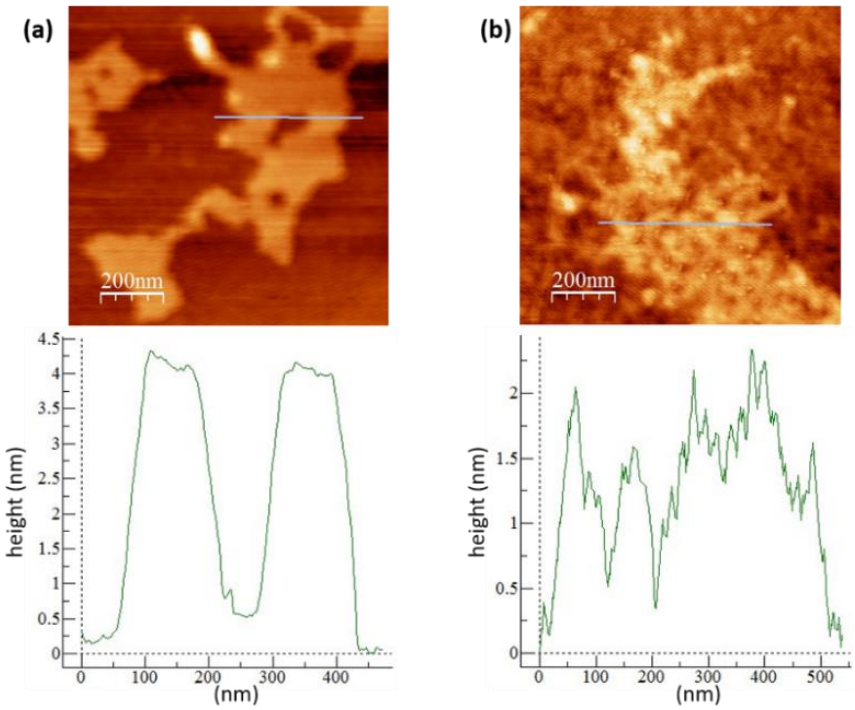

Figure 41: AFM tapping mode images of the on Si^{++}/SiO_2 substrate *spin-coated SiNS-dodecene (a) and oxidized OSiNS-dodecene (b) with their corresponding height profiles along the blue line (under the images respectively). Partly adapted from Helbich et al.* (Helbich, Lyuleeva, Ludwig, et al. 2016)

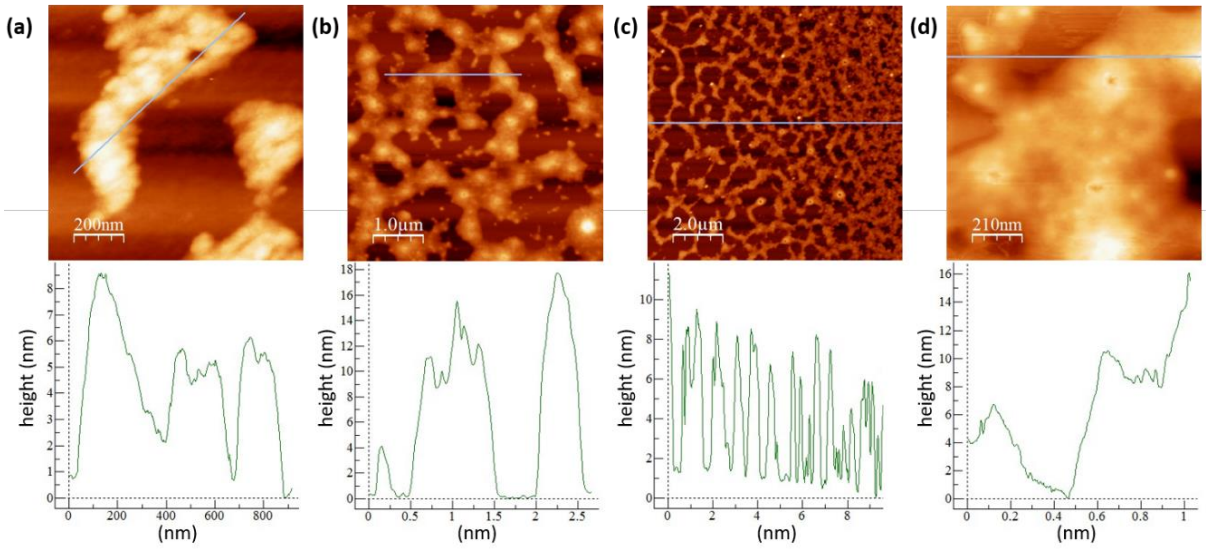

Figure 42. *AFM tapping mode images of OSiNS-MAA dip-deposited on Si^{++}/SiO_2 substrate. Smallest thickness of about 4 nm can be found, followed by stacked nanosheet layers with 8, 12 and 16 nm. The corresponding height diagrams along the blue line are shown under the images. Porous structure of the material is especially visible in 42a. A network of OSiNS-MAA can be built even with dip-deposition (c). Partly adapted from Lyuleeva et al.* (Lyuleeva, Tobias Helbich, Bobbinger, Rieger, et al. 2017)

The scanned OSiNSs with MAA functionalization present a well-distributed structure (Figure 42c) even after the dip-deposition of the material. Especially in figure 42a, the porosity of the oxidized sheets can be recognized. Holes cover the surface with the minimum height of 4 nm. Furthermore, stacked

2D layers on top of each other with 8, 12 and 16 nm heights can be found. Thus, the drop-cast deposition allows fabrication of a highly porous network of the stacked OSiNSs, which enables to establish high surface-to-volume ratio of the sensitive matrix.

The devices were analyzed at 1 kHz, 10 kHz and 100 kHz. Three values were selected to show the frequency response of the devices, although 201 frequency points were recorded.

Figure 43 depicts the capacitance in nF of the OSiNS-MAA layer over time at 1 kHz. Although the shape of the capacitance does not change over time, its nominal value decreases with the factor of 2 until its complete stabilization. The capacitance remains stable after 15 d with the maximum mismatch among curves of less than 0.05% (taken on different days). Looking at this time-response, it is clear that the sensor requires full oxidation of the stacked SiNS-MAA layers to form a highly porous OSiNS-MAA matrix for a constant and reproducible response over time with a mainly capacitive behavior. The capacitance varies with respect to any value of %RH but its changes are significant above 60 %RH.

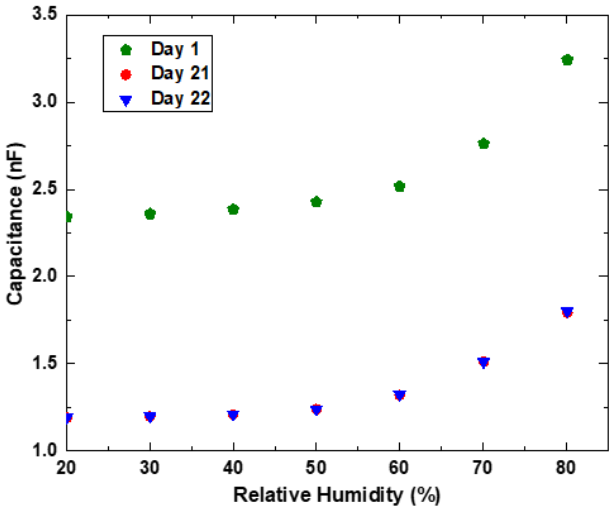

Figure 43. *Capacitance (nF) vs. RH (%) of the hydrolyzed and oxidized film (OSiNS-MAA) over time at 40ºC and 1 kHz. The OSiNS-MAA were drop-deposited on Si^{++}/SiO_2 surface on the pre-patterned Cr/Au IDE structure. Adapted from Lyuleeva et al.* (Lyuleeva, Tobias Helbich, Bobbinger, Rieger, et al. 2017)

From this point, the characterization corresponds to the data obtained after 15 d measurement. With respect to the hysteresis of the sensor, which is well-visible in Figure 44, the maximum error between the ascending (increasing RH (%) values) and descending (decreasing RH (%) values) response of the sensor is about 1% at 1 kHz, while at higher frequencies the maximum hysteresis is below 0.3%.

The capacitance decreases with frequency from about 1.2 nF at 1 kHz to 1.8 nF at 100 kHz, which means that a reduction of two orders of magnitude in two decades takes place. During the dissipation, energy is transformed into other forms and is eventually lost to the environment. Hereby, there are more losses at low frequency and at higher values of RH, whose value is above $5 \cdot 10^{-2}$ when RH > 60%

at 1 kHz. Contrary to that, the dissipation factor is below 10^{-2} in the hereby measured range of RH, studied for frequencies above 8 kHz.

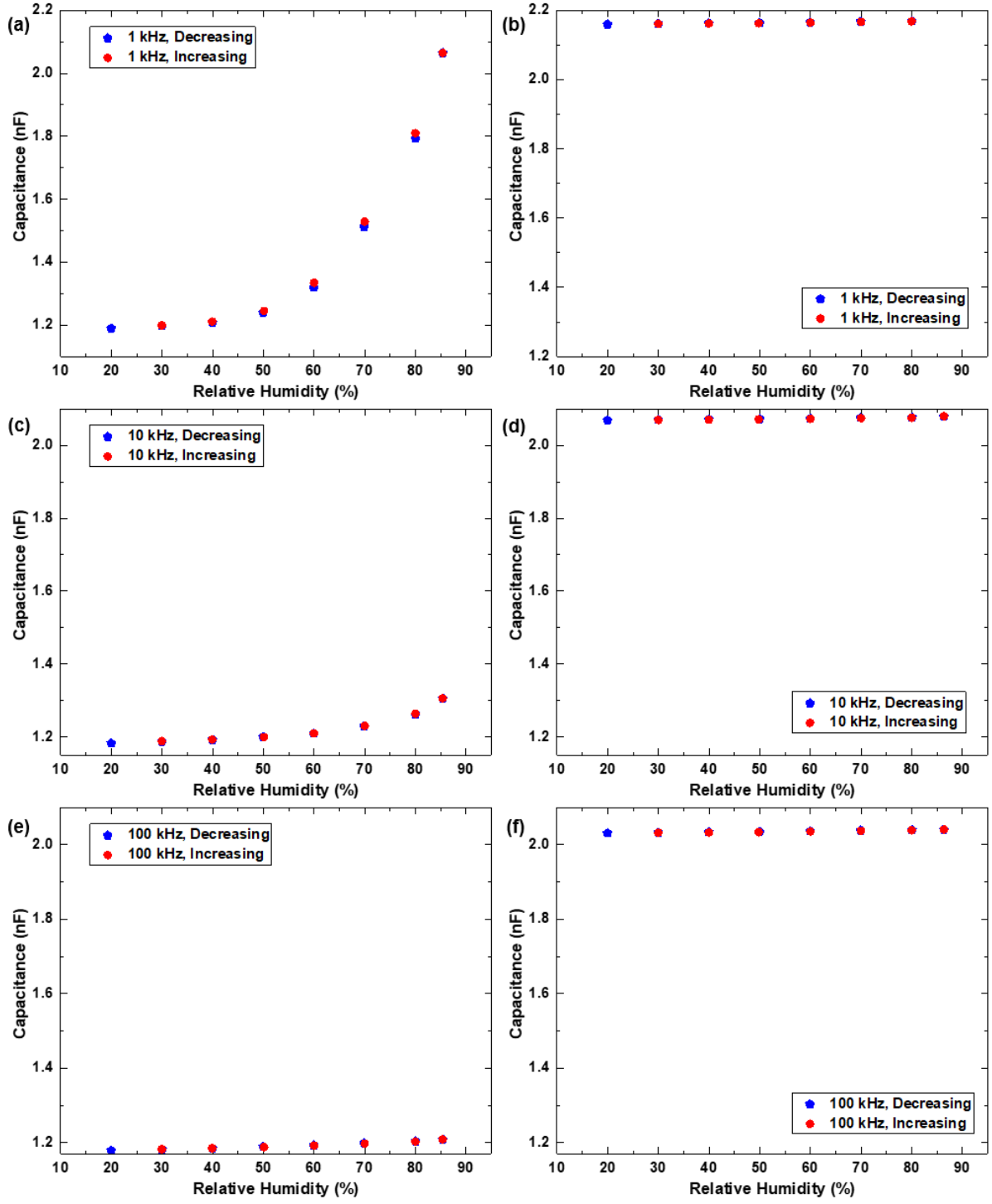

Figure 44. *Capacitance for increasing and decreasing RH at 40°C and 1 kHz of OSiNS-MAA film (a) and OSiNS-^{t}BMA film (b); at 10 kHz of OSiNS-MAA film (c) and OSiNS-^{t}BMA film (d) and at 100 kHz of OSiNS-MAA film (e) and OSiNS-^{t}BMA film (f) on Si^{++}/SiO_2. Adapted from Lyuleeva et al.* (Lyuleeva, Tobias Helbich, Bobbinger, Rieger, et al. 2017)

The humidity sensitive response was measured for both films, SiNS-^{t}BMA and SiNS-MAA, to demonstrate the effect of the hydrolyzation of the ^{t}BMA functional groups. Once again, sensitivity increases with hydrophilicity. Figure 44 illustrates the calibration curves of both OSiNS-MAA (left graphs) and OSiNS-^{t}BMA (right graphs) films at the studied frequencies with increasing and decreasing moisture content.

At lower frequencies, there is a bigger change in capacitance in both films. The initial capacitance for the OSiNS-MAA is about 1.2 nF and is independent of frequency. Its response is quadratic or adjustable by two lines: below and above 60 %RH. Only at 100 kHz is the shape of the curve capacitance (nF) *vs.* RH (%) linear. In contrast to that, for the rather hydrophobic OSiNS-^{t}BMA layer the capacitance is about 2.1 nF. However, this value is negligible, since it shows values less than 0.1 nF in the studied RH range (20 %RH to 80 %RH).

The temperature was also varied during the measurements. During the sensing process it is one of the most influential environmental factors. Both hereby presented devices were evaluated and their capacitance at different temperatures is shown in Figure 45.

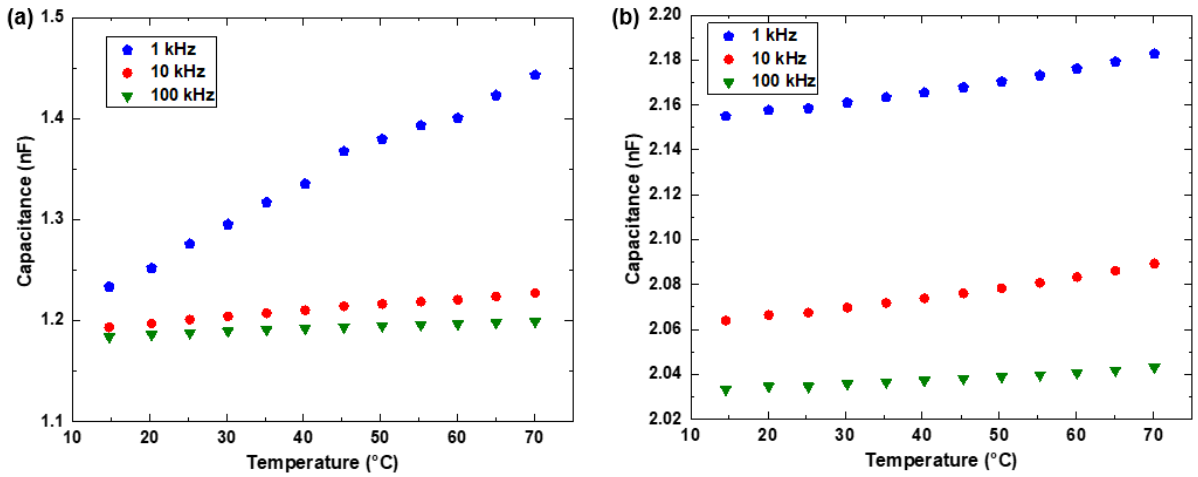

Figure 45. *Capacitance (nF) vs. Temperature (°C) at 60 %RH and different frequencies for the drop-deposited OSiNS-MAA film (a) and the OSiNS-^{t}BMA film (b) on Si^{++}/SiO_2 surface with pre-patterned Cr/Au IDE structure. Adapted from Lyuleeva et al.* (Lyuleeva, Tobias Helbich, Bobbinger, Rieger, et al. 2017)

Both films, OSiNS-MAA as well as OSiNS-^{t}BMA are temperature dependent. For OSiNS-MAA at 1 kHz, the thermal drift is 5 times lower compared to the sensitivity towards RH. However, at other frequencies the variation with the temperature is comparable with the frequency *vs.* RH change. In conclusion, it highlights the necessity of thermal compensation to obtain an accurate value of RH.

The sensor response was studied in more detail. Thus, the partial sensitivities of the capacitance to RH (S_{RH}) and the temperature (S_T) were defined as a function of the measurement frequency (f) (Equations 3 & 4).

$$S_{RH}(f) \equiv \frac{\partial C_{T=cte}\,(RH)}{\partial\, RH} \quad (3)$$

$$S_{T}(f) \equiv \frac{\partial C_{\mathrm{RH}=cte}\,(T)}{\partial\, T} \quad (4)$$

All measurements show that the coefficient of correlation is higher than 0.98, indicating a good linearity (Table 4). Sensitivity of the OSiNS-^{t}BMA film towards RH is higher at 100 kHz, which is contrast to the OSiNS-MAA film response. In the case of the thermal sensitivity, both devices show the same trend over frequency.

Table 4: Summary of sensitivities to RH and temperature for both characterized drop-deposited and oxidized films: OSiNS-MAA and OSiNS-^{t}BMA

	Frequency (kHz)	**OSiNS-MAA film**	**OSiNS-^{t}BMA film**
S_{RH} (pF/%RH)	1	1.60 for RH< 60% 28.40 for RH< 60%	0.10
	10	0.70 for RH< 60% 3.60 for RH< 60%	0.10
	100	0.50	0.20
S_T (pF/ºC)	1	3.80	0.50
	10	0.60	0.40
	100	0.30	0.20

The hydroxylation of the ^{t}BMA functional groups on the surface of the SiNSs as a tool to gain hydrophilicity, which is suitable for the goal sensitivity, can lead to a good response of the silicon-based nanomaterial towards RH. The hereby studied MAA functionalized and oxidized SiNSs films show a capacitance of 1.2 nF at 1 kHz in ambient conditions and a sensitivity of about 1.6 pF/%RH below 60 %RH and 28.4 pF/%RH above this RH value. The response is not linear, but it exhibits good reproducibility and small hysteresis (less than 0.2% in the whole RH range).

As expected, no change with RH could be detected with the rather hydrophobic OSiNS-^{t}BMA layer. Its response towards temperature is 5 times higher at 1 kHz than its variation with moisture content. By comparing the response of common polymer humidity sensors with our device, one will realize that these significant changes in capacitance are extremely high. In polymer based sensors the capacitance increases by only a few units (Rivadeneyra et al. 2016; Trung et al. 2017). However, this thermal drift

can be easily compensated by adding a meandered metal line as resistive temperature sensor. (Molina-Lopez et al. 2012; Kinkeldei et al. 2011)

Wang *et al.* demonstrated the characteristics of humidity sensing devices based on macroporous silicon, which was modified with a metal oxide layer. (Y. Wang et al. 2010) This sensor has shown a maximum hysteresis of 3.3 % at 200 kHz. Additionally, it presented good repeatability and long-term stability. The capacitance of this sensor increased with RH increase with a behavior in frequency, comparable with the hereby studied OSiNS-MAA films. Wang *et al.* demonstrated that substitution in the porous space of air by adsorbed water molecules, which caused the variation in capacitance during the exposure to RH. This process could also be found in the hereby studied system, explaining the sensitivity of the highly porous layered OSiNS-MAA. With respect to the sensitivity, the sensor of Wang *et al.* was twice as sensitive as our OSiNS-MAA based device. However, the OSiNS-MAA sensor is one order of magnitude smaller than the sensor made by Wang *et al.* The importance of this finding is that capacitance (and therefore sensitivity) is proportional to the area of a device. Thus, for an order of magnitude reduction in size, one would expect an order of magnitude reduction in sensitivity, which we are clearly showing isn't the case.

Finally, it is important to notice that the surface modification of our sensor can be further used for subsequent (bio)molecules immobilization. These (bio)molecules could target the precise detection of, for example, various surrounding substrates (Melzer et al. 2016; Caterino et al. 2015) or gas molecules (Balasubramanian & Burghard 2005; Lim et al. 2010), depending on the functionality of the attached enzyme, or molecular group respectively.

4.3.3. Summary

These results present an important surface modification technique as an approach, which can be applied to achieve sensor array selectivity. The devices described in this work show how the functionalization of SiNSs with hydrophilic functional groups can be used to improve the sensitivity of OSiNSs based devices towards RH. These sensors and the hereby presented technique can be helpful for novel technology, which is in search of cheap and reproducible methods, without sacrificing the quality of the sensor systems. Furthermore, it enables manufacturing of devices that are sensitive to specific molecules. The hereby presented work uses straightforward syntheses in materials' chemistry, which can be applied as a tool for new and promising fabrication solutions.

5. SUMMARY AND OUTLOOK

This dissertation presents cutting-edge research, combining Chemistry, Physics and Engineering, which helps to improve and broaden the spectrum of novel approaches in nanotechnology. The results presented in this work do not only build a fundamental bridge between the theoretical research and the preparative studies, but also provide solid ground for a new mind-set for reaching the desired goals in novel sensing and (opto)electronic technologies. The main goal is to provide guidance for scientists who work in the currently vital area of 2D nanomaterials - especially on the interface between the mentioned research fields - and with it help them benefit from the herein presented results.

Freestanding 2D silicon was recently introduced to the nanomaterials community and became the main material for our research. It is believed to exhibit not only new, but also outstanding (opto)electronic properties. These properties were predicted and confirmed with a variety of theoretical calculations, followed eventually by experimental confirmation.

In this work, chemical exfoliation was used for the synthesis of hydrogenated SiNSs, starting with the deintercalation of calcium ions from the crystalline $CaSi_2$ compound. As a result, slightly buckled free-standing 2D silicon sheets ranging from hundreds of nanometers to micrometers in size were obtained. These sheets have been used for further radical hydrosilylation steps to chemically functionalize the surface of the nanomaterial. Being nearly planar, the small dimensions of SiNSs open up new properties and possibilities. Some examples are the green PL at around 510 nm, whose exact origin was studied with the help of TRPL and TIPL measurements. Understanding the origin of the band gap, the ability to tune it with functional groups covalently attached to the surface and the application of the semiconducting behavior of the SiNSs were the main subjects of this work.

To enable the use of these nanomaterials in ambient conditions and especially for facile and big scale fabrication, they need to be stabilized. The 2D-sheets tend to agglomerate easily due to their high surface-to-volume ratio. Furthermore, they can be destroyed by high energy light (UV light) and reaction with oxygen. As a result, the formation of silicon oxide, or silicon dioxide takes place, forming an insulator with a wide energy band gap. This makes SiNSs not suitable for electronic applications as semiconductor material. The stabilization of SiNSs can be reached with the help of covalent surface functionalization, which was carried out in close collaboration with the group of Prof. Rieger at the chair of Macromolecular Chemistry (TU Munich). Organic groups such as dodecene, styrene or *tert*-butyl methacrylate (^{t}BMA) were successfully attached using diazonium salt initiators for the first, or thermal/AIBN induced reactions for the last two examples. As the related work, described in the

dissertation of Dr. Helbich (TUM, Chair of Macromolecular Chemistry, 2017) presents, the lifetime of these silicon monolayers can be increased dramatically. Additionally, their fabrication is facilitated with different material deposition techniques, such as for example spray-deposition or spin-coating. Furthermore, dispersed solutions can be used in the future for the fabrication of highly precise, reproducible and ultra-low-cost conductive patterns *via* inkjet printing technique, which is currently under further investigation in our group.

Physical strain on the SiNSs, the underlying substrate, external electrical fields and surface functionalization are predicted to have an influence on the band gap of the 2D silicon. These external influences may be able to manipulate the range of the band gap and need to be investigated in more detail. They are believed to be useful for direct manipulation of the PL, leading to light emission of different wavelengths.

The results presented herein, describe the attempt to shift the PL with the help of chemical surface modification. Nevertheless, no promising results could be achieved so far. Interestingly, all these SiNSs based composites, hybrid materials and bare freestanding sheets (SiNS-H) exhibit the consistent green PL at around 510 nm. As already mentioned, this PL could neither be shifted with the various covalent functionalizations on the surface, nor with the temperature. No one has studied and understood the origin of this light emission of the SiNSs so far. Thus, for the first time time-resolved PL and time-integrated PL studies have been carried out in combination with measurements at different temperatures (from room temperature down to 5 K). As a result, our group could confirm that the PL is band-like. Additionally, we observed a long exponential tail, also referred to as the Urbach tail, which is due to the band-tail states. It arises from the 'locked-in' structural disorder in the sheets, present due to the nature of the SiNSs after their chemical exfoliation. To liberate the sheets from their packed structure in the crystalline $CaSi_2$, harsh conditions, such as various solvents, ultra-sonication, freeze-drying, chemical treatment with hydrochloric acid and hydrofluoric acid have been undertaken. Each step causes damage to the 2D structure, which might result in additional disorder of the surface and holes in the sheets. This disorder additionally ranges with the type of the molecules which were covalently attached to the surface. This has exclusively an impact on the Urbach band-tail and could be clearly observed with our measurements. Already these results do not only build a fundamental bridge between the knowledge of the physics of the herein described material and the preparative studies, but also provide solid ground for a so far not described behavior of the disorder dependent band-tail states in 2D systems.

Based on the investigations described, new devices such as *e.g.,* SiNSs based field-effect transistors, photonic or humidity sensors can be fabricated. We showed that SiNSs-polymer based composites can

be formed *via* simultaneous radical functionalization of SiNSs and polymer matrix formation (polymer = polystyrene, poly(acrylic acid)). As a result, a three-dimensional network is formed, which opens up even more new possibilities for application due to the added features of the polymer. New photosensitive devices can be built based on these composites. Especially in the case of polystyrene, SiNS-PS@PS can be synthesized and melted on top of pre-patterned gold electrodes, forming an optoelectronic sensor. Highly sensitive optical response can be detected using this device, while exposing it to a light source with wavelengths under around 450 nm.

Another successful way to realize the SiNSs in the applied nanotechnology field was found to be the improvement of the already well-known P3HT based solution-gated FETs. For the desired combination with the up to now widely used organic semiconducting polymer P3HT, the surface of the SiNSs was modified with various functional groups. The choice of these groups was concentrated on the precise engineering of the nanomaterial's surface, with the aim to establish best interaction with the polymer chains. Thus, most homogeneous thin films could be fabricated for the desired SGFETs. At the same time, its remarkable properties, such as the green PL, ambipolarity and semiconductivity were preserved. Surface modification with thiophene acetylene functional molecules has proven to be the best approach, due to the molecule's chemical and physical similarity to the repeating units, which are found within the P3HT. As a result, the herein mentioned combination of chemically modified SiNSs with P3HT lead to the fabrication of an improved hybrid material based SGFET with ON currents 4 times higher than the ones of the solely P3HT based devices.

Up to now, protection of the SiNSs from external influences, such as oxygen and light for further application as ambipolar semiconducting material was the main aim of the herein described research.

Nevertheless, with the next application we went beyond the classic approach of SiNSs' synthesis, functionalization and incorporation into the already well-known fabrication techniques: our group concentrated on the application possibilities of the byproducts, namely the silicon (di)oxide, which were by now rather avoided than intended. With the third application we demonstrate that the oxidation of SiNSs leads to a highly porous material OSiNSs, which shows remarkable sensitivity towards humidity. Additional functionalization with hydrophilic molecules enables precise engineering of the surface. It allows the surrounding water molecules to approach and interact with the sensitive material directly at the interface and also within the pores, yielding a highly sensitive response to humidity and temperature changes. Herein, ^{t}BMA was used as the organic molecule for modification of the surface. The *tert*-butylic ester group of the methacrylic acid, can be exposed to hydroxylation. This reaction step leads to the formation of carboxylic groups on top of the surface and thus results in a facile transformation of the properties of the hybrid material from hydrophobic to

hydrophilic. Due to the surrounding water molecules, which can now easily interact with the hydrophilic hybrid material and influence its dielectric behavior, a change in the capacitance can be detected. The material's response to humidity (25 %RH to 95 %RH) and temperature were successfully detected.

In conclusion, these results do not only build a fundamental bridge between theoretical research, understanding of the basic physical and chemical behavior of the inorganic material and its fabrication techniques, but also provide solid ground for a new mind-set for reaching the desired goals in nanotechnology. This original work can be applied to further novel nanomaterials and facilitate their treatment and subsequent application in novel devices. For example, SiNS can be combined with other monolayered nanostructures such as phosphorene, germanene, graphene and further newly synthesized 2D monolayers. The 2D research community is concentrating on the fabrication of self-stacking heterostructures, relying on the basic physical forces such as van der Waals interactions between the sheets. They promise to open new possibilities for application by widening the range of the fundamental and so far unexplored properties.

6. REFERENCES

Abdellah, A. et al., 2009. Exploring spray technology for the fabrication of organic devices based on poly(3-hexylthiophene). *2009 9th IEEE Conference on Nanotechnology (IEEE-NANO)*, 8, pp.831–834.

Abdellah, A. & Abdelhalim, A., 2013. Flexible Carbon Nanotube Based Gas Sensors Fabricated by Large-Scale Spray Deposition. *IEEE Sensors Journal*, 13(October), pp.4014–4021. Available at: http://ieeexplore.ieee.org/iel7/7361/6583958/06527935.pdf?arnumber=6527935.

Adamson, A.W. & Gast, A.P., 1997. *Physical Chemistry of Surfaces* 6th ed., New York. Available at: http://www.degruyter.com/doi/10.1524/zpch.1999.210.Part_1.134.

Al-Ibrahim, M. et al., 2005. The influence of the optoelectronic properties of poly(3-alkylthiophenes) on the device parameters in flexible polymer solar cells. *Organic Electronics: physics, materials, applications*, 6(2), pp.65–77.

Allen, B.L., Kichambare, P.D. & Star, A., 2007. Carbon nanotube field-effect-transistor-based biosensors. *Advanced Materials*, 19(11), pp.1439–1451.

Anslyn, E. V. & Dougherty, D.A., 2005. Modern Physical Organic Chemistry. In *Modern Physical Organic Chemistry*. University Science Books.

Apeloig, Y. et al., 2000. Polysilyl radicals: EPR study of the formation and decomposition of star polysilanes. *Applied Magnetic Resonance*, 18(3), pp.425–434.

Arivalagan, K. et al., 2011. Nanomaterials and its potential applications. *International Journal of ChemTech Research*, 3(2), pp.534–538.

Aswal, D.K. et al., 2006. Self assembled monolayers on silicon for molecular electronics. *Analytica Chimica Acta*, 568(1–2), pp.84–108.

Aufray, B. et al., 2010. Graphene-like silicon nanoribbons on Ag(110): A possible formation of silicene. *Applied Physics Letters*, 96(18), pp.1–4.

Balasubramanian, K. & Burghard, M., 2005. Chemically functionalized carbon nanotubes. *Small*, 1(2), pp.180–192.

Balendhran, S. et al., 2015. Elemental analogues of graphene: Silicene, germanene, stanene, and phosphorene. *Small*, 11(6).

Barkelid, M. & Zwiller, V., 2013. Photocurrent generation in semiconducting and metallic carbon

nanotubes. *Nature Photonics*, 8(January), pp.47–51. Available at: http://dx.doi.org/10.1038/nphoton.2013.311%5Cnhttp://www.nature.com/doifinder/10.1038/nphoton.2013.311.

Barreda, J.L. et al., 2017. Multiple Schottky Barrier-Limited Field-Effect Transistors on a Single Silicon Nanowire with an Intrinsic Doping Gradient. *ACS Applied Materials and Interfaces*, 9(13), pp.12046–12053.

Baum, M. & Brittain, W.J., 2002. Synthesis of Polymer Brushes on Silicate Substrates via Reversible Addition Fragmentation Chain Transfer Technique. *Society*, pp.610–615.

Bekyarova, E. et al., 2009. Chemical Modification of Epitaxial Graphene:Spontaneous Grafting of Aryl Groups. *Journal of American Chemical Society*, 131(2), pp.1336–1337.

Bianco, E. et al., 2013. Stability and Exfoliation of Germanane : A Germanium Graphane Analogue. , (5), pp.4414–4421.

Blanksby, S.J. & Ellison, G.B., 2003. Bond dissociation energies of organic molecules. *Accounts of Chemical Research*, 36(4), pp.255–263.

Bo, X.Z. et al., 2005. Carbon nanotubes-semiconductor networks for organic electronics: The pickup stick transistor. *Applied Physics Letters*, 86(18), pp.1–3.

Böhm, J.; Hassel, O., 1927. Die Kristallstruktur des Calciumsilicids CaSi,. *Z. anorg. allg. Chem.*, 160, p.152.

Borini, S. et al., 2013. Ultrafast Graphene Oxide Humidity Sensors. *ACS Nano*, 7(12), pp.11166–11173.

Brennan, M.D., Morishita, T. & Spencer, M.J.S., 2016. Tuning the band gap of silicene by functionalisation with naphthyl and anthracyl groups. *The Journal of Chemical Physics*, 144(11), p.114704. Available at: http://scitation.aip.org/content/aip/journal/jcp/144/11/10.1063/1.4943880.

Brennan, M.D., Morishita, T. & Spencer, M.J.S., 2016. Tuning the band gap of silicene by functionalisation with naphthyl and anthracyl groups. *Journal of Chemical Physics*, 144(11). Available at: http://dx.doi.org/10.1063/1.4943880.

Brinkmann, M. & Rannou, P., 2007. Effect of molecular weight on the structure and morphology of oriented thin films of regioregular poly(3-hexylthiophene) grown by directional epitaxial solidification. *Advanced Functional Materials*, 17(1), pp.101–108.

Brumfiel, G., 2013. Sticky problem snares wonder material. *Nature*, 495, p.152.

Brus, L., 1994. Luminescence of Silicon Materials: Chains, Sheets, Nanocrystals, Nanowires, Microcrystals, and Porous Silicon. *The Journal of Physical Chemistry*, 98(14), pp.3575–3581.

Buriak, J.M., 2002. Organometallic chemistry on silicon and germanium surfaces. *Chemical Reviews*, 102(5), pp.1271–1308.

Buscema, M. et al., 2015. Photocurrent generation with two-dimensional van der Waals semiconductors. *Chem. Soc. Rev.*, 44, pp.3691–3718. Available at: http://xlink.rsc.org/?DOI=C5CS00106D.

Cahangirov, S. et al., 2013. Electronic structure of silicene on Ag(111): Strong hybridization effects. *Physical Review B*, 88(3), p.35432.

Cahangirov, S. et al., 2009. Two- and one-dimensional honeycomb structures of silicon and germanium. *Physical Review Letters*, 102(June), pp.1–4.

Canham, L.T., 1990. Silicon quantum wire array fabrication by electrochemical and chemical dissolution of wafers. *Applied Physics Letters*, 57(10), pp.1046–1048.

Caterino, R. et al., 2015. Photocurrent generation in diamond electrodes modified with reaction centers. *ACS applied materials & interfaces*, 7(15), pp.8099–107.

Ceuster, J. De et al., 2001. High-frequency (95 GHz) electron paramagnetic resonance study of the photoinduced charge transfer in conjugated polymer-fullerene composites. *Physical Review B*, 64(19), p.195206. Available at: https://link.aps.org/doi/10.1103/PhysRevB.64.195206.

Chakraborty, S. et al., 1999. Moisture sensitive field effect transistors using \mathrm{SiO_2/Si_3N_4/Al_2O_3} gate structure. *Smart Materials and Structures*, 8(2), pp.274–277. Available at: http://iopscience.iop.org/0964-1726/8/2/014.

Chandiramouli, R. & Nagarajan, V., 2016. Adsorption studies of NH3 molecules on functionalized germanene nanosheet - A DFT study. *Chemical Physics Letters*, 665, pp.22–30. Available at: http://dx.doi.org/10.1016/j.cplett.2016.10.048.

Chen, W. et al., 2007. Surface Transfer p-Type Doping of Epitaxial Graphene Surface Transfer p-Type Doping of Epitaxial Graphene. *J. Am. Chem. Soc.*, 129(16), pp.10418–10422.

Chen, Z. & Lu, C., 2005. Humidity Sensors: A Review of Materials and Mechanisms. *Sensor Letters*, 3(4), pp.274–295. Available at: http://www.ingentaselect.com/rpsv/cgi-bin/cgi?ini=xref&body=linker&reqdoi=10.1166/sl.2005.045.

Chiappe, D. et al., 2012. Local electronic properties of corrugated silicene phases. *Advanced Materials*,

24(37), pp.5088–5093.

Chiappe, D. et al., 2014. Two-dimensional Si nanosheets with local hexagonal structure on a MoS 2 surface. *Advanced Materials*, 26(13), pp.2096–2101.

Chimene, D., Alge, D.L. & Gaharwar, A.K., 2015. Two-Dimensional Nanomaterials for Biomedical Applications: Emerging Trends and Future Prospects. *Advanced Materials*, 27(45), pp.7261–7284.

Chow, W.L. et al., 2017. High Mobility 2D Palladium Diselenide Field-Effect Transistors with Tunable Ambipolar Characteristics. *Advanced Materials*, 29(21), pp.1–8.

Chowdhury, S. & Jana, D., 2016. A theoretical review on electronic, magnetic and optical properties of silicene. *Reports on Progress in Physics*, 79(12), p.126501.

Chuang, C.M. et al., 2014. Through Band Alignment Engineering. *Nat Mater.*, 13(8), pp.796–801.

D'apuzzo, M. et al., 2000. Sol-Gel Synthesis of Humidity-Sensitive P2O5-SiO2 Amorphous Films. *Journal of Sol-Gel Science and Technology*, 17, pp.247–254.

Dahn, J.R. et al., 1993. Structure of siloxene and layered polysilane (Si6H6). *Physical Review B*, 48(24), pp.17872–17877.

Dalgarno, A. & Kingston, A.E., 1959. Van der Waals Forces. *Proc. Phys. Soc.*, 73, p.455.

Dasog, M. et al., 2013. Chemical insight into the origin of red and blue photoluminescence arising from freestanding silicon nanocrystals. *ACS Nano*, 7(3), pp.2676–2685.

Dasog, M. et al., 2016. Silicon nanocrystals and silicon-polymer hybrids: Synthesis, surface engineering, and applications. *Angewandte Chemie - International Edition*, 55(7), pp.2322–2339.

Dasog, M. et al., 2014. Size vs Surface: Tuning the Photoluminescence of Freestanding Silicon Nanocrystals Across the Visible Spectrum via Surface Groups. *ACS Nano*, 8(9), pp.9636–9648.

Degoli, E. & Ossicini, S., 2000. The electronic and optical properties of Si/SiO2 superlattices: role of confined and defect states. *Surface Sc*, 470, pp.32–42.

Delerue, C., Allan, G. & Lannoo, M., 1993. Theoretical aspects of the luminescence of porous silicon. *Physical Review B*, 48(15), pp.11024–11036.

Delley, B. & Steigmeier, E.F., 1993. Quantum confinement in Si nanocrystals. *Physical Review B*, 47(3), pp.1397–1400. Available at: http://link.aps.org/doi/10.1103/PhysRevB.47.1397.

Derr, J. et al., 2009. Quantum confinement regime in silicon nanocrystals. *Physica E: Low-Dimensional*

Systems and Nanostructures, 41(4), pp.668–670.

Dettlaff-Weglikowska, U. et al., 1997. Structure and optical properties of the planar silicon compounds polysilane and Wohler siloxene. *Physical Review B*, 56(20), pp.13132–13140.

Dietmueller, R. et al., 2009. Light-induced charge transfer in hybrid composites of organic semiconductors and silicon nanocrystals. *Applied Physics Letters*, 94(11).

Ding, Y. & Wang, Y., 2012. Electronic structures of silicene fluoride and hydride. *Applied Physics Letters*, 100(8), p.83102.

Du, Y. et al., 2014. Device perspective for black phosphorus field-effect transistors: Contact resistance, ambipolar behavior, and scaling. *ACS Nano*, 8(10), pp.10035–10042.

Edmondson, S., Osborne, V.L. & Huck, W.T.S., 2004. Polymer brushes via surface-initiated polymerizations. *Chemical Society Reviews*, 33(1), p.14. Available at: http://xlink.rsc.org/?DOI=b210143m.

Elias, D.C. et al., 2009. Control of Graphene's Properties by Reversible Hydrogenation: Evidence for Graphane. *Science*, 323(January), pp.610–613.

Erickson, D. et al., 2008. Nanobiosensors: Optofluidic, electrical and mechanical approaches to biomolecular detection at the nanoscale. *Microfluidics and Nanofluidics*, 4(1–2), pp.33–52.

Feng, B. et al., 2012. Evidence of silicene in honeycomb structures of silicon on Ag (111). *Nano letters*, 12(7), pp.3507–3511.

Fiori, G. et al., 2014. Electronics based on two-dimensional materials. *Nature nanotechnology*, 9(October), pp.768–779.

Fleurence, A. et al., 2012. Experimental evidence for epitaxial silicene on diboride thin films. *Physical Review Letters*, 108(24), pp.1–5.

Fuchs, H.D. et al., 1992. Visible luminescence from porous silicon and siloxene. *Physica Scripta*, T45, pp.309–313.

Gang, C., Peng-Fei, L. & Zi-Tao, L., 2013. Influence of strain and electric field on the properties of silicane. *Chinese Physics B*, 22(4), p.46201. Available at: http://stacks.iop.org/1674-1056/22/i=4/a=046201?key=crossref.3bacdff018b241cd7fd800c368c89f03.

Gao, N., Zheng, W.T. & Jiang, Q., 2012. Density functional theory calculations for two-dimensional silicene with halogen functionalization. *Physical Chemistry Chemical Physics*, 14(1), p.257.

Available at: http://www.ncbi.nlm.nih.gov/pubmed/22083171.

Gatoo, M.A. et al., 2014. Physicochemical properties of nanomaterials: Implication in associated toxic manifestations. *BioMed Research International*, p.498420.

Geim, A.K. & Novoselov, K.S., 2007. The rise of graphene. *Nature materials*, 6, pp.183–191.

Gong, M.-S., Joo, S.-W. & Choi, B.-K., 2002. Humidity-sensitive properties of a cross-linked polyelectrolyte prepared from mutually reactive copolymers. *Journal of Materials Chemistry*, 12(4), pp.902–906. Available at: http://xlink.rsc.org/?DOI=b108647m.

Gong, M.S., Joo, S.W. & Choi, B.K., 2002. Humidity sensor using mutually reactive copolymers containing quaternary ammonium salt and reactive function. *Sensors and Actuators, B: Chemical*, 86(1), pp.81–87.

Grazianetti, C., Cinquanta, E. & Molle, A., 2016. Two-dimensional silicon: the advent of silicene. *2D Materials*, 3(1), p.12001. Available at: http://www.scopus.com/inward/record.url?eid=2-s2.0-84964452703&partnerID=tZOtx3y1.

Guo, Q. et al., 2016. Black phosphorus mid-infrared photodetectors with high gain. *Nano Letters*, 16(7), pp.4648–4655.

Guo, Z.-X. et al., 2013. Absence of Dirac Electrons in Silicene on Ag(111) Surfaces. *Journal of the Physical Society of Japan*, 82(6), p.63714.

Guo, Z.X. et al., 2015. Structural evolution and optoelectronic applications of multilayer silicene. *Physical Review B - Condensed Matter and Materials Physics*, 92(20), pp.1–13.

Guzmán-Verri, G.G. & Lew Yan Voon, L.C., 2011. Band structure of hydrogenated Si nanosheets and nanotubes. *Journal of physics. Condensed matter : an Institute of Physics journal*, 23(14), p.145502. Available at: http://www.ncbi.nlm.nih.gov/pubmed/21430307.

Guzmán-Verri, G.G. & Lew Yan Voon, L.C., 2007. Electronic structure of silicon-based nanostructures. *Physical Review B - Condensed Matter and Materials Physics*, 76(7).

Handy, J., 2014. The Biggest Problem Facing Semiconductors. *online*. Available at: https://www.forbes.com/sites/jimhandy/2014/04/30/the-biggest-problem-facing-semiconductors/#53725cd35093.

Harun, N.I. et al., 2012. Resistive-type Humidity Sensor Based on CA-NH4BF4-PEG600 Thin Films. *Physics Procedia*, 25, pp.221–226. Available at: http://linkinghub.elsevier.com/retrieve/pii/S1875389212004919.

Helbich, T. et al., 2017. Diaryliodonium salts as hydrosilylation initiators for the surface functionalization of silicon nanomaterials and their collaborative effect as ring opening polymerization initiators. *Nanoscale*, 9(23).

Helbich, T. et al., 2017. Lewis Acid Induced Functionalization of Photoluminescent Two-Dimensional Silicon Nanosheets for the Fabrication of Functional Hybrid Films. *Advanced Functional Materials*, p.1606764.

Helbich, T., Lyuleeva, A., Ludwig, T., et al., 2016. One-Step Synthesis of Photoluminescent Covalent Polymeric Nanocomposites from 2D Silicon Nanosheets. *Advanced Functional Materials*, 26(37), pp.6711–6718.

Helbich, T., Lyuleeva, A., Höhlein, I.M.D., et al., 2016. Radical-Induced Hydrosilylation Reactions for the Functionalization of Two-Dimensional Hydride Terminated Silicon Nanosheets. *Chemistry - A European Journal*, 22(18), pp.6194–6198.

Hengge, E. & Grupe, H., 1964. Bestimmung der Substituentenorientierung am Siloxen durch Brückenbildung. *Farbe und Fluoreszenz ringformiger Si-Verbindungen*, 4, pp.1783–1788.

Hess, L.H. et al., 2011. Graphene transistor arrays for recording action potentials from electrogenic cells. *Advanced materials*, 23, pp.5045–9. Available at: http://www.ncbi.nlm.nih.gov/pubmed/21953832 [Accessed November 14, 2014].

Hess, L.H. et al., 2014. Graphene Transistors with Multifunctional Polymer Brushes for Biosensing Applications. *ACS Appl. Mater. Interfaces*, 6, pp.9705–9710.

Hoffmann, R.W., 2004. Stereoselective synthesis using diastereotopic groups. *Synthesis*, (13), pp.2075–2090.

Houssa, M. et al., 2011. Electronic properties of hydrogenated silicene and germanene. *Applied Physics Letters*, 98(22), pp.96–99.

Hu, M. et al., 2001. Structure and morphology of self-assembled layers on silicon oxide. *Applied Surface Science*, 181, pp.307–316. Available at: http://www.sciencedirect.com/science/article/pii/S0169433201003993.

Hu, P. et al., 2013. Highly responsive ultrathin GaS nanosheet photodetectors on rigid and flexible substrates. *Nano Letters*, 13(4), pp.1649–1654.

Huang, B., Xiang, H.J. & Wei, S.-H., 2013. Chemical Functionalization of Silicene: Spontaneous Structural Transition and Exotic Electronic Properties. *Physical Review Letters*, 111(14),

p.145502. Available at: http://link.aps.org/doi/10.1103/PhysRevLett.111.145502 [Accessed November 28, 2014].

Huang, J., Su, J.-H. & Tian, H., 2012. The development of anthracene derivatives for organic light-emitting diodes. *Journal of Materials Chemistry*, 22(22), p.10977. Available at: http://xlink.rsc.org/?DOI=c2jm16855c.

Huffaker, D.L. et al., 1998. 1.3 μm room-temperature GaAs-based quantum-dot laser. *Applied Physics Letters*, 73(18), pp.2564–2566. Available at: http://aip.scitation.org/doi/10.1063/1.122534.

Hünenberger, P.H. & McCammon, J.A., 1999. Ewald artifacts in computer simulations of ionic solvation and ion–ion interaction: A continuum electrostatics study. *The Journal of Chemical Physics*, 110(4), pp.1856–1872. Available at: http://aip.scitation.org/doi/10.1063/1.477873.

Huntley, D.J., 2006. An explanation of the power-law decay of luminescence. *Journal of Physics: Condensed Matter*, 18(4), pp.1359–1365. Available at: http://stacks.iop.org/0953-8984/18/i=4/a=020?key=crossref.1373fed3399e6bc6f2950816c2bc7ec9.

Hussain, T. et al., 2014. Enhancement of energy storage capacity of Mg functionalized silicene and silicane under external strain. *Applied Physics Letters*, 105(12).

Hussain, T. et al., 2013. Functionalization of hydrogenated silicene with alkali and alkaline earth metals for efficient hydrogen storage. *Phys. Chem. Chem. Phys. Phys. Chem. Chem. Phys*, 15(15), pp.18900–18905.

Intartaglia, R. et al., 2012. Influence of organic solvent on optical and structural properties of ultra-small silicon dots synthesized by UV laser ablation in liquid. *Physical Chemistry Chemical Physics*, 14(44), p.15406. Available at: http://xlink.rsc.org/?DOI=c2cp42195j.

Islam, M.A. et al., 2016. Grafting Poly(3-hexylthiophene) from Silicon Nanocrystal Surfaces: Synthesis and Properties of a Functional Hybrid Material with Direct Interfacial Contact. *Angewandte Chemie - International Edition*, 55(26), pp.7393–7397.

Jiang, S. et al., 2015. Covalently-controlled properties by design in group IV graphane analogues. *Accounts of Chemical Research*, 48(1), pp.144–151.

Jiang, S. et al., 2014. Improving the stability and optical properties of germanane via one-step covalent methyl-termination. *Nature Communications*, 5, pp.1–6. Available at: http://dx.doi.org/10.1038/ncomms4389.

Jonscher, A.K. & De Polignac, A., 1984. The time dependence of luminescence in solids. *Journal of*

Physics C: Solid State Physics, 17(35), pp.6493–6519.

Kabashin, A. V. & Meunier, M., 2003. Synthesis of colloidal nanoparticles during femtosecond laser ablation of gold in water. *Journal of Applied Physics*, 94(12), pp.7941–7943.

Kairdolf, B.A. et al., 2013. Semiconductor Quantum Dots for Bioimaging and Biodiagnostic Applications. *Annual Review of Analytical Chemistry*, 6(1), pp.143–162. Available at: http://www.annualreviews.org/doi/10.1146/annurev-anchem-060908-155136.

Kanemitsu, Y., 2002. Efficient light emission from crystalline and amorphous silicon nanostructures. *J. Lumin.*, 100, pp.209–217.

Kao, H.-L. et al., 2016. DuoSkin: Rapidly Prototyping On-Skin User Interfaces Using Skin-Friendly Materials. *ACM*, pp.16–23.

Kara, A. et al., 2009. Physics of silicene stripes. *Journal of Superconductivity and Novel Magnetism*, 22(3), pp.259–263.

Kataoka, K., Harada, A. & Nagasaki, Y., 2001. Block copolymer micelles for drug delivery: Design, characterization and biological significance. *Advanced Drug Delivery Reviews*, 47(1), pp.113–131.

Kautsky, H., 1952. Probleme der Siliciumchemie - Zweidimensionale Kristallstrukturen. *Zeitschrift fur Naturforschung - Section B Journal of Chemical Sciences*, 7(3), pp.174–183.

Kautsky, H. & Herzberg, G., 1925. Permutoid-Strukturen. Von. *Z. anorg. u. allg. Chem.*, 147, pp.81–92.

Kelley, S.O. et al., 2014. Advancing the speed, sensitivity and accuracy of biomolecular detection using multi-length-scale engineering. *Nature Nanotechnology*, 9(12), pp.969–980. Available at: http://dx.doi.org/10.1038/nnano.2014.261.

Kergoat, L. et al., 2012. DNA detection with a water-gated organic field-effect transistor. *Organic Electronics*, 13(1), pp.1–6. Available at: http://linkinghub.elsevier.com/retrieve/pii/S1566119911003430 [Accessed November 28, 2014].

Kim, H.J. et al., 2011. Magnetic nanoparticle-based separation of metallic and semiconducting carbon nanotubes. *Nanotechnology*, 22(4), p.45703.

Kim, N.S. et al., 2003. Leakage Current: Moore's Law Meets Static Power. *IEEE Computer Society*, pp.68–75.

Kim, S. et al., 2009. Realization of a high mobility dual-gated graphene field-effect transistor with

Al2O3 dielectric. *Applied Physics Letters*, 94(6), p.62107.

Kim, U. et al., 2011. Synthesis of Si nanosheets by a chemical vapor deposition process and their blue emissions. *ACS Nano*, 5(3), pp.2176–2181.

King, B.R., 2006. Bond Energies. In *Encyclopedia of Inorganic Chemistry*. pp. 1–4. Available at: http://doi.wiley.com/10.1002/0470862106.id098.

Kinkeldei, T. et al., 2011. A textile integrated sensor system for monitoring humidity and temperature. *Solid-State Sensors*, June, pp.1156–1159.

Kong, L.B., Zhang, L.Y. & Yao, X., 1997. Preparation and properties of a humidity sensor based on LiCl-doped porous silica. *Journal of Materials Science Letters*, 16(10), pp.824–826. Available at: http://link.springer.com/article/10.1023/A:1018534626228.

Kong, Y.L. et al., 2014. 3D printed quantum dot light-emitting diodes. *Nano Letters*, 14(12), pp.7017–7023.

Koski, K.J. & Cui, Y., 2013. The new skinny in two-dimensional nanomaterials. *ACS Nano*, 7(5), pp.3739–3743.

Kramer, I.J. et al., 2015. Efficient spray-coated colloidal quantum dot solar cells. *Advanced materials*, 27(1), pp.116–121.

Kumai, Y., Shirai, S., et al., 2011. Properties and Mechanism of Layered Polysilane (Si 6 H 6) Anode. *IOP Conference Series: Materials Science and Engineering*, 18(12), p.122005. Available at: http://stacks.iop.org/1757-899X/18/i=12/a=122005.

Kumai, Y., Kadoura, H., et al., 2011. Si–C composite anode of layered polysilane (Si6H6) and sucrose for lithium ion rechargeable batteries. *Journal of Materials Chemistry*, 21(32), p.11941.

Kumai, Y. & Nakano, H., 2015. Characteristics of layered polysilane and its application to lithium ion battery anodes. *Japanese Journal of Applied Physics*, 54(3), p.35201.

Lambert, J.M., 2005. The Nature of Platinum in Silicones for Biomedical and Healthcare Use. *Journal of Biomedical Materials Research Part B: Applied Biomaterials*, 83(2), pp.167–180.

Le Lay, G., Salomon, E. & Angot, T., 2016. Silicene: silicon conquers the 2D world. *Europhysics News*, 47(1), pp.17–21. Available at: http://www.europhysicsnews.org/10.1051/epn/2016101.

Ledentsov, N.N., 2011. Quantum dot laser. *Semiconductor Science and Technology*, 26(1), p.14001. Available at: http://stacks.iop.org/0268-

1242/26/i=1/a=014001?key=crossref.a2bf994e4439d6835d3d6013518c5b95.

Lee, J. et al., 2016. Two-Dimensional Semiconductor Optoelectronics Based on van der Waals Heterostructures. *Nanomaterials*, 6(12), p.193. Available at: http://www.mdpi.com/2079-4991/6/11/193.

Lee, J., Cho, D. & Jeong, Y., 2013. A resistive-type sensor based on flexible multi-walled carbon nanotubes and polyacrylic acid composite films. *Solid-State Electronics*, 87, pp.80–84. Available at: http://dx.doi.org/10.1016/j.sse.2013.05.001.

Lew Yan Voon, L.C. et al., 2010. Hydrogen compounds of group-IV nanosheets. *Applied Physics Letters*, 97(16), pp.13–16.

Leyden, M.R. et al., 2010. Fabrication and characterization of carbon nanotube field-effect transistor biosensors. *SPIE Photonic Devices+ Applications*, p.77790H.

Li, F. et al., 2013. Geometric and Electronic Structures as well as Thermodynamic Stability of Hexyl-Modi fi ed Silicon Nanosheet. *J. Phys. Chem. C*, 117(25), pp.13283–13288. Available at: http://dx.doi.org/10.1021/jp402875t.

Li, J. & Zhu, J.-J., 2013. Quantum dots for fluorescent biosensing and bio-imaging applications. *The Analyst*, 138(9), p.2506. Available at: http://xlink.rsc.org/?DOI=c3an36705c.

Li, L. et al., 2014. Suppl.: Black phosphorus field-effect transistors. *Nature nanotechnology*, 9(5), pp.1–17. Available at: http://www.ncbi.nlm.nih.gov/pubmed/24584274%5Cnhttp://www.nature.com/doifinder/10.1038/nnano.2014.35.

Li, X. et al., 2013. Intrinsic electrical transport properties of monolayer silicene and MoS2 from first principles. *Physical Review B - Condensed Matter and Materials Physics*, 87(11), pp.1–9.

Li, X., Zeng, X.C. & Wu, X., 2017. Embedded silicene nanostructures in partly-dehydrogenated polysilane. *Phys. Chem. Chem. Phys.* Available at: http://xlink.rsc.org/?DOI=C7CP01020F.

Liao, C. & Yan, F., 2013. Organic semiconductors in organic thin-film transistor-based chemical and biological sensors. *Polymer Reviews*, 53(3), pp.352–406.

Lim, J.-H. et al., 2010. Electrical and gas sensing properties of polyaniline functionalized single-walled carbon nanotubes. *Nanotechnology*, 21, p.75502.

Lin, C.L. et al., 2012. Structure of silicene grown on Ag(111). *Applied Physics Express*, 5(4), pp.5–8.

Lin, J., Heurich, M. & Obermeier, E., 1993. Manufacture and examination of various spin-on glass films with respect to their humidity-sensitive properties. *Sensors and Actuators: B. Chemical*, 13(1–3), pp.104–106.

Liu, C.-Y., Holman, Z.C. & Kortshagen, U.R., 2009. Hybrid Solar Cells from P3HT and Silicon Nanocrystals. *Nano Letters*, 9(1), pp.449–452. Available at: http://pubs.acs.org/doi/abs/10.1021/nl8034338.

Liu, C.C., Feng, W. & Yao, Y., 2011. Quantum spin Hall effect in silicene and two-dimensional germanium. *Physical Review Letters*, 107(AUGUST), pp.1–4.

Liu, F. et al., 2013. D+id' chiral superconductivity in bilayer silicene. *Physical Review Letters*, 111(6), pp.1–5.

Liu, G., Lei, X.L., et al., 2014. Comparison of the stability of free-standing silicene and hydrogenated silicene in oxygen: a first principles investigation. *Journal of Physics: Condensed Matter*, 26(35), p.355007. Available at: http://stacks.iop.org/0953-8984/26/i=35/a=355007?key=crossref.1d799c652431bf3090039d6720adcc9f.

Liu, G. et al., 2014. Is silicene stable in O2? —First-principles study of O2 dissociation and O2-dissociation–induced oxygen atoms adsorption on free-standing silicene. *EPL (Europhysics Letters)*, 106, p.47001.

Liu, G., Lei, X. & Wu, M., 2014. Comparison of the stability of free-standing silicene and hydrogenated silicene in oxygen: a first principles investigation. *Journal of Physics: Condensed Matter*, 26, p.355007. Available at: http://iopscience.iop.org/0953-8984/26/35/355007.

Liu, H. et al., 2014. Phosphorene : An Unexplored 2D Semiconductor with a High Hole. *American Chemical Society*, 8(4), pp.4033–4041.

Liu, N. et al., 2012. Functionalization of silicon nanowire surfaces with metal-organic frameworks. *Nano Research*, 5(2), pp.109–116.

Liu, S. & Guo, X., 2012. Carbon nanomaterials field-effect-transistor-based biosensors. *NPG Asia Materials*, 4(8), pp.e23-10. Available at: http://dx.doi.org/10.1038/am.2012.42.

Lodish, H. et al., 2000. Molecular Cell Biology, 4th Edition. In W. H. Freeman, ed. *Molecular Cell Biology*. NCBI Bookshelf, pp. 12–13.

Lomeda, J.R. et al., 2008. Diazonium functionalization of surfactant-wrapped chemically converted graphene sheets. *Journal of the American Chemical Society*, 130(48), pp.16201–16206.

Lu, N., Li, Z. & Yang, J., 2009. Electronic structure engineering via on-plane chemical functionalization: A comparison study on two-dimensional polysilane and graphane. *Journal of Physical Chemistry C*, 113(38), pp.16741–16746.

Lu, X. et al., 2012. Hydrogen induced silicon surface layer cleavage Hydrogen induced silicon surface layer cleavage. , 1804(1997).

Luppi, M. & Ossicini, S., 2005. Ab initio study on oxidized silicon clusters and silicon nanocrystals embedded in SiO2: Beyond the quantum confinement effect. *Physical Review B*, 71(3), p.35340.

Lyuleeva, A., Narreto, M.A.B., Helbich, T., Veinot, J.G.C., et al., 2017. Band-tail Photoluminescence Dynamics of Functionalized Two-dimensional Silicon Nanosheets. *manuscript in preparation*.

Lyuleeva, A., Holzmüller, P., Helbich, T., Stutzmann, M., et al., 2017. Charge Transfer Doping in Functionalized Silicon Nanosheets/P3HT Hybrid Material for the Application in Solution-Gated Field-Effect Transistors. *subitted to Adv. Funct. Mater.*

Lyuleeva, A., Helbich, T., Bobbinger, M., Rieger, B., et al., 2017. Functionalized and Oxidized Silicon Nanosheets (OSiNSs): Customized Design for Enhanced Sensitivity Towards Relative Humidity. *submitted to 2D Materials*.

Lyuleeva, A., Helbich, T., Rieger, B. & Lugli, P., 2017. Polymer-silicon nanosheet composites: bridging the way to optoelectronic applications. *Journal of Physics D: Applied Physics*, 50(13), p.135106. Available at: http://stacks.iop.org/0022-3727/50/i=13/a=135106?key=crossref.dcb1e4685c788ea2a701f1ac5a985ba8.

Lyuleeva, A., Helbich, T., Lugli, P., Becherer, M., et al., 2017. Silicon Nanosheets New Materials for Future Applications. , pp.11–12.

Macdiarmid, A., 1987. Conducting polymers: What does the future hold? *Synthetic Metals*, 21(1–3), pp.79–83. Available at: http://linkinghub.elsevier.com/retrieve/pii/0379677987900695.

Machui, F., 2014. *Formulation of Semiconductor Solutions for Organic Photovoltaic Devices*. Friedrich-Alexander Universität Erlangen-Nürnberg.

Mak, K.F. et al., 2010. Atomically thin MoS2: A new direct-gap semiconductor. *Physical Review Letters*, 105(13), pp.2–5.

Manceau, M. et al., 2011. Light-induced degradation of the P3HT-based solar cells active layer. *Solar Energy Materials and Solar Cells*, 95(5), pp.1315–1325.

Mathlouthi, M., 2001. Water content, water activity, water structure and the stability of foodstuffs.

Food Control, 12(7), pp.409–417.

Matthes, L., Pulci, O. & Bechstedt, F., 2014. Optical properties of two-dimensional honeycomb crystals graphene, silicene, germanene, and tinene from first principles. *New Journal of Physics*, 16.

Mazzaro, R., Romano, F. & Ceroni, P., 2017. Long-lived luminescence of silicon nanocrystals: from principles to applications. *Physical chemistry chemical physics*, p.Perspectives (invited), Submitted.

McCafferty, E. & Zettlemoyer, A.C., 1971. Adsorption of water vapour on α-Fe2O3. *Discussions of the Faraday Society*, 52, p.239.

McCulloch, I. et al., 2006. Liquid-crystalline semiconducting polymers with high charge-carrier mobility. *Nature materials*, 5(April), pp.328–333.

McNeil, I.J. et al., 2012. Power-law kinetics in the photoluminescence of dye-sensitized nanoparticle films: Implications for electron injection and charge transport. *Journal of Physical Chemistry C*, 116(30), pp.15888–15899.

Mecklenburg, M. et al., 2012. Aerographite: Ultra lightweight, flexible nanowall, carbon microtube material with outstanding mechanical performance. *Advanced Materials*, 24, pp.3486–3490.

Melzer, K. et al., 2014. Characterization and simulation of electrolyte-gated organic field-effect transistors. *Faraday Discuss.*, 174, pp.399–411. Available at: http://xlink.rsc.org/?DOI=C4FD00095A.

Melzer, K. et al., 2016. Enzyme assays using sensor arrays based on ion-selective carbon nanotube field-effect transistors. *Biosensors and Bioelectronics*, 84, pp.7–14. Available at: http://dx.doi.org/10.1016/j.bios.2016.04.077.

Meng, L. et al., 2013. Buckled silicene formation on Ir(111). *Nano Letters*, 13(2), pp.685–690.

Merali, Z., 2013. Exotic conductors from lab and nature. *Nature*, 146802(2005), p.146802.

Miyamoto, A. et al., 2017. Inflammation-free, gas-permeable, lightweight, stretchable on-skin electronics with nanomeshes. *Nature Nanotechnology*, 12(September), pp.1–7. Available at: http://www.nature.com/doifinder/10.1038/nnano.2017.125.

Mohan, B. et al., 2015. Shape and edge dependent electronic and magnetic properties of silicene nano-flakes. , 140054(2015), p.140054. Available at: http://scitation.aip.org/content/aip/proceeding/aipcp/10.1063/1.4918263.

Mohan, B., Kumar, A. & Ahluwalia, P.K., 2013. A first principle calculation of electronic and dielectric properties of electrically gated low-buckled mono and bilayer silicene. *Physica E: Low-Dimensional Systems and Nanostructures*, 53, pp.233–239. Available at: http://dx.doi.org/10.1016/j.physe.2013.05.014.

Molina-Lopez, F. et al., 2012. All-additive Inkjet Printed Humidity and Temperature Sensors Fabricated and Encapsulated at Foil Level. *IMCS 2012 - The 14th International Meeting on Chemical Sensors*, pp.1122–1125. Available at: http://www.ama-science.org/home/details/1091.

Morimoto, T., Nagao, M. & Tokuda, F., 1969. Relation between the amounts of chemisorbed and physisorbed water on metal oxides - The Journal of Physical Chemistry (ACS Publications). *The Journal of Physical Chemistry*, 73(1), pp.243–248. Available at: http://pubs.acs.org/doi/abs/10.1021/j100721a039.

Musumeci, A.W. et al., 2007. Structure and conductivity of multi-walled carbon nanotube/poly(3-hexylthiophene) composite films. *Polymer*, 48(6), pp.1667–1678.

Nakano, H. et al., 2012. Preparation of alkyl-modified silicon nanosheets by hydrosilylation of layered polysilane (Si 6H 6). *Journal of the American Chemical Society*, 134(12), pp.5452–5455.

Nakano, H. et al., 2006. Soft synthesis of single-crystal silicon monolayer sheets. *Angewandte Chemie - International Edition*, 45(38), pp.6303–6306.

Nakano, H., 2014. Synthesis and modi fi cation of two-dimensional crystalline silicon nanosheets. *Jounal of the Ceramic Society of Japan*, 122(9), pp.748–754.

Nakano, H., Ishii, M. & Nakamura, H., 2005. Preparation and structure of novel siloxene nanosheets. *Chemical communications (Cambridge, England)*, 2(23), pp.2945–2947.

Ni, Z. et al., 2014. Tunable band gap and doping type in silicene by surface adsorption: towards tunneling transistors. *Nanoscale*, 6, pp.7609–18. Available at: http://www.ncbi.nlm.nih.gov/pubmed/24896227.

Ni, Z. et al., 2012. Tunable bandgap in silicene and germanene. *Nano Letters*, 12(1), pp.113–118.

Nishimura, K. et al., 1996. Characterization of layered polysilane. *Japanese Journal of Applied Physics, Part 2: Letters*, 35(3 A).

Niu, M., Cheng, D. & Cao, D., 2014. SiH/TiO2 and GeH/TiO2 heterojunctions: promising TiO2-based photocatalysts under visible light. *Scientific reports*, 4, p.4810. Available at: http://www.pubmedcentral.nih.gov/articlerender.fcgi?artid=4007092&tool=pmcentrez&rende

rtype=abstract.

Noor, M.O. & Krull, U.J., 2014. Silicon nanowires as field-effect transducers for biosensor development: A review. *Analytica Chimica Acta*, 825, pp.1–25. Available at: http://dx.doi.org/10.1016/j.aca.2014.03.016.

Novoselov, K.S. et al., 2004. Electric Field Effect in Atomically Thin Carbon Films. *Science*, 306(5696), pp.666–669. Available at: http://arxiv.org/ftp/cond-mat/papers/0410/0410550.pdf.

Öğüt, S., Chelikowsky, J.R. & Louie, S.G., 1997. Quantum Confinement and Optical Gaps in Si Nanocrystals. *Physical Review Letters*, 79(9), pp.1770–1773. Available at: https://link.aps.org/doi/10.1103/PhysRevLett.79.1770.

Ohno, Y., Maehashi, K. & Matsumoto, K., 2010. Label-Free Biosensors Based on Aptamer-Modified Graphene Field-Effect. , pp.18012–18013.

Ohshita, J. et al., 2016. Preparation and Photocurrent Generation of Silicon Nanosheets with Aromatic Substituents on the Surface. *The Journal of Physical Chemistry C*, p.acs.jpcc.6b03014. Available at: http://pubs.acs.org/doi/abs/10.1021/acs.jpcc.6b03014.

Okamoto, H. et al., 2010. Silicon nanosheets and their self-assembled regular stacking structure. *Journal of the American Chemical Society*, 132(8), pp.2710–2718.

Okamoto, H. et al., 2015. Surface Modification of Layered Polysilane with n-Alkylamines, α,ω-Diaminoalkanes, and ω-Aminocarboxylic Acids. *Chemistry of Materials*, 27, pp.1292–1298.

Okamoto, H., Sugiyama, Y. & Nakano, H., 2011. Synthesis and modification of silicon nanosheets and other silicon nanomaterials. *Chemi. Eur. J.*, 17(36), pp.9864–87. Available at: http://www.ncbi.nlm.nih.gov/pubmed/21780200 [Accessed January 8, 2015].

Osborn, T.H. et al., 2011. Ab initio simulations of silicene hydrogenation. *Chemical Physics Letters*, 511(1–3), pp.101–105. Available at: http://dx.doi.org/10.1016/j.cplett.2011.06.009.

Patolsky, F., Zheng, G. & Lieber, C.M., 2006. Nanowire-based biosensors. *Analytical Chemistry*, 78(13), pp.4260–4269.

Pelant, I. & Valenta, J., 2012. Phonons and their participation in optical phenomena. In *Luminescence Spectroscopy of Semiconductors*. Oxford University Press: New York.

Peng, Q., Wen, X. & De, S., 2013. Mechanical stabilities of silicene. *RSC Advances*, 3(33), p.13772. Available at: http://xlink.rsc.org/?DOI=c3ra41347k.

Perez-Taborda, J.A., Caballero-Calero, O. & Marisol, M.-G., 2017. Silicon - Germanium (SiGe) Nanostructures for Thermoelectric Devices : Recent Advances and New Approaches to High Thermoelectric Efficiency. In V. I. Talanin, ed. *N e w R e s e a r c h o n S ic l i o n - S t r u c t u r e , P r o p e r t i e s , T e c h n o l o gy*. pp. 183–206.

Prasankumar, R.P. & Taylor, A.J., 2011. *Optical Techniques for Solid-State Materials CHaracterization*, CRC Press.

Privalov, P.L. & Gill, S.J., 1988. Stability of Protein Structure and Hydrophobic Interaction. *Advances in Protein Chemistry*, 39(C), pp.191–234.

Purkait, T.K. et al., 2014. Borane-catalyzed room-temperature hydrosilylation of alkenes/alkynes on silicon nanocrystal surfaces. *Journal of the American Chemical Society*, 136(52), pp.17914–17917.

Qian, L. et al., 2011. Stable and efficient quantum-dot light-emitting diodes based on solution-processed multilayer structures. *Nature Photonics*, 5(9), pp.543–548. Available at: http://www.nature.com/doifinder/10.1038/nphoton.2011.171.

Quhe, R.-G., Wang, Y.-Y. & Lü, J., 2015. Silicene transistors— A review. *Chinese Physics B*, 24(8), p.88105. Available at: http://stacks.iop.org/1674-1056/24/i=8/a=088105?key=crossref.be7adc52f2c5f4738db4667deb5a94f9.

Rahman, M.Z. et al., 2016. 2D phosphorene as a water splitting photocatalyst: fundamentals to applications. *Energy Environ. Sci.*, 9(3), pp.709–728. Available at: http://xlink.rsc.org/?DOI=C5EE03732H.

RamanathanT. et al., 2008. Functionalized graphene sheets for polymer nanocomposites. *Nat Nano*, 3(6), pp.327–331. Available at: http://dx.doi.org/10.1038/nnano.2008.96%5Cnhttp://www.nature.com/nnano/journal/v3/n6/full/nnano.2008.96.html%5Cnhttp://www.nature.com/nnano/journal/v3/n6/pdf/nnano.2008.96.pdf.

Rauen, K.L. et al., 1993. Humidity sensor based on conductivity measurements of a poly(dimethyldiallylammonium chloride) polymer film. *Sensors and Actuators: B. Chemical*, 17(1), pp.61–68.

Ray, P.C., Yu, H. & Fu, P.P., 2009. Toxicity and Environmental Risks of Nanomaterials: Challenges and Future Needs. *J Environ Sci Health C Environ Carcinog Ecotoxicol Rev. 2009*, 27(1), pp.1–35.

Restrepo, O.D., Krymowski, K.E., et al., 2014. A first principles method to simulate electron mobilities

in 2D materials. *New Journal of Physics*, 16.

Restrepo, O.D. et al., 2014. A first principles method to simulate electron mobilities in 2D materials. *New Journal of Physics*, 16(10), p.105009. Available at: http://stacks.iop.org/1367-2630/16/i=10/a=105009?key=crossref.b2837ae9fed79f462338cc90ae617941.

Restrepo, O.D., Mishra, R., et al., 2014. Tunable gaps and enhanced mobilities in strain-engineered silicane. *Journal of Applied Physics*, 115(3).

Rivadeneyra, A. et al., 2016. Printed electrodes structures as capacitive humidity sensors: A comparison. *Sensors and Actuators, A: Physical*, 244, pp.56–65. Available at: http://dx.doi.org/10.1016/j.sna.2016.03.023.

Roger, K. et al., 2016. Controlling water evaporation through self-assembly. *Proceedings of the National Academy of Sciences*, 113(37), pp.10275–10280. Available at: http://www.pnas.org/lookup/doi/10.1073/pnas.1604134113.

Ronkainen, N.J., Halsall, H.B. & Heineman, W.R., 2010. Electrochemical biosensors. *Chemical Society Reviews*, 39(5), p.1747. Available at: http://xlink.rsc.org/?DOI=b714449k.

Roome, N.J. & Carey, J.D., 2014. Beyond graphene: Stable elemental monolayers of silicene and germanene. *ACS Applied Materials and Interfaces*, 6(10), pp.7743–7750.

Rosenbauer, M. et al., 1993. Preparation and properties of Siloxene films on silicon. In *Optical Properties of Low Dimensional Silicon Structures*. Springer Netherlands, pp. 43–54. Available at: https://link.springer.com/chapter/10.1007%2F978-94-011-2092-0_5.

Rubin, M., Schwier, T. & Gevorgyan, V., 2002. Highly efficient B(C6F5)3-catalyzed hydrosilylation of olefins. *Journal of Organic Chemistry*, 67(6), pp.1936–1940.

Rupp, C.J. et al., 2015. The effect of impurities in ultra-thin hydrogenated silicene and germanene: a first principles study. *Phys. Chem. Chem. Phys.*, 17(34), pp.22210–22216. Available at: http://xlink.rsc.org/?DOI=C5CP03489B.

Sakai, Y., Sadaoka, Y. & Matsuguchi, M., 1996. Humidity sensors based on polymer thin films. *Sensors and Actuators B: Chemical*, 35(1–3), pp.85–90. Available at: http://linkinghub.elsevier.com/retrieve/pii/S0925400596020199.

Salh, R., 2011. Defect related luminescence in silicon dioxide network: a review. In S. Basu, ed. *Crystalline Silicon: Properties and Uses*. InTech, pp. 135–172. Available at: http://www.intechopen.com/books/crystalline-silicon- properties-and-uses/silicon-

nanocluster-in-silicon-dioxide-cathodoluminescence-energy-dispersive-x-ray- analysis-infrared.

Sangawar, V.S. & Golchha, M.C., 2013. Evolution of the optical properties of Polystyrene thin films filled with Zinc Oxide nanoparticles. , 4(6), pp.2700–2705.

Scalise, E. et al., 2014. Vibrational properties of epitaxial silicene layers on (1 1 1) Ag. *Applied Surface Science*, 291, pp.113–117. Available at: http://dx.doi.org/10.1016/j.apsusc.2013.08.113.

Scher, H., Shlesinger, M.F. & John, T., 2008. Time-Scale Invariance in. , 26(1991).

Schulz, M., 1999. The end of the road for silicon? *Nature*, 399, pp.729–730. Available at: http://www.nature.com/nature/journal/v399/n6738/full/399729a0.html.

Shiotani, M. et al., 1983. Electron Spin Resonance Studies on Radical Cations of Five-Membered Heteroaromatics. Furan, Thiophene, Pyrrole, and Related Compounds. *J. Phys. Chem.*, 87(23), pp.1170–1174.

Skrypnychuk, V. et al., 2015. Enhanced Vertical Charge Transport in a Semiconducting P3HT Thin Film on Single Layer Graphene. *Advanced Functional Materials*, 25(5), pp.664–670. Available at: http://doi.wiley.com/10.1002/adfm.201403418.

de Smet, L.C.P.M. et al., 2011. World â€™ s largest Science , Technology & Medicine Open Access book publisher c. In A. Hashim, ed. *Nanowires - Implementations and Applications*. pp. 267–288.

Smith, M.B. & March, J., 2006. *March's Advanced Organic Chemistry: Reactions, Mechanisms, and Structure: Sixth Edition*,

Spencer, M.J.S. et al., 2013. Interactions between stacked layers of phenyl-modified silicene. *New Journal of Physics*, 15.

Spencer, M.J.S., 2016. *Silicene Structure, Properties and Applications* M. J. S. Spencer & T. Morishita, eds., Springer Series in Materials Science 235.

Stoppa, M. & Chiolerio, A., 2014. Wearable electronics and smart textiles: A critical review. *Sensors (Switzerland)*, 14(7), pp.11957–11992.

Sudo, T. et al., 1999. Lewis acid catalyzed highly regio- and stereocontrolled trans- hydrosilylation of alkynes and allenes. *Journal of Organic Chemistry*, 64(7), pp.2494–2499.

Sugiyama, Y., Okamoto, H., Mitsuoka, T., et al., 2010. Synthesis and optical properties of monolayer organosilicon nanosheets. *Journal of the American Chemical Society*, 132(17), pp.5946–5947.

Sugiyama, Y., Okamoto, H. & Nakano, H., 2010. Synthesis of Siloxene Derivatives with Organic Groups.

Chemistry Letters, 39(9), pp.938–939. Available at: http://www.journal.csj.jp/doi/10.1246/cl.2010.938.

Sui, Y. & Appenzeller, J., 2009. Screening and Interlayer Coupling in Multilayer Graphene Field-Effect Transistors 2009. *Nano Letters*, 9(8), pp.2973–2977.

Sukhanova, T.E. et al., 2011. Morphology and electronic structure of platinum-containing polymer nanosystems. *Journal of Surface Investigation. X-ray, Synchrotron and Neutron Techniques*, 5(3), pp.440–446. Available at: http://link.springer.com/10.1134/S1027451011050156.

Sun, H.T. et al., 1995. Connectivity of pore networks in chemically sensitive materials. *Sensors and Actuators: B. Chemical*, 25(1–3), pp.865–870.

Sun, Q.Y. et al., 2005. Covalently attached monolayers on crystalline hydrogen-terminated silicon: Extremely mild attachment by visible light. *Journal of the American Chemical Society*, 127(8), pp.2514–2523.

Sun, Y. & Wang, H.H., 2007. High-performance, flexible hydrogen sensors that use carbon nanotubes decorated with palladium nanoparticles. *Advanced Materials*, 19(19), pp.2818–2823.

Svrcek, V. et al., 2016. Environmentally Friendly Processing Technology for Engineering Silicon Nanocrystals in Water with Laser Pulses. *Journal of Physical Chemistry C*, 120(33), pp.18822–18830.

Syaputra, M. et al., 2015. Study of hydrogenated silicene: The initialization model of hydrogenation on planar, low buckled and high buckled structures of silicene. , 80006(2015), p.80006. Available at: http://scitation.aip.org/content/aip/proceeding/aipcp/10.1063/1.4930737.

Takagi, H. et al., 1990. Quantum size effects on photoluminescence in ultratfne Si particles. *Applied Physics Letters*, 56(April), pp.2379–2380.

Takeda, K. & Shiraishi, K., 1994. Theoretical possibility of stage corrugation in Si and Ge analogs of graphite. *Physical Review B*, 50(November), pp.14916–14922.

Tao, L. et al., 2015. Silicene fi eld-effect transistors operating at room temperature. *Nature Nanotechnology*, 10(February), pp.227–231. Available at: http://dx.doi.org/10.1038/nnano.2014.325.

Tiedje, T. & Rose, A., 1980. A Physical Interpretation of Dispersive Transport in Disordered Semiconductors. *Solid State Communications*, 37, pp.49–52.

Torrisi, F. et al., 2012. Inkjet-printed graphene electronics. *ACS Nano*, 6(4), pp.2992–3006.

Traversa, E., 1995. Ceramic sensors for humidity detection: the state-of-the-art and future developments. *Sensors and Actuators: B. Chemical*, 23(2–3), pp.135–156.

Trivedi, S., Srivastava, A. & Kurchania, R., 2014. Silicene and germanene: A first principle study of electronic structure and effect of hydrogenation-passivation. *Journal of Computational and Theoretical Nanoscience*, 11(3).

Trung, T.Q. et al., 2017. Transparent, stretchable, and rapid-response humidity sensor for body-attachable wearable electronics. *Nano Research*, 10(6), pp.2021–2033.

Turner, A.P.F., 2013. Biosensors: sense and sensibility. *Chemical Society Reviews*, 42(8), p.3184. Available at: http://xlink.rsc.org/?DOI=c3cs35528d.

Urien, M. et al., 2007. Field-effect transistors based on poly(3-hexylthiophene): Effect of impurities. *Organic Electronics: physics, materials, applications*, 8(6), pp.727–734.

Velusamy, D.B. et al., 2015. Flexible transition metal dichalcogenide nanosheets for band-selective photodetection. *Nature Communications*, p.8063. Available at: http://www.nature.com/doifinder/10.1038/ncomms9063.

Vinciguerra, V. et al., 2000. Quantum confinement and recombination dynamics in silicon nanocrystals embedded in Si/SiO2 superlattices. *Journal of Applied Physics*, 87(11), pp.8165–8173. Available at: http://aip.scitation.org/doi/10.1063/1.373513.

Vogt, P. et al., 2012. Silicene: Compelling Experimental Evidence for Graphenelike Two-Dimensional Silicon. *Physical Review Letters*, 108(15), p.155501. Available at: http://link.aps.org/doi/10.1103/PhysRevLett.108.155501 [Accessed July 10, 2014].

Wadsworth, C.L. et al., 1985. ESR Spectra for Anion Radicals of Alkylcyclotetrasilanes and -cyclopentasilanes. *Organometallics*, 4(9), pp.1659–1664.

Walbran, S. & Kornyshev, A.A., 2001. Proton transport in polarizable water. *Journal of Chemical Physics*, 114(22), pp.10039–10048.

Walsh, S.T. et al., 2005. The semiconductor silicon industry roadmap: Epochs driven by the dynamics between disruptive technologies and core competencies. *Technological Forecasting and Social Change*, 72(2), pp.213–236.

Wang, P. et al., 2016. Functionalization of Surfaces and Printed Films for Sensors and Optoelectronics Project Abstract / Summary. *Sensors and Actuators B*, 230, pp.477–484. Available at: http://dx.doi.org/10.1016/j.snb.2016.02.056.

Wang, Q.H. & Hersam, M.C., 2011. Nanofabrication of heteromolecular organic nanostructures on epitaxial graphene via room temperature feedback-controlled lithography. *Nano Letters*, 11(2), pp.589–593.

Wang, Q.H. & Hersam, M.C., 2009. Room-temperature molecular-resolution characterization of self-assembled organic monolayers on epitaxial graphene. *Nature Chemistry*, 1(3), pp.206–211. Available at: http://www.nature.com/doifinder/10.1038/nchem.212.

Wang, R. et al., 2015. Density functional theory study on organically surface-modified silicene. *RSC Adv.*, 5(43), pp.33831–33837. Available at: http://xlink.rsc.org/?DOI=C5RA05751E.

Wang, R. et al., 2010. Large-diameter graphene nanotubes synthesized using Ni nanowire templates. *Nano Letters*, 10(12), pp.4844–4850.

Wang, W., Olovsson, W. & Uhrberg, R.I.G., 2016. Band structure of hydrogenated silicene on Ag(111): Evidence for half-silicane. *Physical Review B*, 93, p.81406.

Wang, X.X. et al., 2005. Origin and evolution of photoluminescence from Si nanocrystals embedded in a SiO2 matrix. *Physical Review B - Condensed Matter and Materials Physics*, 72(19), pp.1–6.

Wang, Y. et al., 2010. A capacitive humidity sensor based on ordered macroporous silicon with thin film surface coating. *Sensors and Actuators, B: Chemical*, 149(1), pp.136–142.

Wang, Y. et al., 2015. Stabilization of elusive silicon oxides. *Nature chemistry*, 7(6), pp.509–13. Available at: http://www.ncbi.nlm.nih.gov/pubmed/25991530.

Wei, W. & Jacob, T., 2013. Strong many-body effects in silicene-based structures. *Physical Review B - Condensed Matter and Materials Physics*, 88(4), pp.1–7.

Weil, J.A. & Bolton, J.R., 1994. *Electron Paramagnetic Resonance: Elementary Theory and Practical Applications* 2nd ed., New York: John Wiley & Sons.

Whitener, K.E., 2014. Reversible graphene functionalization for electronic applications: A review. *ACS Symposium Series*, 1183, pp.41–54.

Wilcoxon, J.P., Samara, G.A. & Provencio, P.N., 1999. Optical and electronic properties of Si nanoclusters synthesized in inverse micelles. *Physical Review B*, 60(4), pp.2704–2714. Available at: https://link.aps.org/doi/10.1103/PhysRevB.60.2704.

Wilson, J. A.; Yoffe, A.D., 1969. The transition metal dichalcogenides discussion and interpretation of the observed optical, electrical and structural properties. *Advances in Physics*, 18(73), pp.193–335.

Wöhler, F., 1863. Über Verbindungen des Siliciums znit Sauer- stoff und Wasserstoff. *ANNALEN DER CHEMIE UND PHARMACIE*, 127(3), pp.257–274.

Wolkin, M. et al., 1999. Electronic States and Luminescence in Porous Silicon Quantum Dots: The Role of Oxygen. *Physical Review Letters*, 82(August 2015), pp.197–200.

Wu, Q. et al., 2014. Boundary and symmetry determined exciton distribution in two dimensional silicon nanosheets. *Journal of Physical Chemistry C*, 118(35), pp.20070–20076.

Xie, T. et al., 2016. Ammonia gas sensors based on poly (3-hexylthiophene)-molybdenum disulfide film transistors. *Nanotechnology*, 27(6), p.65502. Available at: http://stacks.iop.org/0957-4484/27/i=6/a=065502?key=crossref.d608ada0bf37259d034e56c963b68fe7.

Xu, C. et al., 2012. Giant magnetoresistance in silicene nanoribbons. *Nanoscale*, 4(10), p.3111. Available at: http://xlink.rsc.org/?DOI=c2nr00037g.

Xu, Y. et al., 2013. Large-gap quantum spin hall insulators in tin films. *Physical Review Letters*, 111(13), p.136804(5).

Yamanaka, S., Matsu-ura, H. & Ishikawa, M., 1996. New deintercalation reaction of calcium from calcium disilicide. Synthesis of layered polysilane. *Materials Research Bulletin*, 31(3), pp.307–316.

Yan, Y.H. et al., 2007. Systematic studies of covalent functionalization of carbon nanotubes via argon plasma-assisted UV grafting. *Nanotechnology*, 18(11), p.115712. Available at: http://stacks.iop.org/0957-4484/18/i=11/a=115712?key=crossref.c45ce694657cac7f6f12a729f951963d.

Yoffe, a. D., 1993. Advances in Physics Low-dimensional systems : Quantum size effects and electronic properties of semiconductor microcrystallites (zero- dimensional systems) and some quasi-two-dimensional systems. In *Advances in Physics*. pp. 173–262. Available at: http://dx.doi.org/10.1080/00018739300101484.

Yokota, T. et al., 2016. Ultraflexible organic photonic skin. *Science Advances*, 2(4), pp.e1501856–e1501856. Available at: http://advances.sciencemag.org/cgi/doi/10.1126/sciadv.1501856.

Yue, D. et al., 2016. Passivated ambipolar black phosphorus transistors. *Nanoscale*, 8(25), pp.12773–12779. Available at: http://xlink.rsc.org/?DOI=C6NR02554D.

Yue, Z. et al., 2013. Quantum-dot-based photoelectrochemical sensors for chemical and biological detection. *ACS Applied Materials and Interfaces*, 5(8), pp.2800–2814.

Zhang, P. et al., 2012. First-principles studies of the hydrogenation effects in silicene sheets. *Physics Letters, Section A: General, Atomic and Solid State Physics*, 376(14), pp.1230–1233.

Zhang, R. et al., 2014. Silicane as an Inert Substrate of Silicene: A Promising Candidate for FET. *The Journal of Physical Chemistry C*, 118(43), pp.25278–25283. Available at: http://pubs.acs.org/doi/abs/10.1021/jp508253x.

Zhao, J. et al., 2016. Rise of silicene: A competitive 2D material. *Progress in Materials Science*, 83, pp.24–151. Available at: http://dx.doi.org/10.1016/j.pmatsci.2016.04.001.

Zheng, F.-B. & Zhang, C.-W., 2012. The electronic and magnetic properties of functionalized silicene: a first-principles study. *Nanoscale research letters*, 7(1), p.422. Available at: http://www.pubmedcentral.nih.gov/articlerender.fcgi?artid=3460763&tool=pmcentrez&rendertype=abstract.

7. PUBLICATIONS

Lyuleeva, A.; Narreto, M.A.; Helbich, T.; Veinot, J.; Lugli, P.; Rieger, B.; Hegmann, F.: Photoluminescence Dynamics of Functionalized Two-dimensional Silicon Nanosheets, *manuscript in preparation.*

Lyuleeva, A.; Holzmüller, P.; Helbich, T.; Stutzmann, M; Brandt, S. M.; Becherer, M.; Lugli P.; Rieger, B.: Charge Transfer Doping in Functionalized Silicon Nanosheets/P3HT hybrid Material with Effect on the Application in Solution-Gated Field-Effect Transistors, *manuscript submitted, **2018***.

Lyuleeva, A.; Helbich, F.; Bobinger, M.; Rieger, B., Becherer, M.; Lugli, P.; Rivadeneyra, A.: Functionalized and Oxidized Silicon Nanosheets: Customized Design for Enhanced Sensitivity towards Relative Humidity, *manuscript submitted*, **2017**.

Lyuleeva, A.; Rivadeneyra, A.; Helbich, F., Rieger, B., Lugli, P.; Becherer, M.: *Modified 2D Silicon Nanosheets in Electronics: From Synthesis to Application*", Graphene Week 2017, Athens, Greece, September 25th – 29th **2017**.

Lyuleeva, A.; Rivadeneyra, A.; Helbich, T., Narreto, M. A., Hegmann, F., Rieger, B., Lugli, P.: Silicane: The New 2D Silicon Nanomaterial For Sensing and Electronics, Faculty of Engineering Graduate Research Symposium, Edmonton, Canada, June27th – 28th **2017**.

Lyuleeva, A.; Rivadeneyra, A.; Helbich, T., Narreto, M. A., Hegmann, F., Rieger, B., Lugli, P.: Fabrication of Low-Cost Devices Based on Chemically Modified 2D Silicon Nanosheets, 9th International Conference on Materials for Advanced Technologies, Singapore, Singapore, June 18th – 23th, **2017**.

Lyuleeva, A.; Helbich, T.; Rieger, B.; Becherer, M; Lugli, P.: Modified Silicon Nanosheets and Their Composites – Novel 2D Material for Photonic Sensor Applications, 4th Annual Alberta NANO Research Symposium **2017**, Calgary, Canada, May 4th – 5th.

Lyuleeva, A.; Helbich, T.; Holzmüller, P.; Narreto, M. A.; Hegmann, F.; Rieger, B.; Lugli P.: Surface Modification of 2D Silicon Nanosheets for Enhanced (Opto)Electronic Device Fabrication, 100th Canadian Chemistry Conference and Exhibition (CSC 2017), Toronto, Canada, Mai 28 – June 01, **2017**.

Lyuleeva, A.; Helbich, T.; Rieger, B.; Lugli, P.: Polymer–Silicon Nanosheet Composites: Bridging the Way to Optoelectronic Applications. *J. Phys. D: Appl. Phys.*, **2017**, 50, 135106.

Helbich, T.; Lyuleeva, A.; Marx, P.; Scherf, L. M.; Purkait, T. K.; Fässler, T. F.; Lugli, P.; Veinot, J. G. C.; Rieger, B.: Lewis Acid Induced Functionalization of Photoluminescent Two-Dimensional Silicon Nanosheets for the Fabrication of Functional Hybrid Films, *Advanced Functional Materials*, **2017**, p.1606764.

Helbich, T.; Lyuleeva, A.; Ludwig, T.; Scherf, L.M.; Fässler, T. F.; Lugli, P.; Rieger, B.: One-Step Synthesis of Photoluminescent Covalent Polymeric Nanocomposites from 2D Silicon Nanosheets, *Adv. Funct. Mater*., **2016**, 26, 6711.

Helbich, T.; Lyuleeva, A.; Höhlein, I. M. D.; Marx, P.; Scherf, L. M.; Kehrle, J.; Fässler, T. F.; Lugli, P.; Rieger, B.: Radical-induced Hydrosilylation Reactions for the Functionalization of Two-Dimensional Hydride Terminated Silicon Nanosheets, *Chem. Eur. J.*, **2016**, online.

Lyuleeva, A.; Helbich, T.; Narreto, M. A.; Falco, A.; Hegmann, F.; Rieger, B.; Lugli, P.: 99th Canadian Chemistry Conference and Exhibition, 05-09 June 2016, Halifax NS USA, **2016.**

Lyuleeva, A.; Helbich, T.; Narreto, M.A.; Hegmann, F.; Rieger, B.; Lugli, P.: Graphene Flagship EU-US Workshop on 2D Materials, Heterostructures and Devices 2016 Manchester, United Kingdom, 10-12 June, **2016**.

Caterino, R.; Csiki, R.; Lyuleeva, A.; Pfisterer, J.; Wiesinger, M.; Janssens, S. D.; Haenen, K.; Cattani-Scholz, A.; Stutzmann, M.; Garrido, J. A.: Photocurrent Generation in Diamond Electrodes Modified With Reaction Centers, *ACS Applied Materials & Interfaces*, **2015**, 7 (15), 8099-8107.

Hess, L.; Lyuleeva, A.; Blaschke, B. M.; Sachsenhauser, M.; Seifert, M.; Deubel, F.; Garrido, J. A.: Graphene Transistors with Multi-functional Polymer Brushes for Biosensing Applications, *ACS Applied Materials & Interfaces,* **2014**, 6 (12), 9705-9710.

Lyuleeva, A.; Hess, L. H.; Blaschke B. M.; Sachsenhauser, M.; Seifert M.; Deubel, F.; Garrido, J. A.: Functionalization of Graphene for Bioelectronic Applications, DPG Spring Conference, Dresden, Germany, **2014**.

Cover Pages:

Helbich, T.; Lyuleeva, A.; Ludwig, T.; Scherf, L.M.; Fässler, T. F.; Lugli, P.; Rieger, B.: Nanocomposites: One-Step Synthesis of Photoluminescent Covalent Polymeric Nanocomposites from 2D Silicon Nanosheets (Adv. Funct. Mater. 37/2016).

Helbich, T.; Lyuleeva, A.; Marx, P.; Scherf, L. M.; Purkait, T. K.; Fässler, T. F.; Lugli, P.; Veinot, J. G. C.; Rieger, B.: Silicon Nanosheets: Lewis Acid Induced Functionalization of Photoluminescent 2D Silicon Nanosheets for the Fabrication of Functional Hybrid Films (Adv. Funct. Mater. 21/2017)

8. APPENDIX

8.1. ONLINE ARTICLE: SILICON NANOSHEETS. NEW MATERIALS FOR FUTURE APPLICATIONS (Lyuleeva, Tobias Helbich, Lugli, Becherer, et al. 2017)

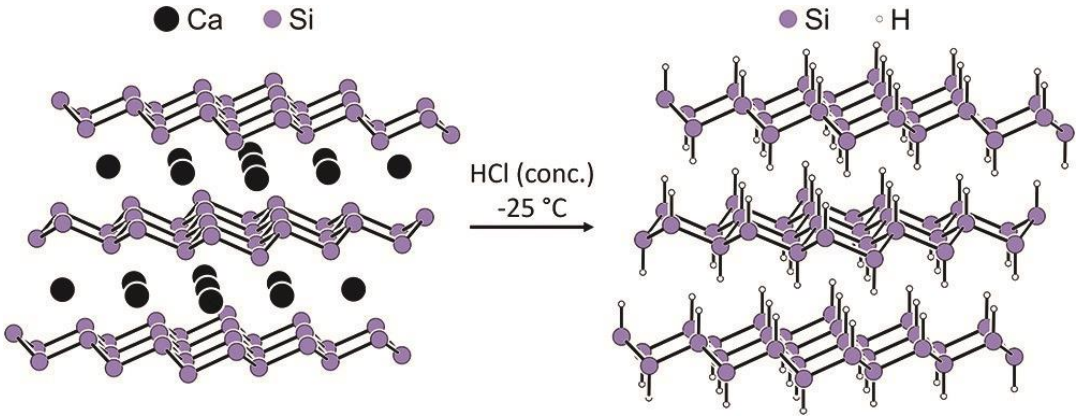

Figure 46: Synthesis of silicanes from the Zintl salt $CaSi_2$. (Lyuleeva, Tobias Helbich, Lugli, Becherer, et al. 2017)

Two-dimensional silicon nanosheets have attracted the attention of researchers from different fields. They exhibit the structural properties of graphene - one of the key players in nanotechnology - but are made from silicon, which forms the basis of information technology. Silicon nanosheets also combine anisotropic structural characteristics with exceptional (opto)electronic properties. As such, they show photoluminescence and in first applications were used in photonic sensors as well as field-effect transistors and lithium ion batteries. In the future, the ease of their processing combined with their outstanding properties might enable the production of printable and flexible electronics.

8.2. TRPL MEASUREMENTS:

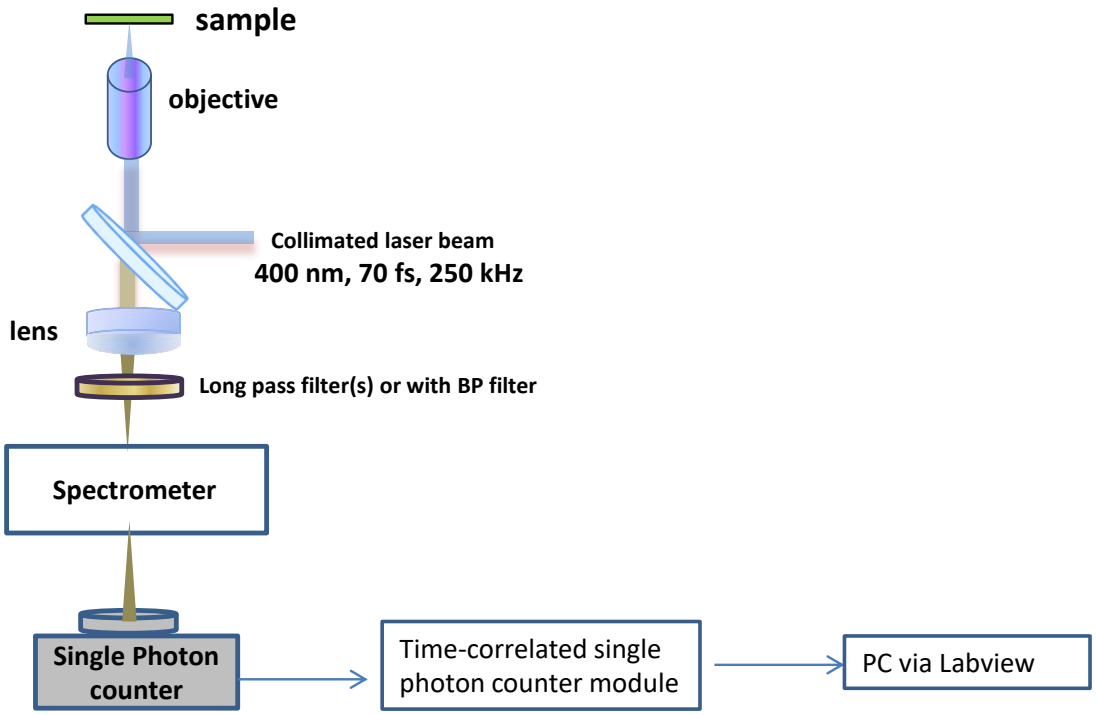

Figure 47: Simplified version of the Confocal setup for measuring Steady-state Photoluminescence, Time-integrated Photoluminescence, and Time-resolved Photoluminescence. (Measurements were carried out at the University of Alberta, Edmonton, Canada)

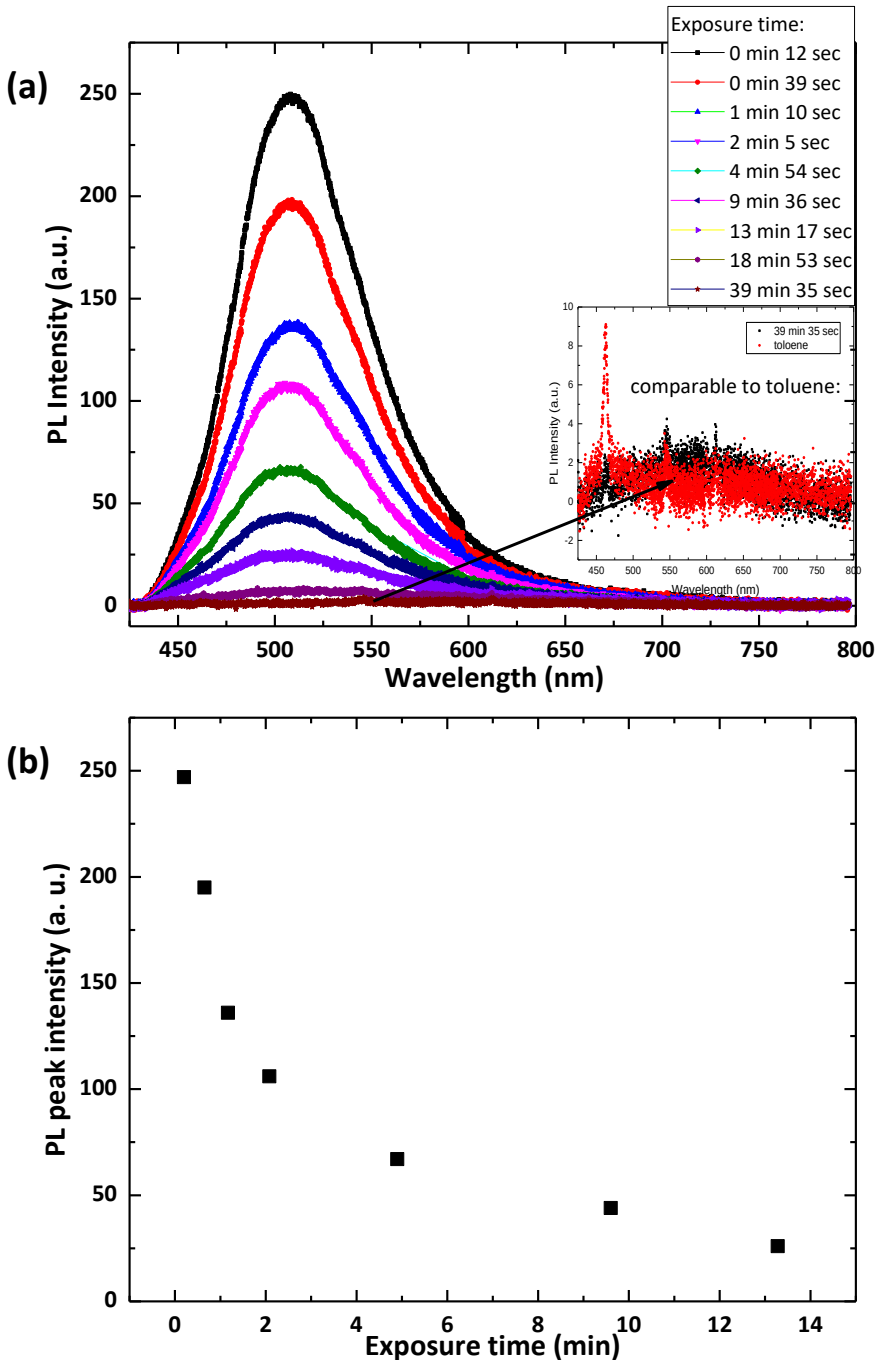

Figure 48: (a) Decay of PL intensity of SiNS-H (dispersed in toluene) over time. The inset in (a) indicates measurements of bare toluene. (b) PL peak intensity vs. Exposure time demonstrates degradation of the PL intensity with UV light radiation.

8.2.1. PL and TRPL Measurements of SiNS-Dodecene/P3HT blends

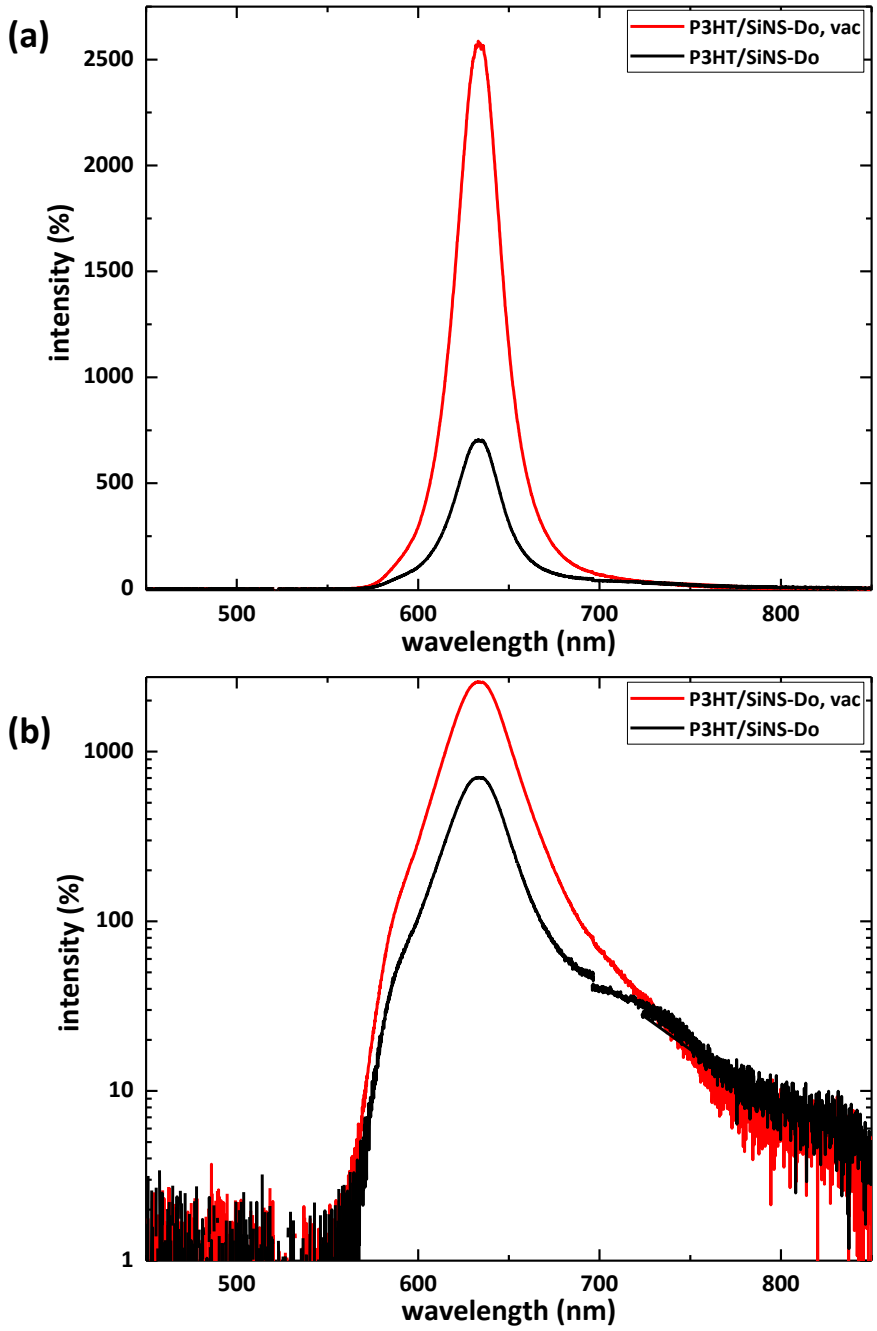

Figure 49: Full CCD spectrum (20 sec each scan) PL of SiNS-Do/P3HT films, drop-deposited on quartz glass. Measurements were carried out in air (black line) and in vacuum (red line). Linear plots (a) and semi-log plots (b) are shown. Laser power is 53 ± 1 µW, measured before the experiment.

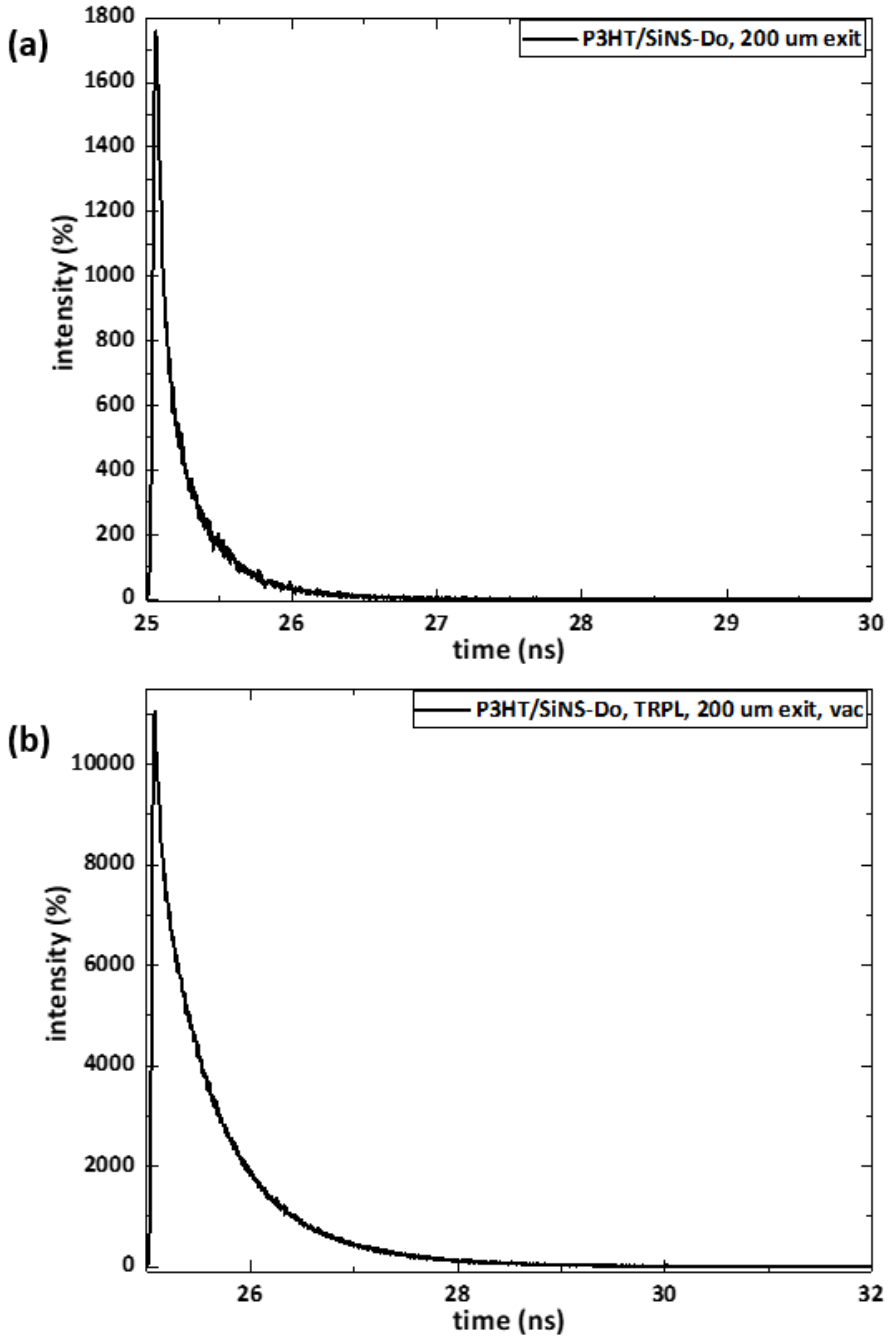

Figure 50: TRPL of SiNS-Do/P3HT films drop-deposited on quartz glass, measured in air (a) and in vacuum (b). TRPL were measured in 20 mins at 200 µm exit slit. Laser power is 53 ± 1 µW, measured before the experiment.

8.2.2. PL and TRPL Measurements of SiNS-PhAc/P3HT blends

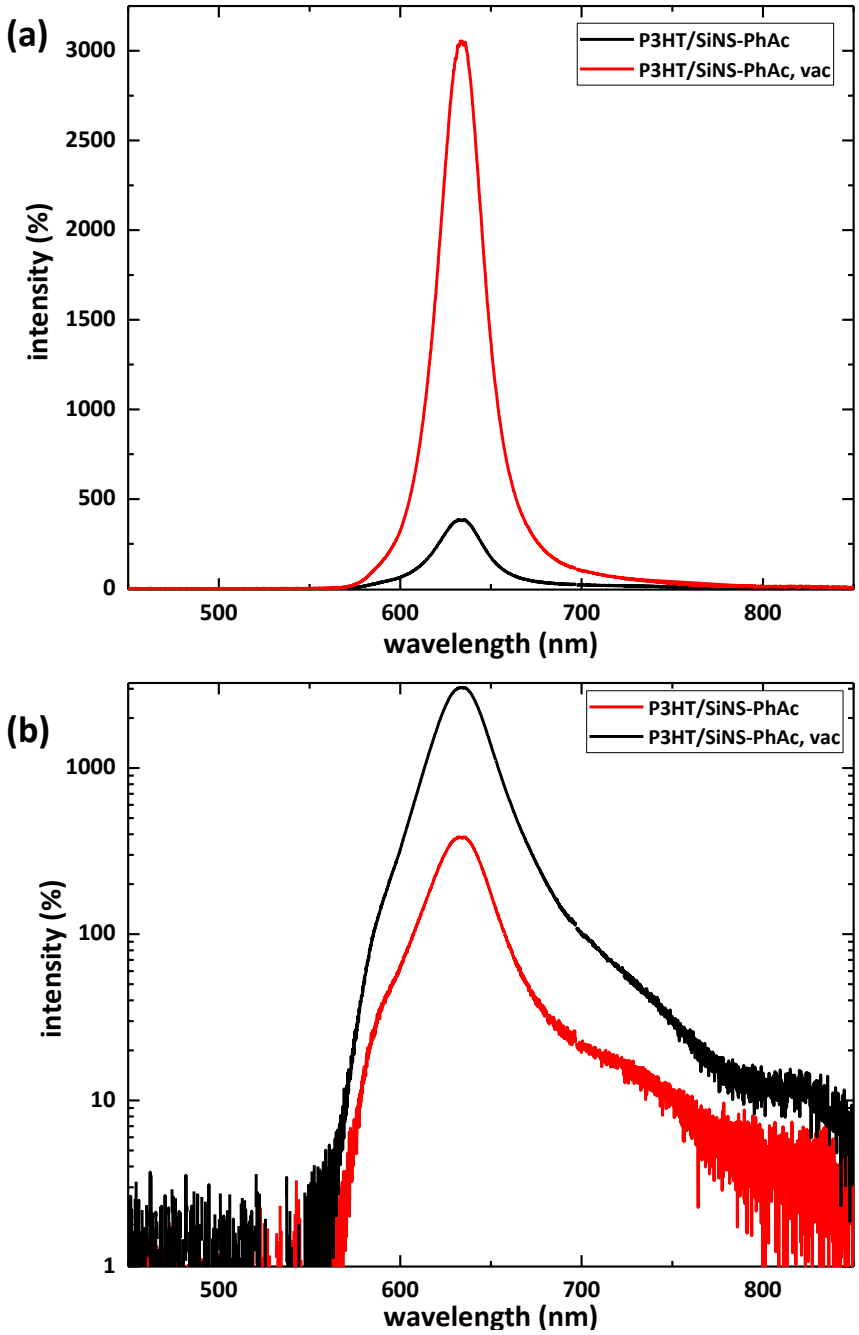

Figure 51: Full CCD spectrum (20 sec each scan) PL intensity (%) vs. wavelength (nm) measurements of SiNS-PhAc/P3HT films, drop-deposited on quartz glass. Measurements were carried out in air (black line) and in vacuum (red line). Linear plots (a) and semi-log plots (b) are shown. Laser power is 53 ± 1 μW, measured before the experiment.

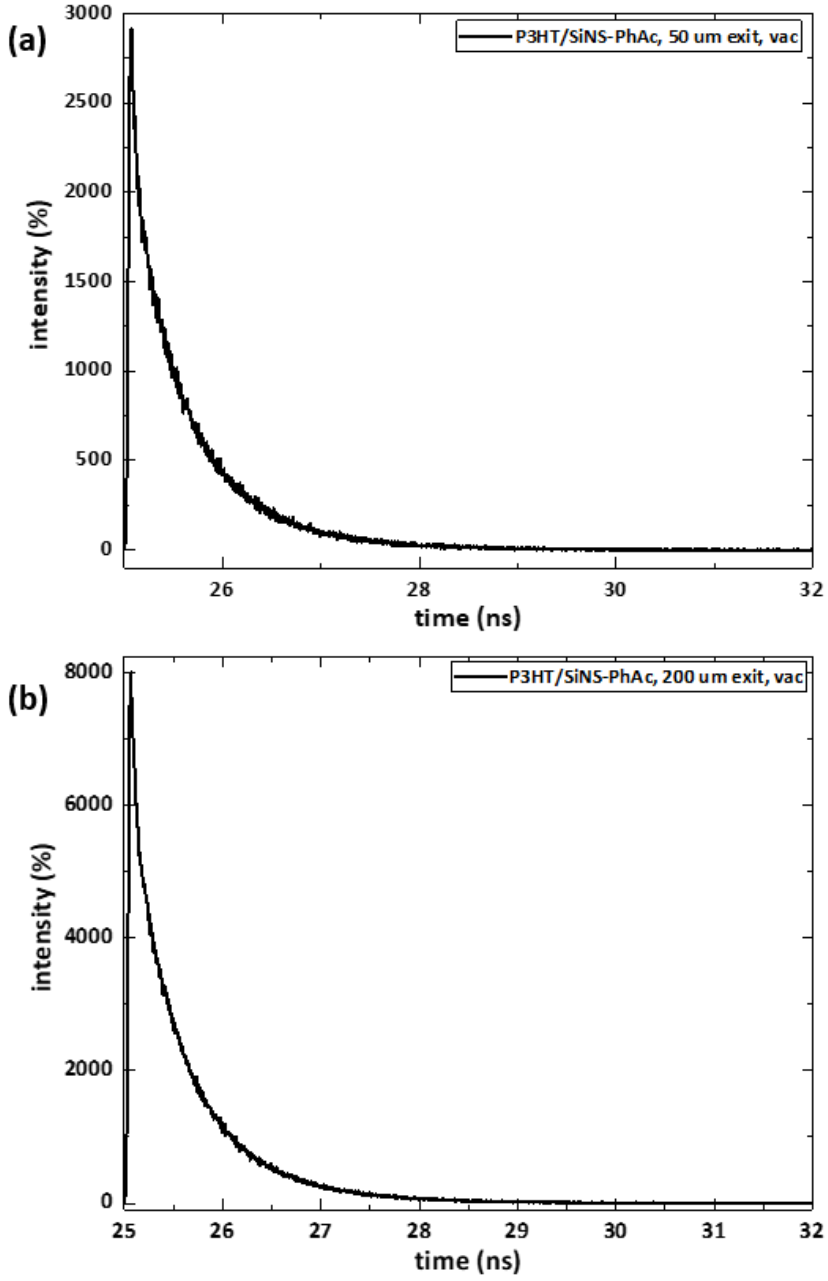

Figure 52: TRPL of SiNS-PhAc/P3HT films drop-deposited on quartz glass, measured in vacuum with 50 µm exit slit size (a) and with 200 µm exit slit size (b). Laser power is 53 ± 1 µW, measured before the experiment.

8.2.3. PL and TRPL Measurements of SiNS-ThAc/P3HT blends

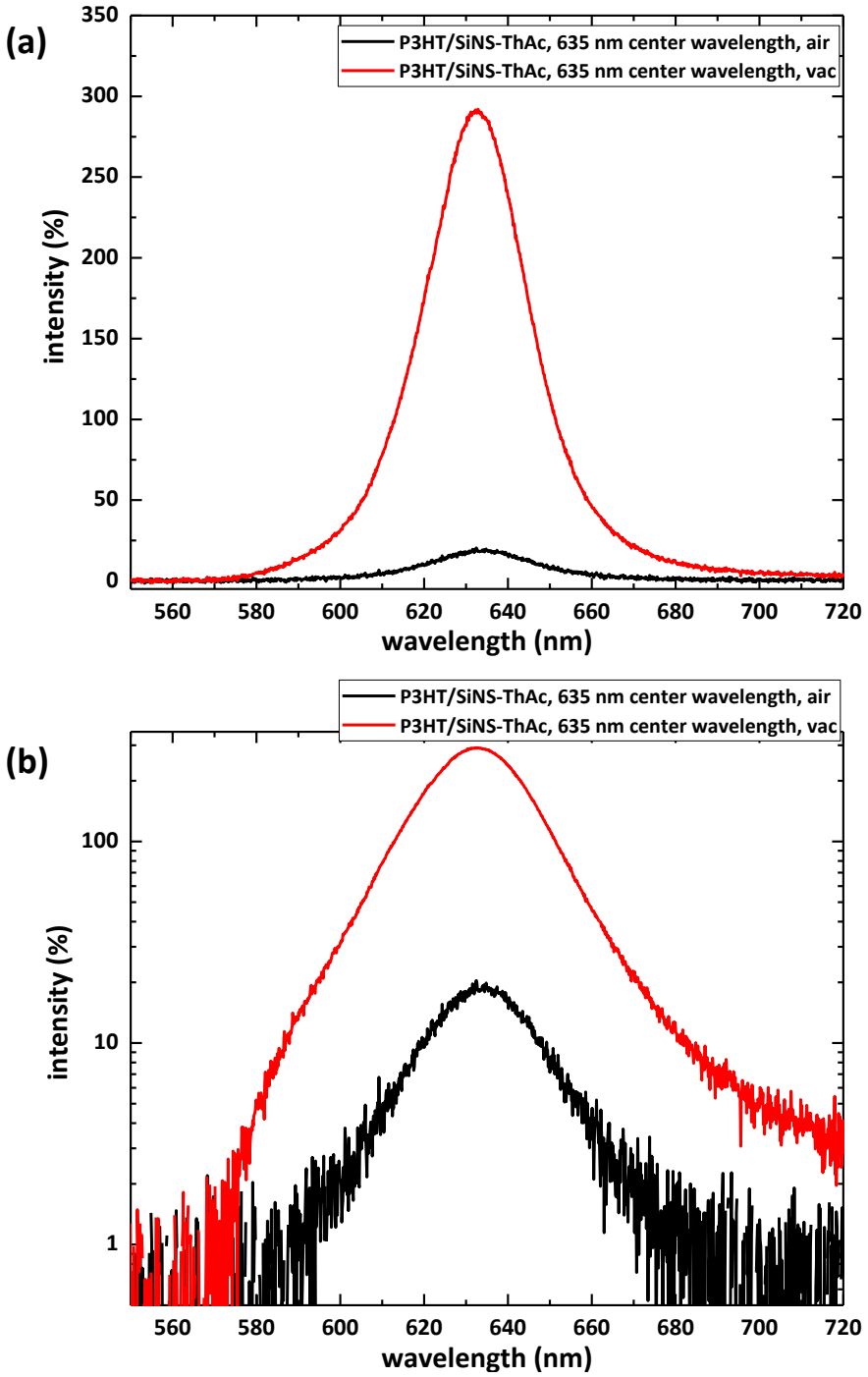

Figure 53: PL intensity (%) vs. wavelength (nm) measurements of SiNS-ThAc/P3HT films, drop-deposited on quartz glass. Measurements were carried out in air (black line) and in vacuum (red line) with the measurement center wavelength of 635 nm. Linear plots (a) and semi-log plots (b) are shown. Laser power is 53 ± 1 µW, measured before the experiment.

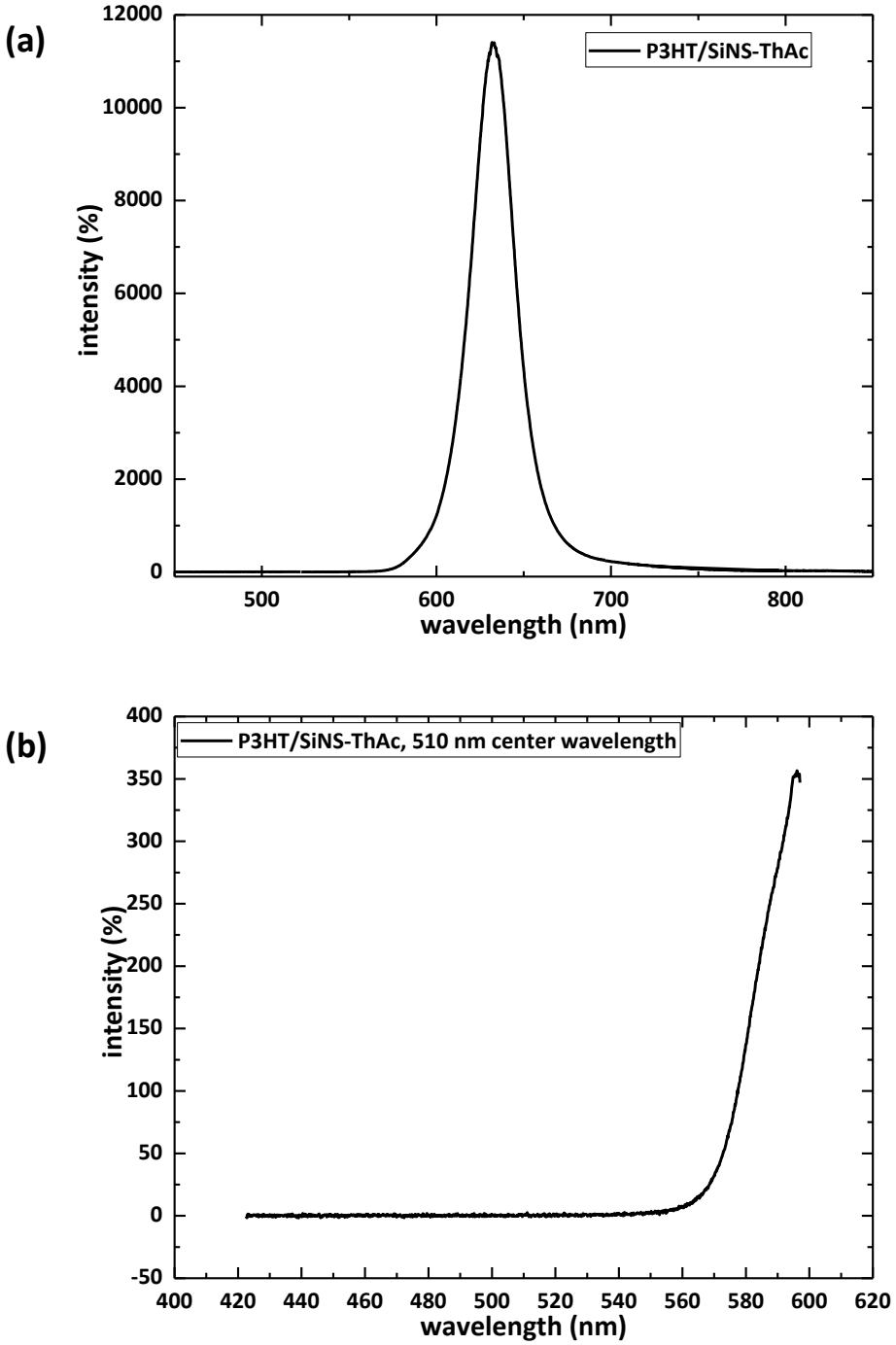

Figure 54: (a) Full CCD spectrum (20 sec each scan) PL intensity (%) vs. wavelength (nm) measurements of drop-casted SiNS-ThAc/P3HT films and PL intensity (%) vs. wavelength (nm) measurements of drop-casted SiNS-ThAc/P3HT films at 510 nm center wavelength. Laser power is 53 ± 1 μW, measured before the experiment.

8.3. LEPR MEASUREMENTS:

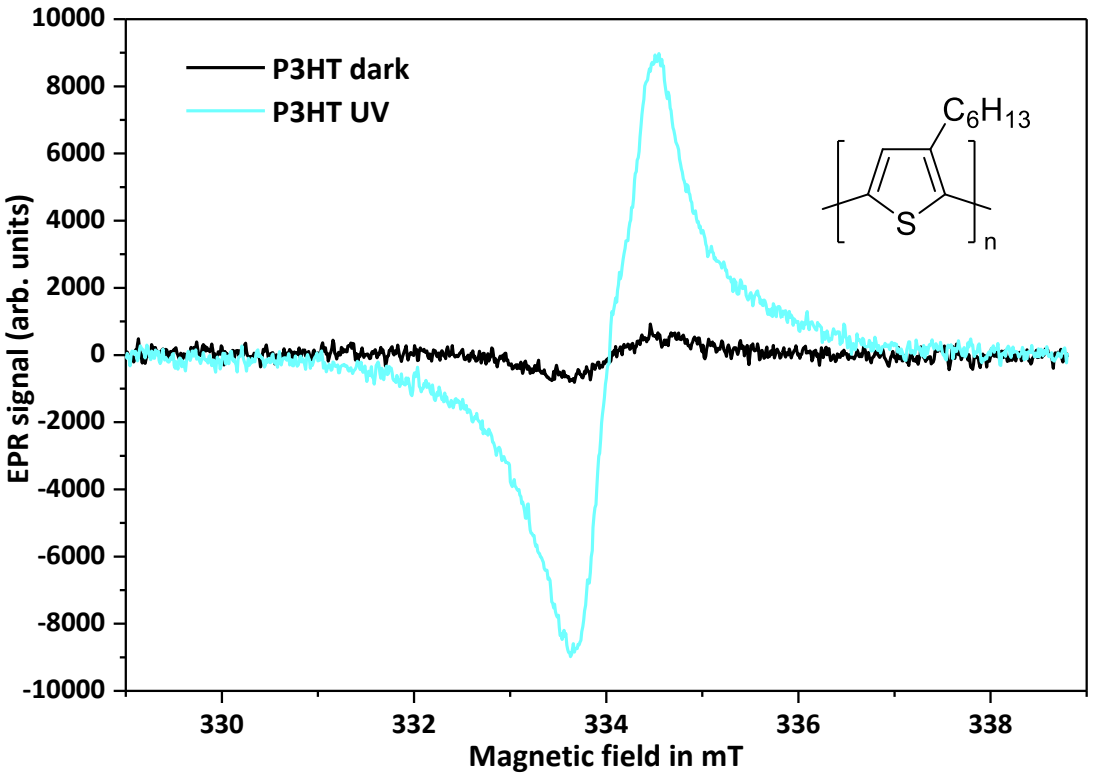

Figure 55: LEPR Measurements of a P3HT film in dark (black line) and under UV light radiation (cyan line).

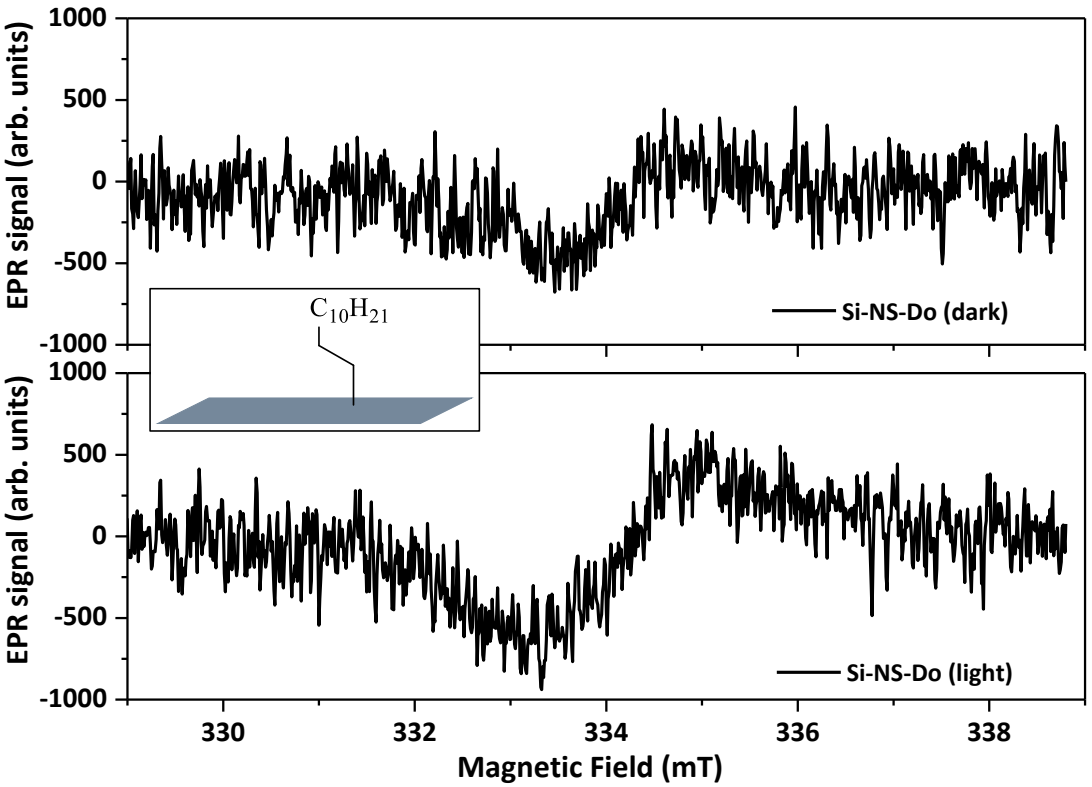

Figure 56: LEPR measurements of SiNS-$C_{12}H_{25}$ film in dark and under visible light radiation.

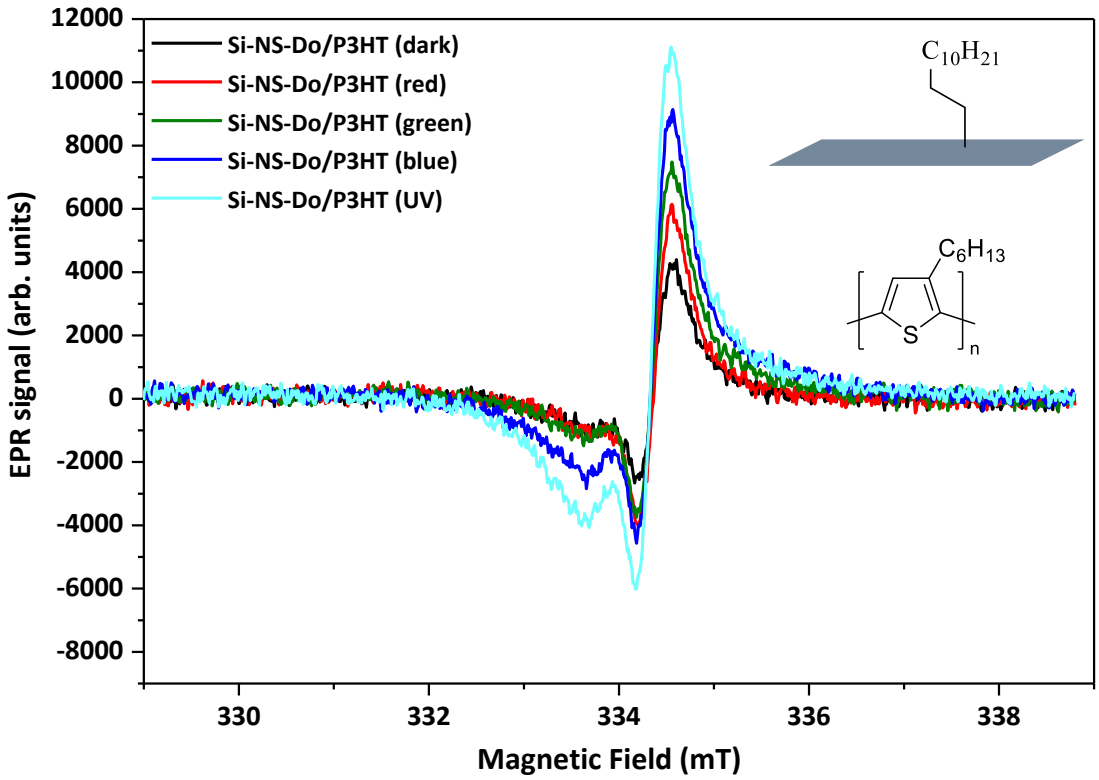

Figure 57: LEPR Measurements of a SiNS-$C_{12}H_{25}$/P3HT film in dark (black), under red light (red line), green light (green line), blue light (blue line) and UV light radiation (cyan line).

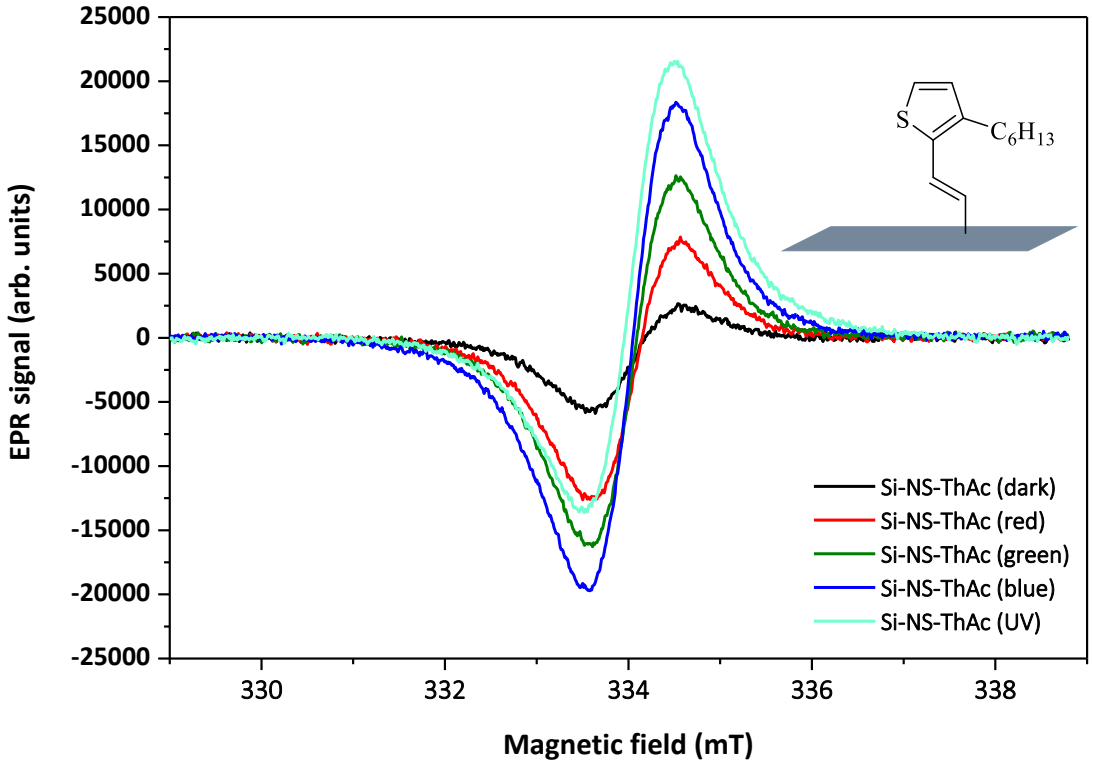

Figure 58: LEPR Measurements of a SiNS-ThAc film in dark (black line), under red light (red line), green light (green line), blue light (blue line) and UV light radiation (cyan line).

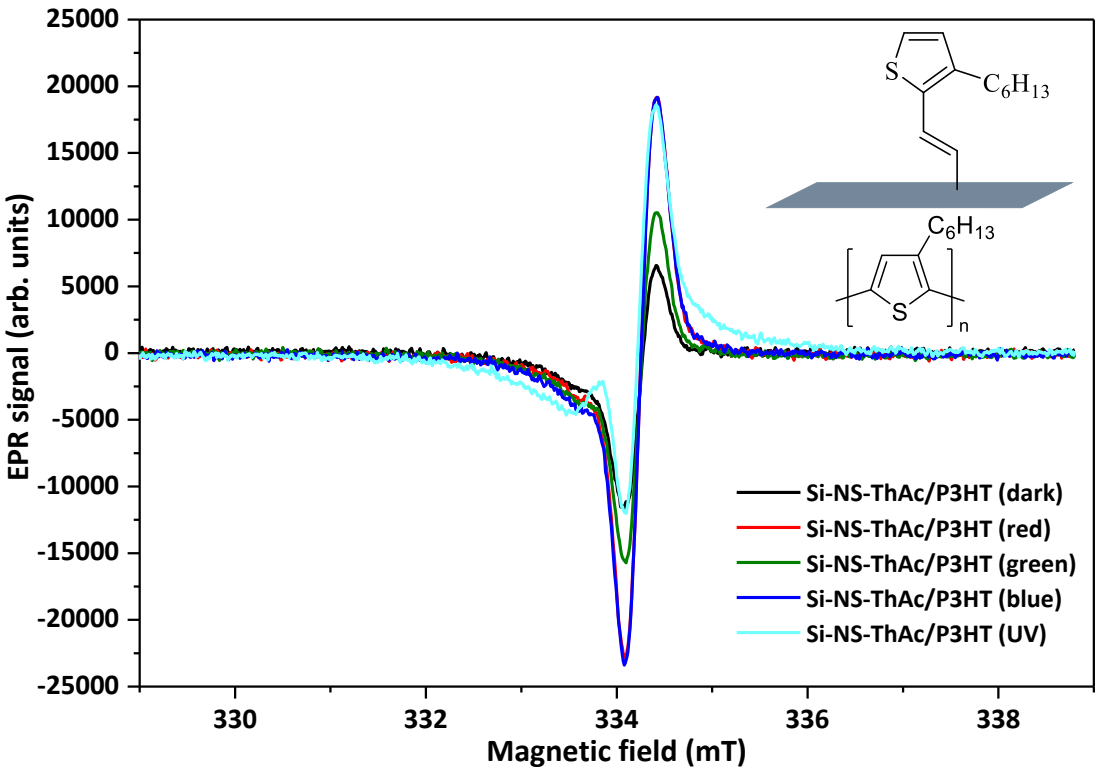

Figure 59: LEPR Measurements of a SiNS-ThAc/P3HT film in dark (black line), under red light (red line), green light (green line), blue light (blue line) and UV light radiation (cyan line).

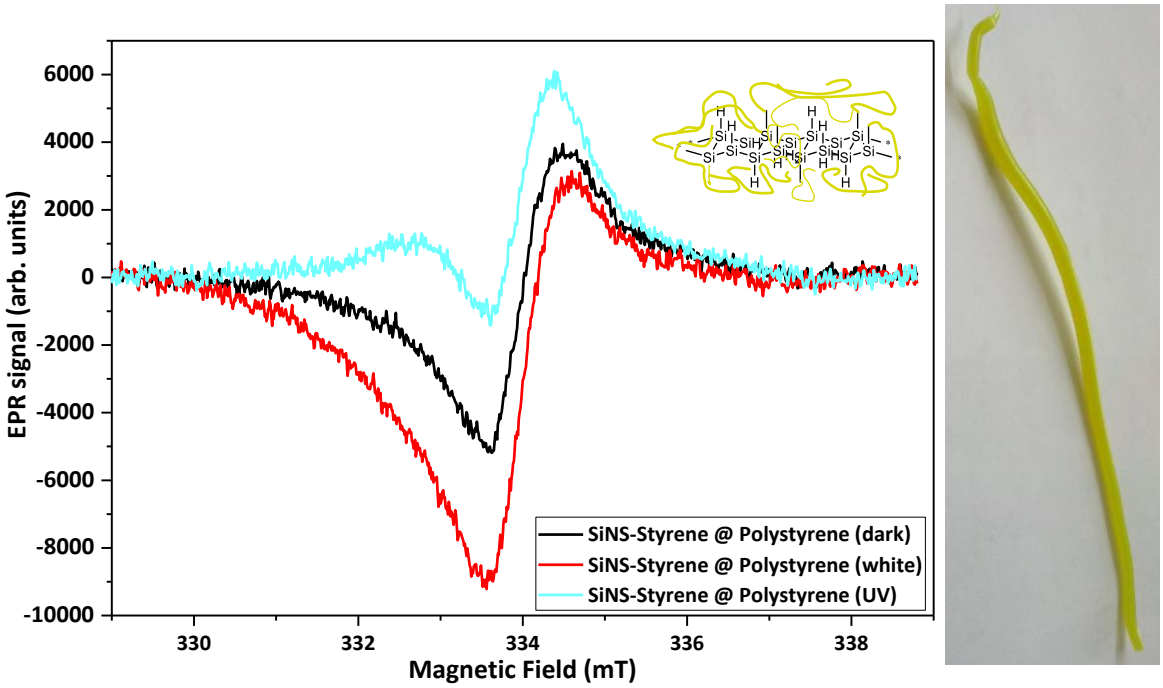

Figure 60: LEPR Measurements of a SiNS-PS@PS composite in solid in dark (black), under visible light (red line) and UV light radiation (cyan line).

8.4. Grazing-Incidence Wide-Angle X-ray Scattering (GIWAXS) Measurements

GIWAXS measurements were carried out with *Ganesha SAXSLAB* (λ = 1.54 Å, sample-detector distance = 106.2 m, incident angle = 0.2°, vertical beam size = 100 µm, horizontal beam size of 200 µm). The scattering pattern was detected with a *Pilatus300K* with a total of 487 x 619 pixels (pixel size 172 µm x 172 µm).

Incident angle of 0.2 ° was chosen, as critical angle of Si is around 0.224 ° and critical angle of P3HT is at 0.162 °. Total reflection from the substrate (less background) is the result after penetration through the polymer thin film.

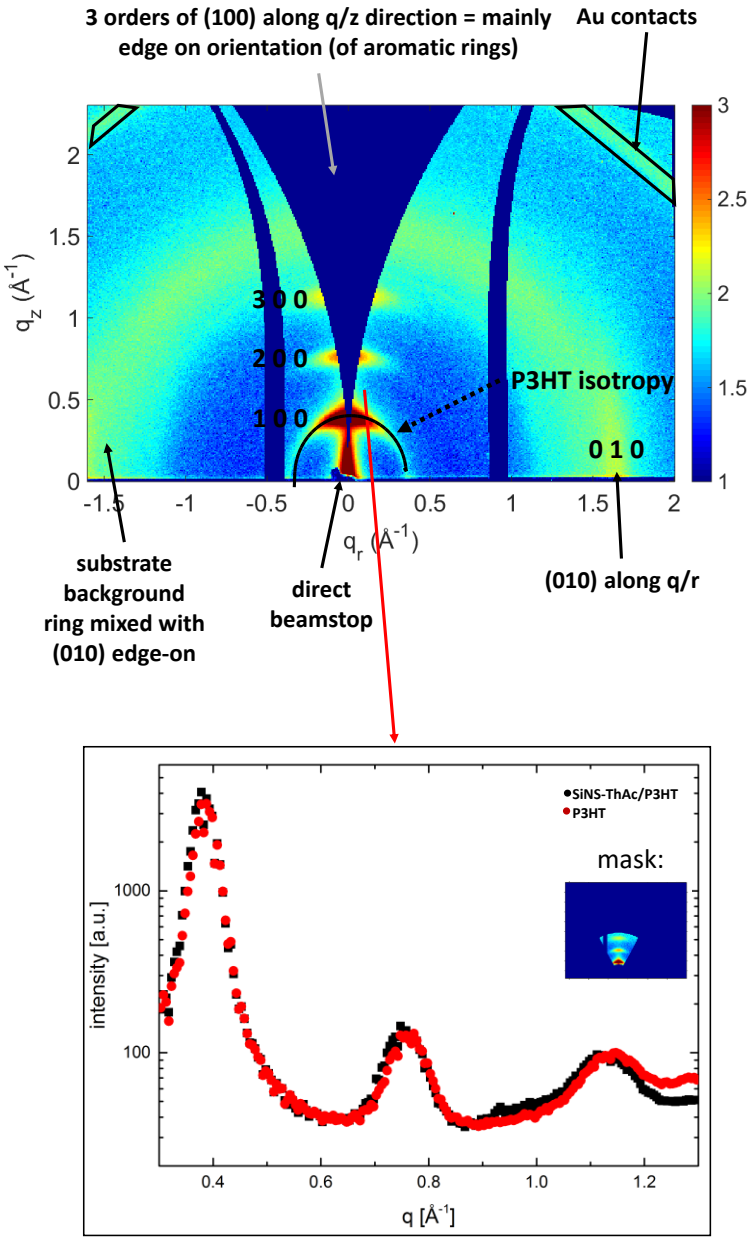

Figure 61: GIWAXS measurements show lamellar (100) stacking around 0.4 A^{-1}, π- π (010) stacking around 1.6 A^{-1} and 3 orders of 100 along q/z-direction → mainly edge on orientation (of aromatic rings).

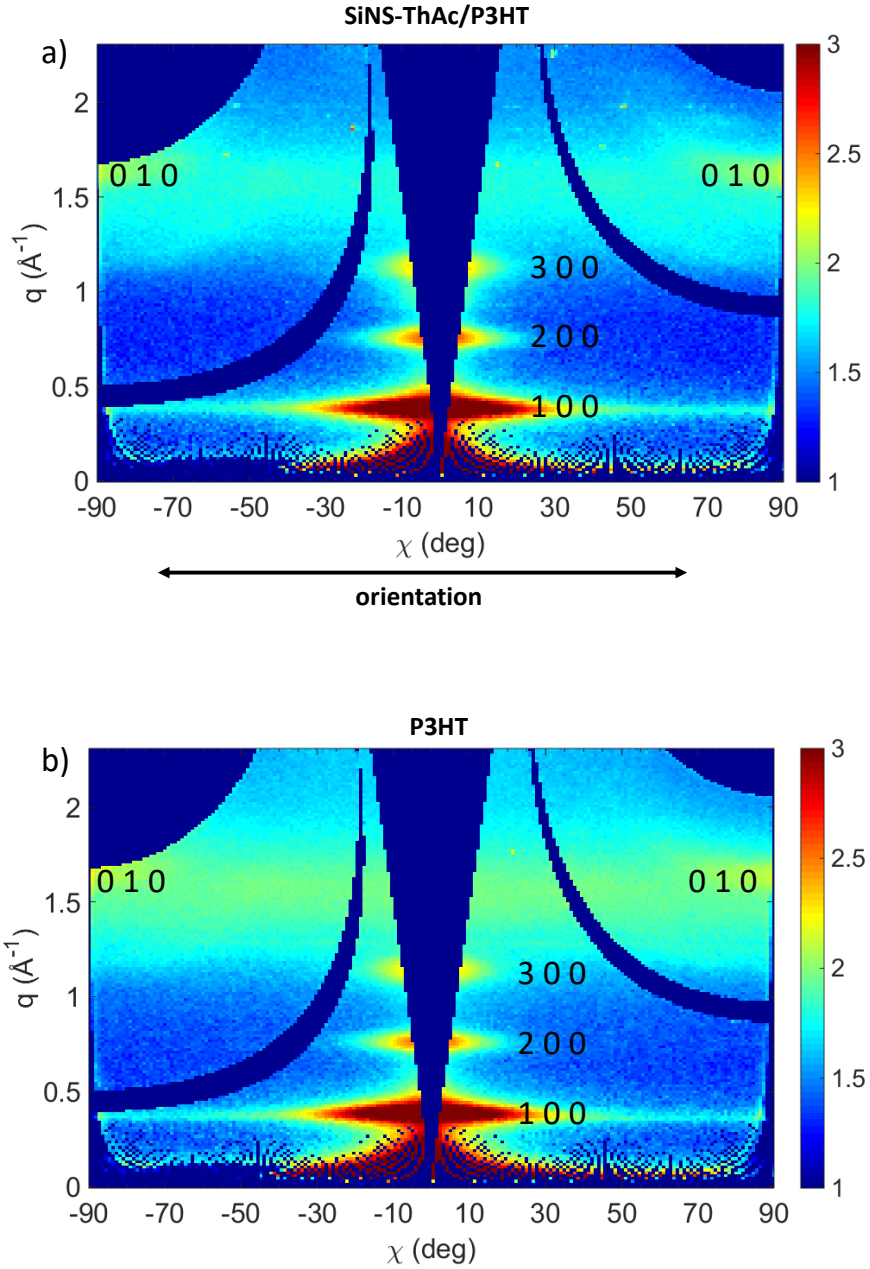

Figure 62: Chi plot presentation of bare P3HT and SiNS-ThAc/P3HT hybrid materials which were spin-coated on Si/SiO_2 substrate.

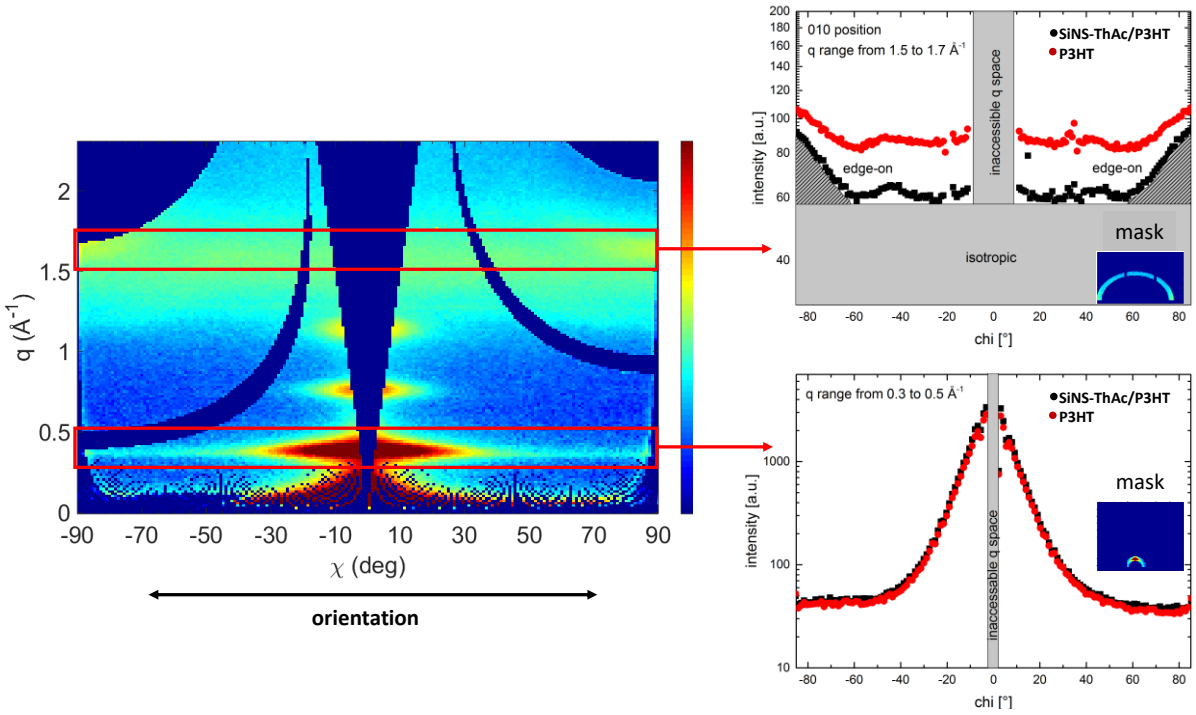

Figure 63: The measurements show increased π- π stacking for SiNS with an "edge-on" orientation, or "face-on" π- π is suppressed. Rratio of "isotropic" to "edge-on" is slightly higher for SiNS containing films.

8.5. SiNS-substrate and SiNS-polymer@polymer Quantum Yields

Emission spectra were measured on a *Hamamatsu Absolute PL Quantum Yield C11347* spectrometer.

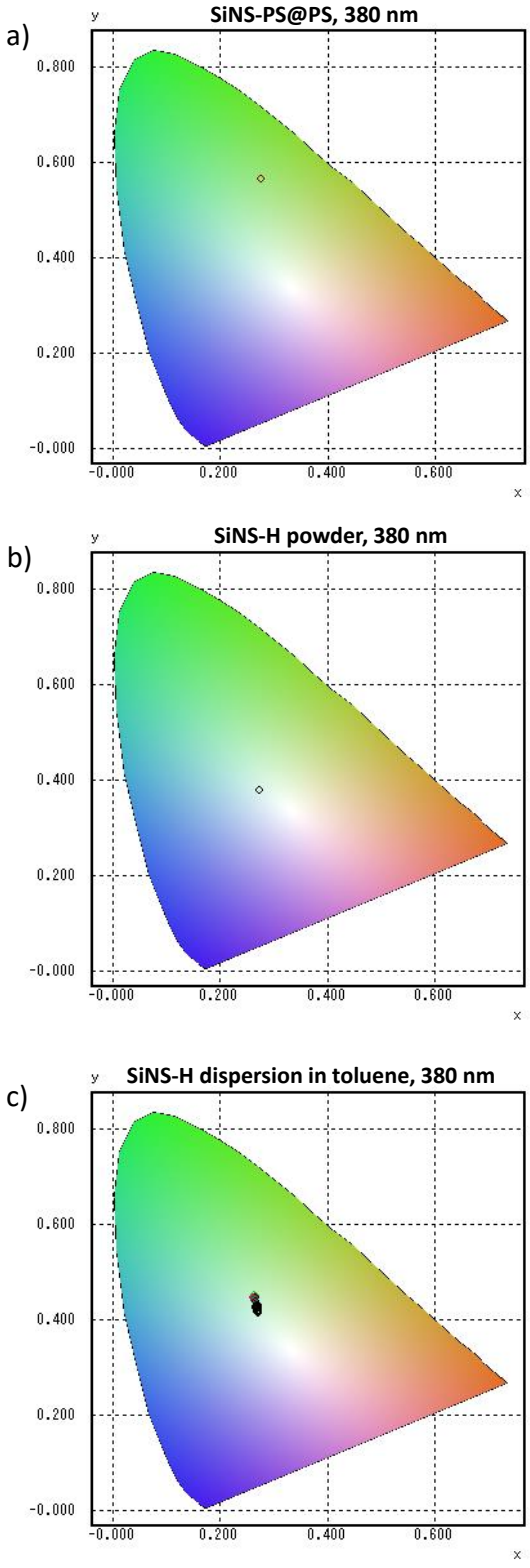

Figure 64: Quantum Yield of SiNS-PS@PS (a), SiNS-H in toluene (b) and SiNS-H in toluene (c) excited with light with the wavelength of λ = 380 nm.

Table 5: Absolute Average Quantum Yield (%) of solution and solid samples.

SiNS-H (toluene)	**SiNS-$C_{12}H_{25}$ (toluene)**	**SiNS-$C_{12}H_{25}$ (powder)**	**SiNS-PS@PS**
0.98	2.10	0.91	2.33

8.6. COVER PAGES

8.6.1. Nanocomposites: One-Step Synthesis of Photoluminescent Covalent Polymeric Nanocomposites from 2D Silicon Nanosheets (Adv. Funct. Mater. 37/2016)

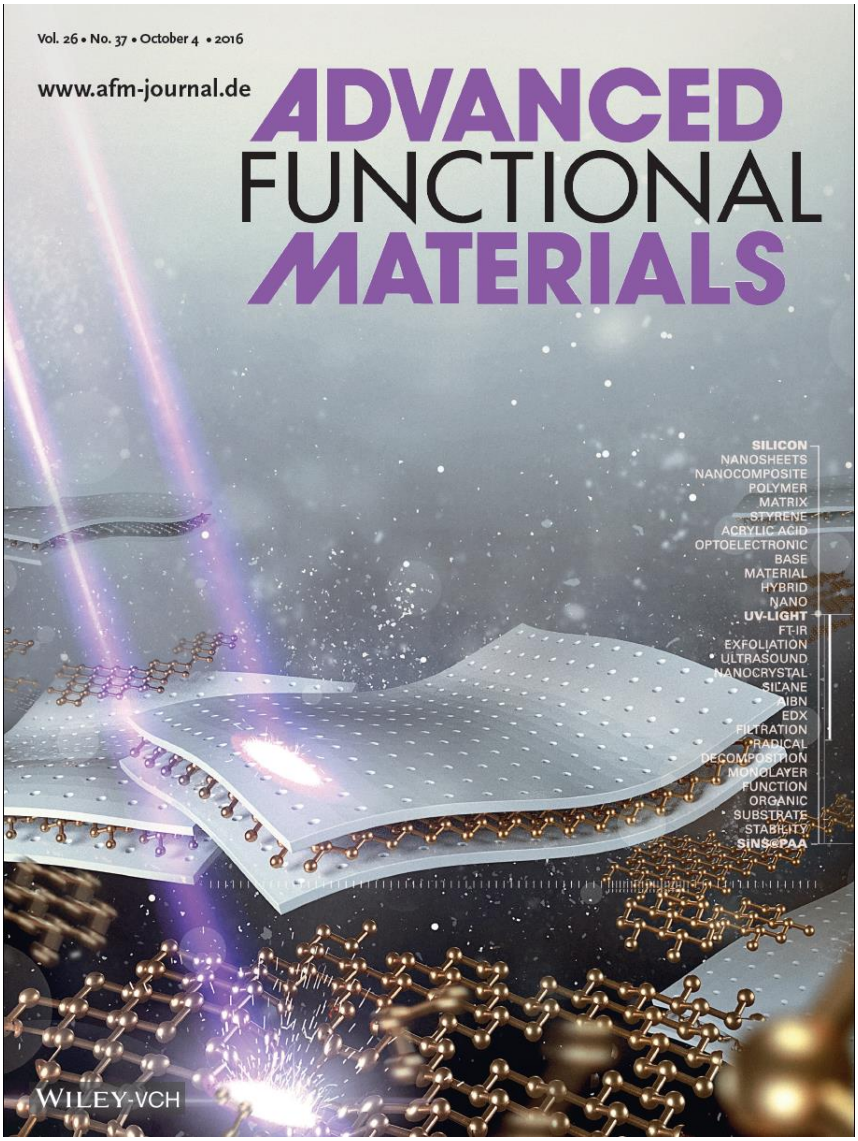

Figure 65: Back cover page of the 26th volume, 37th issue of the Advanced Functional Materials Journal showing an image of exfoliated sheets wrapped in a coating material, which helps to protect the SiNSs from light radiation. The content of the image is related to the publication "One-Step Synthesis of Photoluminescent Covalent Polymeric Nanocomposites from 2D Silicon Nanosheets". (Helbich, Lyuleeva, Ludwig, et al. 2016)

8.6.2. Silicon Nanosheets: Lewis Acid Induced Functionalization of Photoluminescent 2D Silicon Nanosheets for the Fabrication of Functional Hybrid Films (Adv. Funct. Mater. 21/2017)

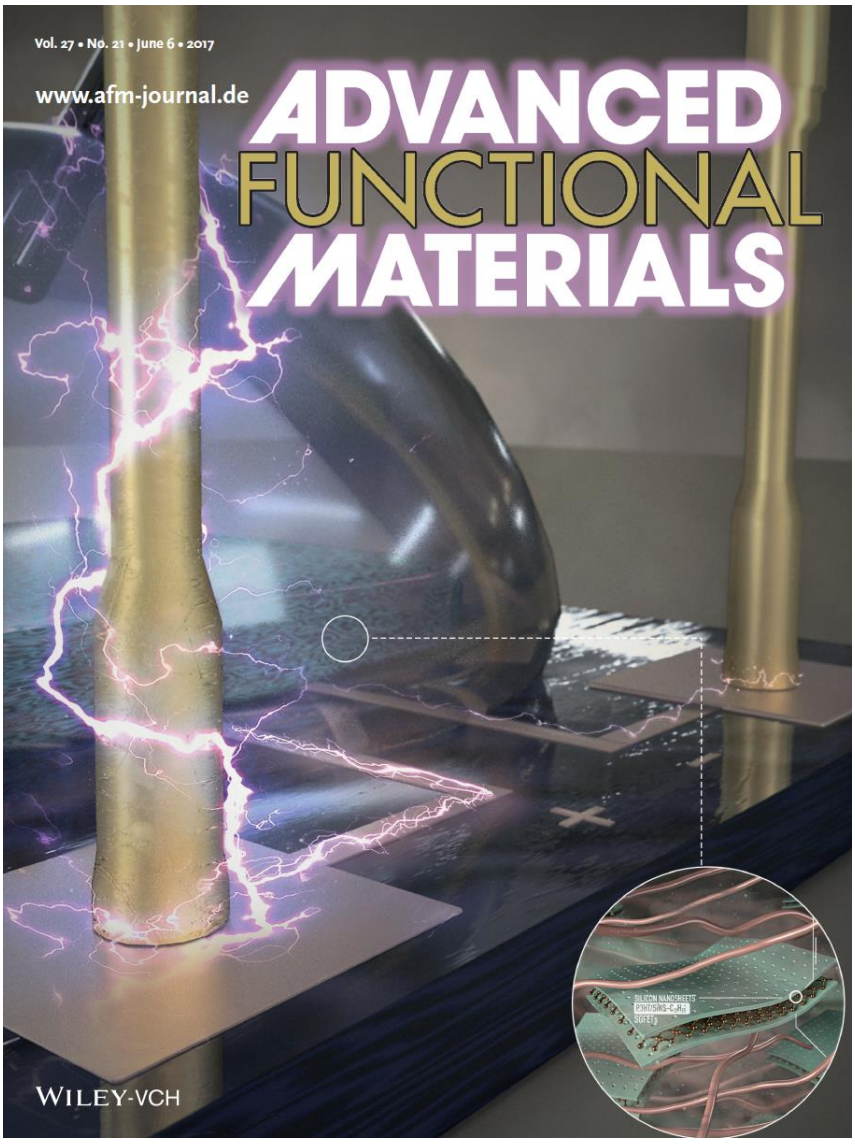

Figure 66: Cover page of the 27th volume, 21st issue of the Advanced Functional Materials Journal showing a part of the Solution-Gated Field-effect Transistor set-up based on SiNS-Dodecene/P3HT hybrid material. The content of the image is related to the publication "Lewis Acid Induced Functionalization of Photoluminescent 2D Silicon Nanosheets for the Fabrication of Functional Hybrid Films". (Tobias Helbich et al. 2017)

9. LICENSES FOR COPYRIGHT CONTENT

Agreement between: Samuel Wright; swright@cvdequipment.com

And: Lyuleeva, Alina

Date: 23 October 2017

Subject: RE: [Salesforce Web to Submission] General Contact Us Form

Dear Alina,

Yes, you can use the image. We would be very interested to receive an electronic copy of the thesis if possible. Attached is a full resolution version of the image.

Thank you,

Best regards,

Samuel Wright, PhD

Application Engineer, 355 S. Technology Dr., Central Islip, NY 11722
Phone: (631) 981-7081
Fax: (631) 981-7095
www.cvdequipment.com

enabling tomorrow's technologies™
CVD Production
R&D Processing
Gas & Chemical Delivery

InTech's Publishing Ethics and Legal Affairs Department

Agreement between: Ivan Šuljić

And: Lyuleeva, Alina

Date: 24.10.2017

Dear Alina,

My name is Ivan Šuljić and I am writing you from InTech's Publishing Ethics and Legal Affairs Department.

You may freely use the figure 5 in your publication as long as you cite the source chapter of the original figure, and include the following notice in the figure caption:

© 2017 Pérez-Taborda JA, Caballero-Calero O, Martín-González M. Published in [short citation] under CC BY 3.0 license. Available from: http://dx.doi.org/10.5772/67730.

Hopefully I managed to help you, but if you have any other questions feel free to contact me.

Kind regards,

Ivan Šuljić

Publishing Ethics and Legal Affairs

_____

InTech - open science | open minds
Email: suljic@intechopen.com
Website: www.intechopen.com
Phone: +385 51 688 977
Fax: +385 51 686 166

Janeza Trdine 9
51000 Rijeka, Croatia

NATURE PUBLISHING GROUP LICENSE
TERMS AND CONDITIONS
Dec 07, 2017

This Agreement between Technical University of Munich -- Alina Lyuleeva ("You") and Nature Publishing Group ("Nature Publishing Group") consists of your license details and the terms and conditions provided by Nature Publishing Group and Copyright Clearance Center.

License Number	4241821431749
License date	Dec 04, 2017
Licensed Content Publisher	Nature Publishing Group
Licensed Content Publication	Nature Photonics
Licensed Content Title	Two-dimensional material nanophotonics
Licensed Content Author	Fengnian Xia, Han Wang, Di Xiao, Madan Dubey, Ashwin Ramasubramaniam
Licensed Content Date	Nov 27, 2014
Licensed Content Volume	8
Licensed Content Issue	12
Type of Use	reuse in a dissertation / thesis
Requestor type	academic/educational
Format	print and electronic
Portion	figures/tables/illustrations
Number of figures/tables/illustrations	1
High-res required	no
Figures	Figure 1
Author of this NPG article	no
Your reference number	
Title of your thesis / dissertation	Functionalization of Surfaces for Sensors and Optoelectronics
Expected completion date	Jan 2018
Estimated size (number of pages)	100
Requestor Location	Technical University of Munich Theresienstr. 90/I Munich, 80333 Germany Attn: Technical University of Munich
Billing Type	Invoice
Billing Address	Technical University of Munich Theresienstr. 90/I Munich, Germany 80333 Attn: Technical University of Munich
Total	0.00 EUR

JOHN WILEY AND SONS LICENSE
TERMS AND CONDITIONS
Dec 07, 2017

This Agreement between Technical University of Munich -- Alina Lyuleeva ("You") and John Wiley and Sons ("John Wiley and Sons") consists of your license details and the terms and conditions provided by John Wiley and Sons and Copyright Clearance Center.

License Number	4214860451517
License date	Oct 23, 2017
Licensed Content Publisher	John Wiley and Sons
Licensed Content Publication	Advanced Functional Materials
Licensed Content Title	One-Step Synthesis of Photoluminescent Covalent Polymeric Nanocomposites from 2D Silicon Nanosheets
Licensed Content Author	Tobias Helbich,Alina Lyuleeva,Theresa Ludwig,Lavinia M. Scherf,Thomas F. Fässler,Paolo Lugli,Bernhard Rieger
Licensed Content Date	Jul 28, 2016
Licensed Content Pages	8
Type of use	Dissertation/Thesis
Requestor type	University/Academic
Format	Print and electronic
Portion	Figure/table
Number of figures/tables	5
Original Wiley figure/table number(s)	Figure S2
Will you be translating?	No
Title of your thesis / dissertation	Functionalization of Surfaces for Sensors and Optoelectronics
Expected completion date	Jan 2018
Expected size (number of pages)	100
Requestor Location	Technical University of Munich Theresienstr. 90/I Munich, 80333 Germany Attn: Technical University of Munich
Publisher Tax ID	EU826007151
Billing Type	Invoice
Billing Address	Technical University of Munich Theresienstr. 90/I Munich, Germany 80333 Attn: Technical University of Munich
Total	0.00 USD

ROYAL SOCIETY OF CHEMISTRY LICENSE
TERMS AND CONDITIONS
Dec 07, 2017

This Agreement between Technical University of Munich -- Alina Lyuleeva ("You") and Royal Society of Chemistry ("Royal Society of Chemistry") consists of your license details and the terms and conditions provided by Royal Society of Chemistry and Copyright Clearance Center.

License Number	4214850316293
License date	Oct 23, 2017
Licensed Content Publisher	Royal Society of Chemistry
Licensed Content Publication	RSC Advances
Licensed Content Title	Mechanical stabilities of silicene
Licensed Content Author	Qing Peng,Xiaodong Wen,Suvranu De
Licensed Content Date	May 16, 2013
Licensed Content Volume	3
Licensed Content Issue	33
Type of Use	Thesis/Dissertation
Requestor type	academic/educational
Portion	figures/tables/images
Number of figures/tables/images	1
Format	print and electronic
Distribution quantity	5
Will you be translating?	no
Order reference number	
Title of the thesis/dissertation	Functionalization of Surfaces for Sensors and Optoelectronics
Expected completion date	Jan 2018
Estimated size	100
Requestor Location	Technical University of Munich Theresienstr. 90/I Munich, 80333 Germany Attn: Technical University of Munich
Billing Type	Invoice
Billing Address	Technical University of Munich Theresienstr. 90/I Munich, Germany 80333 Attn: Technical University of Munich
Total	0.00 EUR

ROYAL SOCIETY OF CHEMISTRY LICENSE
TERMS AND CONDITIONS
Dec 07, 2017

This Agreement between Technical University of Munich -- Alina Lyuleeva ("You") and Royal Society of Chemistry ("Royal Society of Chemistry") consists of your license details and the terms and conditions provided by Royal Society of Chemistry and Copyright Clearance Center.

License Number	4214831023929
License date	Oct 23, 2017
Licensed Content Publisher	Royal Society of Chemistry
Licensed Content Publication	Physical Chemistry Chemical Physics
Licensed Content Title	Embedded silicene nanostructures in partly-dehydrogenated polysilane
Licensed Content Author	Xiuling Li,Xiao Cheng Zeng,Xiaojun Wu
Licensed Content Date	Mar 24, 2017
Licensed Content Volume	19
Licensed Content Issue	16
Type of Use	Thesis/Dissertation
Requestor type	academic/educational
Portion	figures/tables/images
Number of figures/tables/images	1
Format	print and electronic
Distribution quantity	5
Will you be translating?	no
Order reference number	
Title of the thesis/dissertation	Functionalization of Surfaces for Sensors and Optoelectronics
Expected completion date	Jan 2018
Estimated size	100
Requestor Location	Technical University of Munich Theresienstr. 90/I Munich, 80333 Germany Attn: Technical University of Munich
Billing Type	Invoice
Billing Address	Technical University of Munich Theresienstr. 90/I Munich, Germany 80333 Attn: Technical University of Munich
Total	0.00 EUR

ROYAL SOCIETY OF CHEMISTRY LICENSE
TERMS AND CONDITIONS
Dec 07, 2017

This Agreement between Technical University of Munich -- Alina Lyuleeva ("You") and Royal Society of Chemistry ("Royal Society of Chemistry") consists of your license details and the terms and conditions provided by Royal Society of Chemistry and Copyright Clearance Center.

License Number	4214800754440
License date	Oct 23, 2017
Licensed Content Publisher	Royal Society of Chemistry
Licensed Content Publication	Physical Chemistry Chemical Physics
Licensed Content Title	Long-lived luminescence of silicon nanocrystals: from principles to applications
Licensed Content Author	Raffaello Mazzaro,Francesco Romano,Paola Ceroni
Licensed Content Date	Sep 28, 2017
Licensed Content Volume	19
Licensed Content Issue	39
Type of Use	Thesis/Dissertation
Requestor type	academic/educational
Portion	figures/tables/images
Number of figures/tables/images	1
Format	print and electronic
Distribution quantity	5
Will you be translating?	no
Order reference number	
Title of the thesis/dissertation	Functionalization of Surfaces for Sensors and Optoelectronics
Expected completion date	Jan 2018
Estimated size	100
Requestor Location	Technical University of Munich Theresienstr. 90/I Munich, 80333 Germany Attn: Technical University of Munich
Billing Type	Invoice
Billing Address	Technical University of Munich Theresienstr. 90/I Munich, Germany 80333 Attn: Technical University of Munich
Total	0.00 EUR

ROYAL SOCIETY OF CHEMISTRY LICENSE
TERMS AND CONDITIONS
Dec 07, 2017

This Agreement between Technical University of Munich -- Alina Lyuleeva ("You") and Royal Society of Chemistry ("Royal Society of Chemistry") consists of your license details and the terms and conditions provided by Royal Society of Chemistry and Copyright Clearance Center.

License Number	4214800514144
License date	Oct 23, 2017
Licensed Content Publisher	Royal Society of Chemistry
Licensed Content Publication	Energy & Environmental Science
Licensed Content Title	2D phosphorene as a water splitting photocatalyst: fundamentals to applications
Licensed Content Author	Mohammad Ziaur Rahman,Chi Wai Kwong,Kenneth Davey,Shi Zhang Qiao
Licensed Content Date	Jan 18, 2016
Licensed Content Volume	9
Licensed Content Issue	3
Type of Use	Thesis/Dissertation
Requestor type	academic/educational
Portion	figures/tables/images
Number of figures/tables/images	1
Format	print and electronic
Distribution quantity	5
Will you be translating?	no
Order reference number	
Title of the thesis/dissertation	Functionalization of Surfaces for Sensors and Optoelectronics
Expected completion date	Jan 2018
Estimated size	100
Requestor Location	Technical University of Munich Theresienstr. 90/I Munich, 80333 Germany Attn: Technical University of Munich
Billing Type	Invoice
Billing Address	Technical University of Munich Theresienstr. 90/I Munich, Germany 80333 Attn: Technical University of Munich
Total	0.00 EUR

Confirmation Number: 11685753
Order Date: 12/07/2017
Journal of Physics D: Applied Physics

- **Order detail ID:** 70841986
- **Order License Id:** 4243570741971
- **ISSN:** 0022-3727
- **Publication Type:** Journal
- **Volume:**
- **Issue:**
- **Start page:**
- **Publisher:** IOP Publishing
- **Permission Status: Granted**
- **Permission type:** Republish or display content
- **Type of use:** Thesis/Dissertation

Requestor type	Author of requested content
Format	Print, Electronic
Portion	image/photo
Number of images/photos requested	5
The requesting person/organization	Alina Lyuleeva
Title or numeric reference of the portion(s)	Article
Title of the article or chapter the portion is from	N/A
Editor of portion(s)	N/A
Author of portion(s)	Alina Lyuleeva
Volume of serial or monograph	N/A
Page range of portion	N/A
Publication date of portion	Jan 2018
Rights for	Main product and any product related to main product
Duration of use	Life of current edition
Creation of copies for the disabled	no
With minor editing privileges	yes
For distribution to	Worldwide
In the following language(s)	Original language of publication
With incidental promotional use	no
Lifetime unit quantity of new product	Up to 499
Title	Functionalization of Surfaces for Sensors and Optoelectronics
Instructor name	n/a
Institution name	n/a
Expected presentation date	Jan 2018

JOHN WILEY AND SONS LICENSE
TERMS AND CONDITIONS
Dec 19, 2017

This Agreement between Technical University of Munich -- Alina Lyuleeva ("You") and John Wiley and Sons ("John Wiley and Sons") consists of your license details and the terms and conditions provided by John Wiley and Sons and Copyright Clearance Center.

License Number	4252470548938
License date	Dec 19, 2017
Licensed Content Publisher	John Wiley and Sons
Licensed Content Publication	Advanced Functional Materials
Licensed Content Title	Nanocomposites: One-Step Synthesis of Photoluminescent Covalent Polymeric Nanocomposites from 2D Silicon Nanosheets (Adv. Funct. Mater. 37/2016)
Licensed Content Author	Tobias Helbich,Alina Lyuleeva,Theresa Ludwig,Lavinia M. Scherf,Thomas F. Fässler,Paolo Lugli,Bernhard Rieger
Licensed Content Date	Oct 4, 2016
Licensed Content Pages	1
Type of use	Dissertation/Thesis
Requestor type	Author of this Wiley article
Format	Print and electronic
Portion	Figure/table
Number of figures/tables	1
Original Wiley figure/table number(s)	Back Cover
Will you be translating?	No
Title of your thesis / dissertation	Functionalization of Surfaces for Sensors and Optoelectronics
Expected completion date	Jan 2018
Expected size (number of pages)	100
Requestor Location	Technical University of Munich Theresienstr. 90/I Munich, 80333 Germany Attn: Technical University of Munich
Publisher Tax ID	EU826007151
Billing Type	Invoice
Billing Address	Technical University of Munich Theresienstr. 90/I Munich, Germany 80333 Attn: Technical University of Munich
Total	0.00 EUR

JOHN WILEY AND SONS LICENSE
TERMS AND CONDITIONS

Dec 20, 2017

This Agreement between Technical University of Munich -- Alina Lyuleeva ("You") and John Wiley and Sons ("John Wiley and Sons") consists of your license details and the terms and conditions provided by John Wiley and Sons and Copyright Clearance Center.

License Number	4252980299360
License date	Dec 20, 2017
Licensed Content Publisher	John Wiley and Sons
Licensed Content Publication	Advanced Functional Materials
Licensed Content Title	Silicon Nanosheets: Lewis Acid Induced Functionalization of Photoluminescent 2D Silicon Nanosheets for the Fabrication of Functional Hybrid Films (Adv. Funct. Mater. 21/2017)
Licensed Content Author	Tobias Helbich,Alina Lyuleeva,Philipp Marx,Lavinia M. Scherf,Tapas K. Purkait,Thomas F. Fässler,Paolo Lugli,Jonathan G. C. Veinot,Bernhard Rieger
Licensed Content Date	Jun 5, 2017
Licensed Content Pages	1
Type of use	Dissertation/Thesis
Requestor type	Author of this Wiley article
Format	Print and electronic
Portion	Figure/table
Number of figures/tables	1
Original Wiley figure/table number(s)	Front Cover
Will you be translating?	No
Title of your thesis / dissertation	Functionalization of Surfaces for Sensors and Optoelectronics
Expected completion date	Jan 2018
Expected size (number of pages)	100
Requestor Location	Technical University of Munich Theresienstr. 90/I Munich, 80333 Germany Attn: Technical University of Munich
Publisher Tax ID	EU826007151
Billing Type	Invoice
Billing Address	Technical University of Munich Theresienstr. 90/I Munich, Germany 80333 Attn: Technical University of Munich
Total	0.00 EUR

– The End? –